

**Methods and Tools for Parametric Modeling and Simulation  
of Microsystems based on Finite Element Methods  
and Order Reduction Technologies**

von der Fakultät für Elektrotechnik und Informationstechnik  
der Technischen Universität Chemnitz

genehmigte

**Dissertation**

zur Erlangung des akademischen Grades

**Doktor-Ingenieur**

**(Dr.-Ing.)**

vorgelegt

**von Vladimir A. Kolchuzhin, M.Sc.**

geboren am 11. Januar 1974 in Novosibirsk

eingereicht am: 12.02.2010

Gutachter: Univ.-Prof. Dr.-Ing. habil. Jan Mehner  
Technische Universität Chemnitz

Univ.-Prof. Dr.rer.nat. Gerhard Wachutka  
Technische Universität München

Tag der Verleihung: 12.05.2010

**URL: <http://archiv.tu-chemnitz.de/pub/2010/0055>**



# **Bibliographische Beschreibung**

Methoden und Werkzeuge zur parametrischen Modellierung und Simulation  
von Mikrosystemen mit Finite Elemente Methoden und Ordnungsreduktionsverfahren

Kolchuzhin, Vladimir – 137 Seiten, 48 Abbildungen, 12 Tabellen, 120 Literaturstellen

Technische Universität Chemnitz  
Fakultät für Elektrotechnik und Informationstechnik  
Dissertation (in englischer Sprache), 2010

## **Stichworte**

Parametrische Simulation	Finite-Elemente-Methode
Automatisches Differenzieren	Ableitungen höherer Ordnung
FE-Netzerstellung und -anpassung Me-	Substrukturtechnik
thode der modalen Superposition	Parametrische Ordnungsreduktion

## **Kurzreferat**

In der vorliegenden Arbeit wird die Entwicklung eines effizienten Verfahrens zur parametrischen Finite Elemente Simulation von Mikrosystemen und zum Export dieser Modelle in Elektronik- und Systemsimulationswerkzeuge vorgestellt.

Parametrische FE-Modelle beschreiben den Einfluss von geometrischen Abmessungen, Schwankungen von Materialeigenschaften und veränderten Umgebungsbedingungen auf das Funktionsverhalten von Sensoren und Aktuatoren. Parametrische FE-Modelle werden für die Auswahl geeigneter Formelemente und deren Dimensionierung während des Entwurfsprozesses in der Mikrosystemtechnik benötigt. Weiterhin ermöglichen parametrische Modelle Sensitivitätsanalysen zur Bewertung des Einflusses von Toleranzen und Prozessschwankungen auf die Qualität von Fertigungsprozessen. In Gegensatz zu üblichen Sample- und Fitverfahren wird in dieser Arbeit eine Methode entwickelt, welche die Taylorkoeffizienten höherer Ordnung zur Beschreibung des Einflusses von Designparametern direkt aus der Finite-Elemente-Formulierung, durch Ableitungen der Systemmatrizen, ermittelt.

Durch Ordnungsreduktionsverfahren werden die parametrische FE-Modelle in verschiedene Beschreibungssprachen für einen nachfolgenden Elektronik- und Schaltungsentwurf überführt. Dadurch wird es möglich, neben dem Sensor- und Aktuatorentwurf auch das Zusammenwirken von Mikrosystemen mit elektronischen Schaltungen in einer einheitlichen Simulationsumgebung zu analysieren und zu optimieren.



# Contents

<b>Abbreviation and Symbol List</b>	<b>9</b>
<b>Vorwort</b>	<b>13</b>
<b>1 Introduction</b>	<b>15</b>
1.1 Previous Related Studies .....	15
1.2 Present Contributions .....	16
1.3 Outline of the Thesis .....	16
<b>2 Modeling and Simulation in MEMS Design</b>	<b>19</b>
2.1 Evolution of Design and Methods.....	19
2.2 FE-Simulations.....	23
2.3 Recent Developments and Challenges in Reduced Order Modeling of MEMS .....	27
2.3.1 Reduced Order Modeling of Fluid-Structural Interactions .....	30
2.3.2 Package-Transducer Interactions .....	31
2.3.3 Assumptions and Restrictions .....	31
<b>3 Theoretical Background of HODM</b>	<b>35</b>
3.1 Power Series Expansion of a Function.....	35
3.1.1 Taylor Series .....	35
3.1.2 Padé Approximant.....	36
3.1.3 Gevrey Series .....	37
3.2 Parameterization of a Static Analysis.....	38
3.2.1 Linear Case.....	38
3.2.2 Non-linear Case.....	39
3.2.3 Secondary Results .....	40
3.3 Parameterization of a Modal Analysis .....	40
3.4 Parameterization of a Harmonic Analysis.....	42
3.4.1 Frequency Sweep .....	43
3.4.1 Parameter Sweep.....	44
3.4.1 Parametric Frequency Sweep .....	44
3.5 Parameterization of a Transient Analysis.....	44
3.5.1 Full Method .....	44
3.5.2 Modal Superposition Method.....	45
3.6 Examples .....	46
3.6.1 Duffing Oscillator .....	46
3.6.2 Mass-Spring System.....	48

<b>4 Implementation of HODM in FEA</b>	<b>53</b>
4.1 Global Architecture .....	53
4.2 The Derivatives of the FE Matrices .....	55
4.2.1 Element Derivatives versus Material Properties .....	57
4.2.2 Derivatives of a FE Matrix versus Geometrical Parameters .....	58
4.2.3 Derivatives of a FE Matrix versus Boundary Conditions .....	59
4.3 Derivatives of the Load Vectors.....	60
4.3.1 Surface Load .....	60
4.3.2 Volume Load.....	61
4.4 Differentiation .....	62
4.4.1 Automatic Differentiation .....	62
4.4.2 Differentiation Rules .....	63
4.5 Parametric Mesh-morphing.....	65
4.5.1 Design Velocity Field.....	65
4.5.2 Smoothing Technique .....	66
4.5.3 Automated Mesh-Morphing Algorithm .....	67
4.6 Data Structure.....	69
4.7 Substructuring Technique .....	70
4.7.1 Static Analysis.....	70
4.7.2 Component Mode Synthesis.....	71
4.8 Error Estimation .....	72
<b>5 Application of HODM</b>	<b>75</b>
5.1 Parametric Structural Analysis.....	75
5.1.1 Linear Static Analysis .....	75
5.1.2 Variation in Material Properties .....	78
5.1.3 Modal Analysis .....	79
5.1.4 Harmonic Analysis.....	79
5.2 Parametric Electrostatic Analysis.....	80
5.3 Parametric Squeeze Film Analysis.....	83
5.4 Advanced Examples .....	85
5.4.1 Discrete Analysis: Perforated Beam .....	85
5.4.2 Substructuring Technique: Folded-Flexure Resonator .....	88
5.4.3 Parametric Sequential Coupled Analysis: Piezoresistive Element .....	88
5.4.4 Non-Linear Static Analysis: Semiconductor Microtube .....	91
5.5 Discussion on Examples.....	93
<b>6 Application of HODM to MEMS Macromodeling</b>	<b>95</b>
6.1 Generation of MEMS Macromodels Using HODM .....	95
6.1.1 Extraction of Strain Energy Functions .....	95
6.1.2 Extraction of Capacitance Functions.....	96

6.1.3 Extraction of Modal Damping Parameters for Squeeze Film Problems .....	96
6.1.4 Example.....	97
6.2 Parameterization of MEMS Reduced Order Models .....	99
6.2.1 Algorithm Description.....	99
6.2.2 Fixed-Fixed Beam.....	100
<b>7 Conclusions and Outlook</b>	<b>109</b>
<b>Appendix A. Isoparametric Finite Elements Formulations</b>	<b>111</b>
<b>Appendix B. Polynomial Index Notation in 2D Case</b>	<b>115</b>
<b>Appendix C. Analytical Models in an Electrostatically Actuated Fixed-Fixed Beam</b>	<b>117</b>
<b>References</b>	<b>119</b>
<b>List of Figures</b>	<b>129</b>
<b>List of Tables</b>	<b>131</b>
<b>Versicherung</b>	<b>133</b>
<b>Theses</b>	<b>135</b>
<b>Lebenslauf</b>	<b>137</b>





# Abbreviation and Symbol List

## Latin symbols

$a$	lattice constant
$A$	area
$\mathbf{B}$	strain-displacement matrix
$C$	binomial coefficient
$\mathbf{C}$	damping matrix
$d_i$	modal damping constants of mode $i$
$D_{max}$	total deflection range of the structure
$\mathbf{D}$	constitutive matrix, material matrix, elasticity matrix
$E$	Young's modulus
$f$	frequency
$\mathbf{F}$	load vector
$G$	goal function
$\mathbf{I}$	identity matrix
$\mathbf{J}$	Jacobian matrix, isoparametric transformation matrix
$Kn$	Knudsen number
$\mathbf{K}$	stiffness matrix
$\mathbf{M}$	mass matrix
$\mathbf{N}$	shape functions
$p$	parameter
$P, P_{amb}$	pressure, ambient pressure
$Q$	quality factor
$R$	curvature radius
$\mathbf{R}$	residual force vector
$\mathbf{S}$	stress stiffness matrix
$t$	time
$T, T_{ref}$	temperature, reference temperature
$\mathbf{T}$	transformation matrix
$\mathbf{u}$	nodal displacement vector
$\mathbf{v}$	nodal velocity vector

$m$	subscript representing master degree of freedom
$s$	subscript representing slave degree of freedom
$x,y,z$	Cartesian coordinates
$w_i$	weighting factor
$W$	energy

## Mathematical symbols

$\propto$	is proportional to
$\forall$	for all
$\exists$	there exists

$\{F\}$	vector
$[M], \mathbf{M}$	matrix
$\text{Trace}(\mathbf{M})$	trace of $\mathbf{M}$
$ \mathbf{M} , \det(\mathbf{M})$	determinant of $\mathbf{M}$
$M_{ij}$	the $i, j$ -th entry of $\mathbf{M}$
$\mathbf{M}^T$	transpose of $\mathbf{M}$

$\frac{d^n f(x)}{dx^n}, \frac{d^n y}{dx^n}$	Leibniz's notation for the $n^{\text{th}}$ derivative of the function $y = f(x)$ at $x$
$f^{(n)}(x)$	Lagrange's notation for the $n^{\text{th}}$ derivative of the function $f$
$D_x^n y, D_x^n f$	Euler's notation for the $n^{\text{th}}$ derivative of the function $f$
$\dot{y}, \ddot{y}$	Newton's notation for differentiation, derivative with respect to time
$\nabla f$	gradient of $f$

## Greek symbols

$\delta$	solution error
$\Delta$	forward difference
$\boldsymbol{\varepsilon}$	strain vector
$\phi_i$	eigenvector of mode $i$
$\Gamma$	boundary of the domain

$\rho$	mass density
$\eta, \eta_{\text{eff}}$	dynamic viscosity, effective viscosity
$\lambda_i$	eigenvalue of mode $i$
$\nu$	Poisson's ratio
$\sigma$	squeeze number
$\sigma$	stress vector
$\omega$	circular frequency
$\omega_i$	circular eigenfrequencies of mode $i$
$\Omega$	structural domain
$\xi_i$	modal damping ratios of mode $i$
$\xi, \eta, \zeta$	local element coordinates

## Abbreviations

AD	Automatic Differentiation
a.u.	arbitrary unit
AWE	Asymptotic Waveform Evaluation
BDRIE	Bonding and Deep Reactive Ion Etching
BEM	Boundary Element Method
CAD	Computer-Aided Design
CAE	Computer-Aided Engineering
CFD	Computational Fluid Dynamics
CMS	Component Mode Synthesis
DAE	Differential Algebraic Equation
DOF	Degree of Freedom
EDA	Electronic Design Automation
FDM	Finite Difference Method
FE-	Finite Element
FEA	Finite Element Analysis
FEM	Finite Element Method
FSI	Fluid-Structural Interaction
FVM	Finite Volume Method
gp	Gauss point
GNA	Gauss-Newton Algorithms

HOD	High Order Derivatives
HODM	High Order Derivatives Method
IC	Integrated Circuit
LHC	Latin Hypercube
LMA	Levenberg-Marquardt Algorithms
MCS	Monté-Carlo Simulation
MEMS	Micro-Electro-Mechanical System
MFM	Mesh Free Method
MOR	Model Order Reduction
MSM	Modal Superposition Method
ODE	Ordinary Differential Equation
PA	Padé approximant
PCB	Printed circuit board
PDE	Partial Differential Equation
pMOR	Parametric Model Order Reduction
pROM	Parametric Reduced Order Modelling
RF	radio frequency
ROM	Reduced Order Modelling
RSM	Response Surface Method
SWA	Spellucci-Wittmeyer Algorithm
TS	Taylor series
2D	two dimensional
3D	three dimensional
et al.	and others (et alii)
etc.	and so on (etceteras)
e.g.	for example (exempli gratia)
i.e.	that is (id est)
vs.	versus

# Vorwort

Die vorliegende Dissertationsschrift stellt die Ergebnisse meiner Forschungsarbeiten innerhalb des Sonderforschungsbereiches 379 „Mikromechanische Sensor- und Aktorarrays“ an der Technischen Universität Chemnitz vor. Wesentliche Entwicklungen und Resultate wurden in Drittmittelprojekten und in Zusammenarbeit mit verschiedenen Firmen erprobt und evaluiert.

Hiermit möchte ich mich bei allen ehemaligen und aktiven Mitarbeitern der Professur Mikrosystem- und Gerätetechnik bedanken. Die freundliche und unkomplizierte Arbeitsatmosphäre hat mir über lange Jahre eine gute und wertvolle Zeit bereitet.

Ein besonders großer Dank gilt Herrn Prof. Dr.-Ing. Wolfram Dötzel. Er hat mich nach Deutschland eingeladen und alle diese Jahre beruflich wie privat unterstützt.

Herrn Prof. Dr.-Ing. habil. Jan Mehner bin ich für die Themenauswahl und die Betreuung meiner Promotion sehr dankbar. Er hat diese Arbeit durch wertvolle Hinweise sehr gefördert.

Herrn Univ.-Prof. Dr.rer.nat. Gerhard Wachutka danke ich für sein Interesse an meiner Arbeit und seinen Einsatz als Gutachter.

Herzlichst bedanke ich mich bei Dr.-Ing. Richard Kiehnscherf, der jederzeit bei technischen oder formalen Problemen hilfsbereit war.

Ebenso bedanke ich mich bei Dr.-Ing. Joachim Markert, Dr.-Ing. Steffen Kurth und Dipl.-Ing. Roman Forke für Unterstützung bei der messtechnischen Charakterisierung.

Ich danke meiner Familie und insbesondere meiner Frau Svetlana, die mich von der anderen Arbeit entlastete und mit Geduld und Verständnis zum Gelingen dieser Arbeit beitrug.

Chemnitz im Dezember 2009

Vladimir Kolchuzhin



# 1.Introduction

The MEMS designing is a very challenging and interdisciplinary task. Smart design methodologies and software algorithms are required to design powerful, reliable and cost efficient microsystems within shortest time. Activities of the MEMS-Design group at the Chemnitz University of Technology are focused on software development for device and system simulations, on modeling and simulation of user-specific applications and practical MEMS design for prototypes manufactured. Beyond the commercial software the thesis deals with advanced computational approaches required to extend the considered effects within the ordinary FE-analyses.

## 1.1 Previous Related Studies

Commonly used numerical simulation methods (FDM, FEM and BEM) provide only results for a given set of geometrical and physical parameters. Any change of design parameters, loads or boundary conditions requires further simulation runs. Many different topics in the field of structural analysis, design sensitivity analysis and optimization are covered in Ph.D. work [1]. Usually, the methods of design sensitivity analysis used the approach, where derivatives of finite element matrices and vectors are approximated by first order finite differences is adopted. Because, it is very difficult to establish analytical relations between the derivatives of finite element matrices and the available types of generalized shape design variables on the general mesh generation and parameterization features. For static problems the semi-analytical method of design sensitivity analysis is prone to large errors for certain types of problems involving shape design variables. The inaccuracy problems may occur for design sensitivities with respect to structural shape design variables in cases where the displacement is characterized by rigid body rotations which are large relative to actual deformations of the finite elements (e.g. beam-like, plate and shell structures). This error problem is entirely due to the finite difference approximation involved in determining various element matrix derivatives [1]. HOD method, based on automatic differentiation, is a way to overcome these drawbacks [2]. E.g., the modified approach to semi-analytical design sensitivity analysis based on exact differentiation of element matrices has been shown to yield accurate sensitivities [1].

A number of numerical techniques to handle MEMS macromodel have appeared over the last decade. The two major ones are: mode superposition technique [3, 4] and Krylov subspace based methods [5, 6]. But the traditional reduced order methods are incapable of dealing with the parametric models. Complete system level simulation requires accounting for the process variations and for the influence of packaging effects [7]. Recently, some parametric methods have been proposed to preserve the parameter during the reduced process [7, 8, 9]. Feng use the pMOR method to preserve the film coefficient as a parameter in the compact thermal model [8]. The work [7] presented a method to generate a parameterized reduced order model

based on MSM by means of fit and interpolation algorithms. The possibilities of design optimization enabled with the method parameterized modal superposition are demonstrated with an angular rate sensor. The result is strongly dependent on excellent fit procedures. Therefore, an optimized approach to generate parameterized MSM ROMs is a challenge task yet [7].

Following previous works, novel HOD method is applied to FEA in order to reduce the computational effort of techniques for parametric macromodel extraction.

## 1.2 Present Contributions

The general objective of this thesis is to investigate in detail capabilities and limitations of the HODM as a novel approaches for the parametric MEMS simulation.

The major contributions of the present work will be focused on the following topics:

- development of a parametric FE-solver based on the derivation of the discretized FE equations and the computation of a Taylor polynomial of the solution from the high order derivatives
- development of a library of parameterized finite elements
- implementation of a parametric mesh-morphing algorithm
- using of an automatic differentiations technique for extraction high order derivatives of the FE matrixes
- testing of developed parametric FE-solvers, preparation some simple benchmarks, comparing parametric models with the result obtained by the ordinary FE-method.

For the extension of possibilities for reduced order methods based on mode superposition technique the following investigations will be performed:

- time effective ROM model generation using HODM
- derivative based parameterization of macromodels.

Prior to discussing the research topics, a literature review on state-of-the-art numerical methods for the MEMS modeling will be conducted.

## 1.3 Outline of the Thesis

The thesis is subdivided into seven chapters. Chapter 2 presents a short survey of MEMS design and methods developed over the past decade. Following this, the FEM is described briefly with particular attention to MEMS application. As part of the outline, the ROM design



framework which implements system simulation of MEMS is summarized. Computational approaches and challenges in reduced order modeling based on mode superposition method of the coupled electrostatic-structural domains, including nonlinear effects, fluid-structure interactions and packaging effects are presented.

In Chapter 3 the mathematical basis of HODM for parameterization of the overall analysis procedures is described. To demonstrate the theory of the proposed method and its possibilities, two simple, easy to check examples are presented. The first example is the model of a Duffing oscillator as the non-linear system. The second example is a 2-DOF mass-spring system with modal and harmonic responses.

Chapter 4 presents the implementation process of the HODM in FEA. First, a brief introduction to automatic differentiation is given. Next the differentiation of the FE-matrices is explained, with special emphases on geometrical parameters. Finally, mesh-morphing and substructuring technique are described.

In Chapter 5 the developed method is assessed on a number of examples in the static, modal, frequency response domains on the basis of the structural, electrostatic and coupled field analyses. To validate the approach, parameterized solutions, using the polynomials and rational fractions are compared to converged FE results, achieved by restarting for each set of parameters. Numerical details, accuracy and observed problems will be discussed on several examples, which come from the MEMS problems.

Chapter 6 demonstrates the viability of HOD methods for automated MEMS macromodel generation using a single FE run for ROM data extraction, which allows accelerating the generation of macromodel. In the second part, HOD technique is applied for extraction geometrically parameterized reduced order models model of the MEMS components. The parameterization of the mode superposition based reduced order model in the coupled-physics domains, numerical details, accuracy and observed problems will be demonstrated by the macromodel generation procedure of an electrostatically actuated fixed-fixed beam.

The thesis closes with conclusions drawn from the performed studies and suggestions for future work in Chapter 7.



## 2. Modeling and Simulation in MEMS Design

In this chapter a short survey of MEMS design and methods developed over the past decade is given. Following this, the FEM is described briefly with particular attention to MEMS application. As part of the outline, the ROM design framework which implements system simulation of MEMS is summarized. Computational approaches and challenges in reduced order modeling based on mode superposition method of the coupled electrostatic-structural domains, including nonlinear effects, fluid-structure interactions and packaging effects are presented.

### 2.1 Evolution of Design and Methods

Microelectromechanical systems, *actuated by electrostatic force* are widely used in various applications such as pressure sensors, microphones, switches, resonators, accelerometers, filters, tunable capacitors and material properties measurements. Nowadays, even the typical economy car contains some fifty MEMS sensors, and high-end models may have more than one hundred [10]. In the near future, major MEMS application segments are consumer electronics and medical applications.

The MEMS design process is a strongly iterative *multilevel* process, Figure 2.1. The levels in design include lumped elements synthesis, process sequence development and mask layout drawing, component and system simulations [11, 12]. Several different software tools are used for this purpose. Numerical simulations are used both as a design tool and for understanding complex device behavior. Design and analysis of MEMS devices is heavily coupled to the fabricated processes.

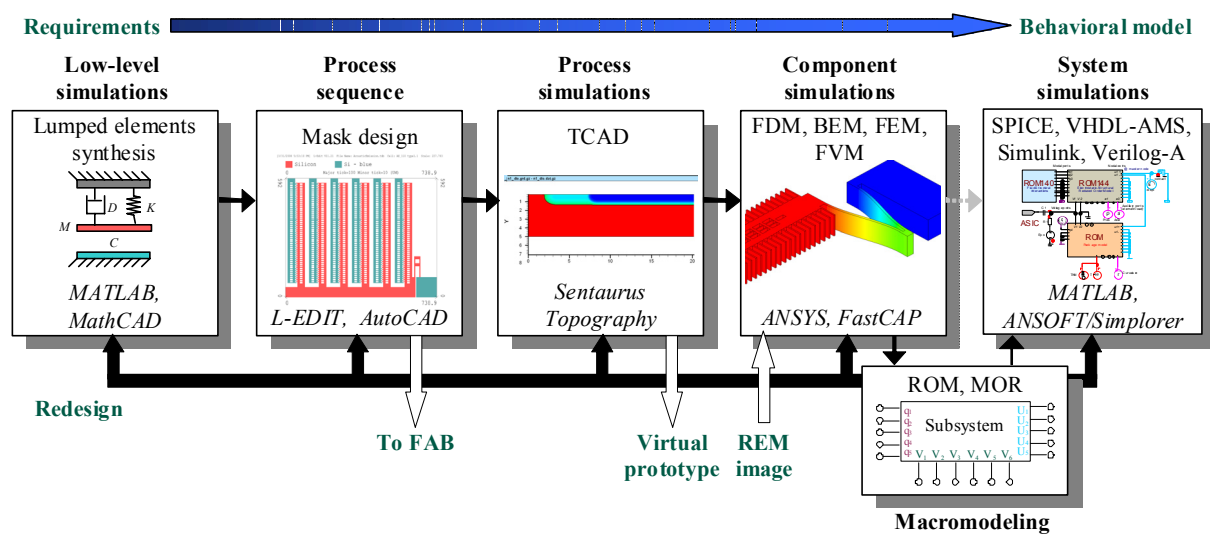


Figure 2.1 Multilevel MEMS design flow process

Recently, many of the MEMS devices were designed, without essentially numerical simulation, by intuition and analytical calculations [13]. Finally, the validation or rejection of ideas typically must be done by fabrication. One iteration of a design loop can take months. Simulations are important, since fabrication and physical evaluation of devices are expensive and time-consuming steps. Modeling and simulation of MEMS is of vital importance to develop innovative products and to reduce time-to-market at lower total costs. Advanced design methodologies and a variety of software tools are utilized in order to analyze complex geometrical structures, to account for interactions among different physical domains. Computer simulations provide a deep understanding of the device behavior and lead to systems with optimized performance parameters. Time-to-market with R&D takes often few years despite growing experience and existing numerical algorithms and commercial tools.

Limitation of computational resources must be considered as a fundamental principle that for algorithm implementation is important as physical laws. In general, it is necessary to use a simplified mathematical model of reality to render a simulation feasible. The algorithms, which do not require an excessively large time and system memory, those are realizable by real computers at least in principle are called effective algorithms. In the formal algorithm theory, an algorithm is called effective if it requires the time limited by some polynomial  $p(n)$  to process an input data of the length  $n$ . Then, the algorithms requiring an exponential time are not effective [14].

The most accurate numerical analysis of complex MEMS devices can be obtained by solving partial differential equations describing 3D physical fields. There are several widely accepted numerical techniques for solving electrical, mechanical, fluid and thermal fields, such as Finite Difference Method, Finite Element Method and Boundary Element Method. For each of these numerical techniques it is essential to produce a geometry model that accurately approximates the real device. The design of MEMS is based on *multiphysics* simulation [15, 16, 17]. Usually, the mechanical domain is modeled by the FEM. For the electrical and fluid domain, both the FEM and BEM can be used, existing advantages and disadvantages for each one. In the coupled electrostatic-structural simulation the electrical domain is constantly changed and it is necessary to modify the mesh for each solution step. The drawback of FEM is the mesh-modification makes the simulation computationally expensive. The FEM generates sparsely populated matrices that are easy to be solved. The BEM avoids modification a mesh for the electrostatic domain and reduces the computational effort. The disadvantage of BEM is the dense matrices. Much of the activity in fluid mechanics has however pursued Finite Difference Method and Finite Volume Method. The meshless methods, which are a novel class of numerical methods, are still under development [18, 19].

CAD systems for MEMS began in the early 1990s, with the primary focus being on 3D model generation, algorithms for fast electrostatic analysis of complicated structures and methods for solving coupled partial differential equations [20, 21, 22]. Like mechanical CAD systems, MEMS CAD systems were integrated with FEM and BEM tools within the design environ-

ment, generating mesh from 3D models or 2D layout. Senturia et al. was among the first people who suggested the architecture of their CAD system for MEMS [20]. Most commercial CAD tools for MEMS have been developed in USA. For example, IntelliSuite [23], from IntelliSense Software Corp. (Woburn, Mass.), CoventorWare [24], from Coventor Inc. (Cary, N.C.) and MEMS Pro [25], from SoftMEMS LLC (Los Gatos, Calif.) are the CAD systems with special focus of MEMS. The two first companies are based on the pioneering MEMCAD system created at the Massachusetts Institute of Technology under the supervision of Professor S. Senturia.

As the importance of MEMS increases, also commercial software vendors for general-purpose simulation have provided integrated tools for MEMS applications [26, 27, 28]. For example, Ansys Inc. (Canonsburg, Pa.) has started to include special element types and algorithms which are useful for electrostatically actuated devices [26].

Specialized tools for widely used micromachined polysilicon foundry process were developed in mid-1990s, and these tools using the specifics of the process to extract the model and simulation [29]. For several years, high aspect ratio technologies based on BDRIE have been used and commercialized for fabrication of MEMS structures [30].

Modern MEMS CAD systems tend to integrate with existing EDA tools generating macro-model from physics based models remains tedious and lacks automatic adaptation tools. This situation is one of the major challenges for integrating analysis into the design environment. The goal of MEMS macromodeling is to create a black-box model with interface input/output ports and internal state variables what can be analyzed within reasonable time and almost the same accuracy as obtained from full models. The developers of general MEMS CAD systems attempted to achieve this goal by focusing on using model-order reduction to extract system level models, which is define by the ODE from the coupled PDE descriptions of MEMS at the physical level, using two strategies: the superposition of basic function based on Rayleigh-Ritz method [3, 4, 31, 32, 33] and the matrix subspace projection based on FE matrices [5, 6]. The advantages and disadvantages of each implementation were analyzed and then some selection principle was proposed in [34, 35]. Reduced order modeling of MEMS allows a tremendous reduction of model size which becomes important for time-domain simulations with several hundreds of steps needed for circuit and control system virtual prototyping [36]. Since reduced order models are based on analytical terms, they can easily transfer from one simulator to others and can be adjusted to experimental data.

Parametric modeling has become the basis for most mechanical CAD systems. In mechanical design, 80% of design tasks are variational [37]. Therefore, parameterized CAD models can be reused in design step. Parametric design is a revolutionary paradigm of CAE systems, which allows designers to take into account the parameters variation of a model in single step without redesign [38]. The parameters can be automatically recognized from the CAD model. Parametric design can help the designer to find the best parameters for a system, or a com-

pletely new design which is uncertain in classical design processes. Parameterization has both advantage and disadvantage. Parameterization increases complexity of the problem as designer must model not only the initial concept, but a structure that guides variation. Changes can cause invalid model. Positively, parameterization can reduce the time and effort required for change and reuse, and can yield better understandings of the conceptual structure.

The number of parameters is a criterion: A model with a few parameters can be deduced from curve fitting or numerical and experimental observations. When the number of parameters grows, it becomes more difficult to span the complete parameter space, since each parameter lets the number of possible variations grow in an exponential way.

Different types of design parameters can be handled in modeling of MEMS component. The most obvious ones are continuous parameters such as geometrical dimensions, material properties, etc. The designer can also deal with discrete parameters such as boundary conditions or loads. Process issues involving dimensional variations can highly change the transfer function of the MEMS components as well as have an influence on the effect of temperature and packaging.

The design variables can be categorized as follows [39]:

- **Geometrical design variables:**

*Sizing design variables:* describe cross-sectional properties of structural components like dimensions, cross-sectional areas or moments of inertia of beams; or thicknesses of membranes, plates and shells

*Configurational design variables:* describe the coordinates of the joints of discrete structures like trusses and frames; or the form of the center-line or mid-surface of continuous structures like curved beams and shells

*Shape design variables:* govern the shape of external boundaries and surfaces, or of interior interfaces of a structure. Examples are the cross-sectional shape of a beam; the boundary shape of a plate or shell; the surface shape of a 3D component; or the shape of interfaces within a structural component made of different materials (*multi-material*)

*Topological design variables:* describe the type of structure, number of interior holes, etc., for a continuous structure. For a discrete structure like a truss or frame, these variables describe the number, spatial sequence, and mutual connectivity of members and joints.

- **Material design variables:** represent constitutive parameters of materials.

- **Support design variables:** describe the support or boundary conditions, i.e., the number, positions, and types of support for the structure.
- **Loading design variables:** describe the positioning and distribution of external loading which in some cases may be at the choice of the designer.
- **Manufacturing design variables:** parameters pertaining to the manufacturing process, which influence the properties and cost of the structure.

There are still many design automation challenges in MEMS design. Other problems are related to the manufacturing of MEMS, more complicated process techniques are used for MEMS, feature sizes decrease. Now also the packaging of MEMS must be included in the MEMS design process. The next frontier is the integration of the CAD tool and topology optimization technique. This combination will make CAD a true design tool. Optimization-driven design can help to develop MEMS by applying the most advanced optimization methods to solve the design problem. Optimization-driven design methodology generates optimal design from supplied input parameters, loads, constraints and required product performance and manufacture conditions in innovative concepts and less time [40].

## 2.2 FE-Simulations

FEM is the dominating numerical method used for simulating the behavior of MEMS components. FEM has various aspects. On an application point of view, the basic steps of FEM are discussed below in generality. Ordinary FE programs are organized in the following [41, 42]:

- Meshing of the simulation domain into elements: numbering the elements and nodes. (*preprocessing*)
- Assembling global stiffness matrix  $\mathbf{K}$  and load vector  $\mathbf{F}$ , element wise: calculate the element stiffness matrix,  $\mathbf{k}^{el}$ , for each element and assemble it into the  $\mathbf{K}$
- Calculate the element load vector,  $\mathbf{f}^{el}$ , for each element and assemble it into the  $\mathbf{F}$
- Modifying global stiffness matrix and global load vector to enforce boundary conditions
- Solving the system of equations for the unknown value at each nodal point
- Obtain secondary results
- Visualization the results (*postprocessing*).

The global stiffness matrix  $\mathbf{K}$  for the entire structure can be assembled if the “*force-displacement*” relationship for each of these discrete elements is known. The terms *displace-*

*ment*, *force* and *stiffness* will be used in this work, it is implied that the concepts apply to all valid effects also. Thermal, fluid and electrostatic analyses are done on an analogous basis by replacing the appropriate terms. The physical significance of the vectors  $\mathbf{u}$  and  $\mathbf{F}$  varies according to the application being modeled, as illustrated in Table 2.1.

Table 2.1 Data for different disciplines nomenclature

Discipline	Structure properties $\mathbf{K}$	Action $\mathbf{F}$	Primary Data	Derived Data		
			Behavior $\mathbf{u}$	Gradient	Flux	Potential energy
elastic	stiffness	force	displacement	stress	strain	elastic
thermal	thermal conductivity	heat source	temperature	temperature gradient	heat flux	thermal
fluidic	dynamic viscosity*	flow rate	pressure	pressure gradient	—	viscous losses
electroconductivity	electro conductivity	current	potential	electric field	flux density	dissipation losses
electrostatic	permittivity	charge	potential	electric field	flux density	electrostatic

The main four *types of structural analyses* are explained below.

- **Static analysis** is used to determine displacements, stresses, etc. under static loading conditions. Both linear and nonlinear static analyses are allowed. There are two kinds of non-linearity:

*geometrical non-linearity* (stress stiffening, large deflection and contact)

*material non-linearity* (large strain and variation of stress with respect to strain).

- **Modal analysis** is used to calculate the natural frequencies and mode shapes of a structure.
- **Harmonic analysis** is used to determine the response of a structure to harmonically time-varying loads.
- **Transient analysis** is used to determine the response of a structure to arbitrarily time-varying loads. Two solutions methods are available to do a transient dynamic analysis:

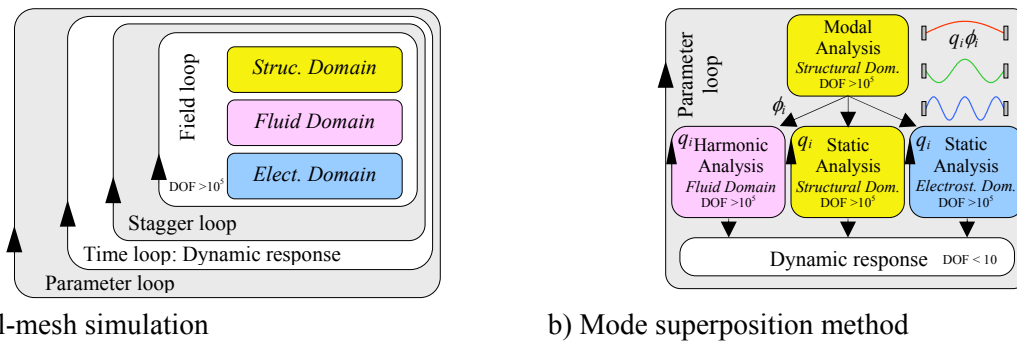
*full* (most general methods allows all types of nonlinearities mentioned under static analysis above to be included)

*mode superposition* (used sum of factored mode shapes from a modal analysis to calculate the response).



Although attention is focused on structural problems, most of the steps translate to other applications problems as noted above in Table 2.1. There are two ways in obtaining the solution of the matrix equations, namely, direct methods and iterative methods. These specific methods are called solvers. It should be emphasized that the solution of the matrix equation is usually computed without taking the inverse of the matrix which will require relatively large computational processes [43].

The multiphysics solution methodology implemented involves a sequential strategy where the each domain are modeled separately and the interaction between them is done by inserting the results of one domain analysis into the other until convergence is reached, Figure 2.2a.



a) Full-mesh simulation

b) Mode superposition method

Figure 2.2 Parametric transient multiphysics simulation

The coupled electrostatic-structural analysis is difficult because the electrostatic pressures are non-uniform and change as the structure deforms. But transient fully-meshed simulations for coupled-domain systems can be quite time consuming using the traditional FE approach. For example, full-mesh transient self-consistent coupled electro-structural simulation of MEMS devices still take a few hours using commercial finite element solvers [43]. One should have in mind that typical electronic simulation runs need several ten thousands of time steps what cannot be processed by FEM in reasonable time [36].

Drawback of existing FE techniques is that those algorithms can only analyze a single model configuration with specified dimensions and physical parameters. A change of a design parameter could be caused by either a parameter variation loop, Figure 2.2. The levels of difficulty of the physical simulations can be classified using three main axes: the parameters, the physical domains and the response, as illustrated in Figure 2.3.

Bottleneck of the transient multiphysics simulation are for-loops that do not run fast. Here are two specific ideas to increase efficiency. First one is to use decomposition based on the MSM, which is an automated approach, Figure 2.2b. MSM method decomposes the problem into single domains and solves the problem on each domain separately. Because of the decoupling, this method is well-suited for parallel computing. The connection between the sub-domains is provided by model amplitudes [4].

Second one is to apply higher order derivatives method to FEA. The complexity ratio of factorization to solution of the matrix increases with the dimension of the system. For large ma-

trix, this time ratio may be rather large. The applications of higher order derivatives method to FE problem as a way to increase the efficiency, accuracy and robustness was started in the 1990s [44, 2, 45, 46]. Paper [47] reviews different techniques for structural design sensitivity analysis, including global finite differences, continuum derivatives, discrete derivatives and automatic differentiation. Parametric technologies have been applied to optimization in mechanical engineering [2, 44, 46], for CFD problem [45, 48] and in electromagnetism [49, 50, 51, 52]. Later this approach was used for microwave device design [53] and parametric model extraction for MEMS [54, 55]. First commercially available software was developed by the French company CADOE S.A. [56].

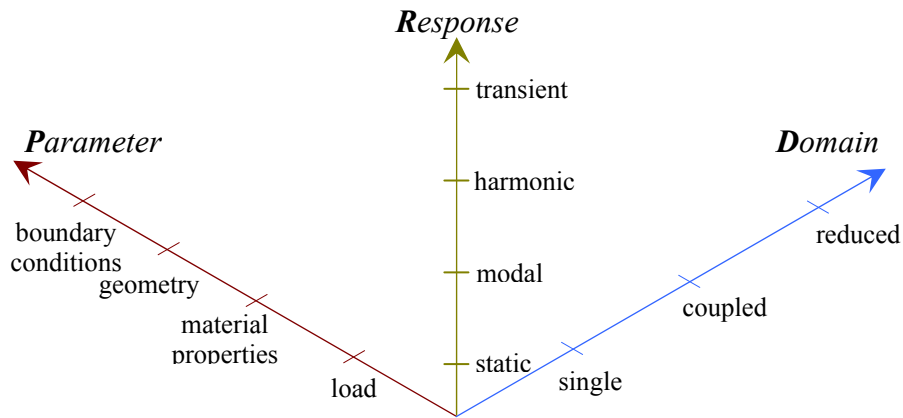


Figure 2.3 The levels of difficulty of the physical simulations

The key idea of the HOD approach is to compute not only the governing system matrices of the corresponding FE problem but also high order partial derivatives with regard to design parameters by means of the AD as shown in Figure 2.4. As result, Taylor vectors of the system's response can be expanded in the vicinity of the initial position capturing dimensions and physical parameter. By using the HOD method, the simulation results become directly polynomial functions in terms of design parameters. Reusing of extracted matrices for different type of analyses (Figure 2.3) can increase the efficiency of HOD method.

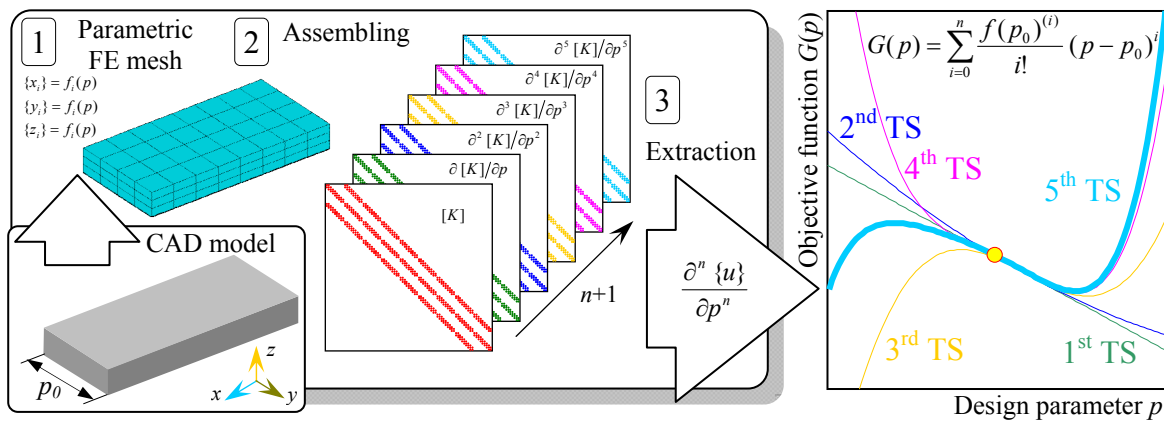


Figure 2.4 Derivatives based parametric FE simulation

## 2.3 Recent Developments and Challenges in Reduced Order Modeling of MEMS

The growth in the MEMS industry in the past ten years has led to the necessity of standardization of the MEMS models and design tools. In the year 2002, Ansys, Inc. shipped the ANSYS Multiphysics software product (Release 7.0) with first version of the reduced order modeling tool for the coupled electrostatic-structural domains. The ANSYS ROM tool has been developed as an extension of mode superposition method to the coupled electrostatic-structural domains [57, 58]. It describes the dynamic behavior of electromechanical flexible components as a system of second order ordinary differential equations. The number of degrees of freedom of this system is equal to the number of chosen modes. Difficulties of consistent modeling arise from the fact that the model types are heterogeneous. Package and transducer models are usually generated by FE tools, controller units are based on signal flows as known from MATLAB/Simulink and electronic circuits are represented by Kirchhoffian networks with languages as Verilog-A or VHDL-AMS. A schematic view on the ROM layout and interfaces is shown in Figure 2.4.

The entity transducer element (the ROM144 functional blocks in Figure 2.5) describes the interface of the macromodel. Each DOF of the ROM element is mapped to one of the across or through quantities of the terminals of the entity. At the modal terminals the modal amplitude  $q_i$  and external modal force  $fm_i$  (e.g. acceleration, angular rate) are available for the chosen modes. The master node terminals provide the displacement  $u_i$  and the inserted forces  $fn_i$  at these nodes. At the electrical terminals the voltages  $V_j$  and currents  $I_j$  are available for the electrodes of the system.

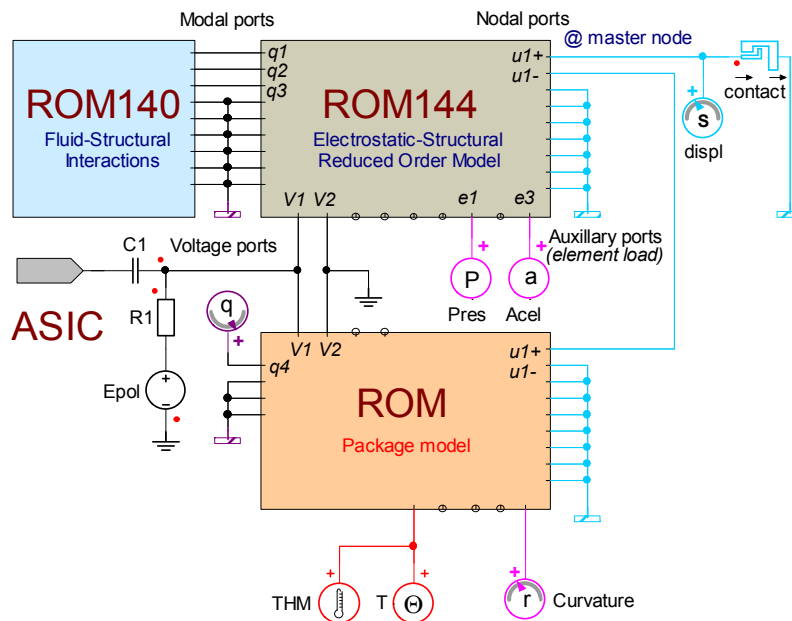


Figure 2.5 A schematic view on the VHDL-AMS exported ROM model in ANSOFT/Simplorer

The governing equations describing an electrostatically actuated structure in terms of modal coordinates in the mechanical domain become

$$m_i \ddot{q}_i + d_i \dot{q}_i + \frac{\partial W_{SENE}}{\partial q_i} = \frac{1}{2} \sum_r \frac{\partial C_{kl}}{\partial q_i} (V_k - V_l)^2 + f_{mi}. \quad (2.1)$$

Where  $r$  is the number of capacitances involved between the multiple electrodes. The capacitance  $C_{kl}$  between the electrodes  $k$  and  $l$  provides the coupling between the mechanical and electrical domains. The current  $I_j$  through the electrode  $j$  can be calculated from the stored charge  $Q_j$ :

$$I_j = \frac{\partial Q_j}{\partial t} = \sum_r \left[ \left( \sum_m \frac{\partial C_{kl}}{\partial q_m} \dot{q}_m \right) (V_k - V_l) + C_{kl} (\dot{V}_k - \dot{V}_l) \right]. \quad (2.2)$$

Efficiency of reduced order models becomes obvious if one considers the total number of differential equations to be solved. There is only one equation for each eigenmodes (basis function) and one equation for each conductor. True structural displacements  $u$  are calculated from modal amplitudes  $q$  by

$$u(x, y, z, t) = u_{ref} + \sum_{i=1}^m \phi_i^E(x, y, z) q_i(t), \quad (2.3)$$

where  $u_{ref}$  are initial displacements,  $\phi_i^E$  are the eigenvectors involved in the reduced order model.

The equations (2.1), (2.2) and (2.3) are defined the transducer ROM macromodel, which fully describe the static, harmonic and dynamic nonlinear behavior of the flexible structure.

All missing parameters of the ROM can be derived from a detailed FE-model of the MEMS component. Geometrical nonlinearities and stress-stiffening are considered by calculating the modal stiffness  $k_{ij}$  from the second derivatives of the strain energy  $W_{SENE}$  [32], which is stored within the structure due to deflection with respect to the modal amplitudes:

$$k_{ij} = \frac{\partial^2 W_{SENE}}{\partial q_i \partial q_j}. \quad (2.4)$$

The modal masses  $m_i$  are calculated from the eigenfrequencies  $\omega_i$  of the modes  $i$  and the entries of the modal stiffness matrix  $k_{ij}$ :

$$m_i = \frac{k_{ii}}{\omega_i^2}. \quad (2.5)$$

The modal damping constants  $d_i$  are calculated from the modal damping ratios  $\xi_i$  that represent the fluidic damping (squeeze and slide film damping) of the structure and can be obtained from analytical calculations, CFD simulations or measurements:

$$d_i = 2\xi_i \omega_i m_i. \quad (2.6)$$

In such a way, the strain energy, the mutual capacitances, the damping coefficients and the modal load forces are the parameters characterizing the coupled electromechanical system. The ROM macromodels are generated by numerical data sampling and subsequent fit algorithms [4]. Each data point must be obtained by a set of separate FE runs in the structural, electrostatic and fluid domains. At each point  $(q_1, q_2, \dots, q_m)$  the microstructure is displaced to a linear combination of  $m$  selected mode shapes in order to calculate the strain energy  $W_{SENE}(q_1, q_2, \dots, q_m)$  in the structural domain. For example, in the case of  $k$  modal amplitudes in each mode direction, the number of orthogonal sampling points would be  $k^m$ . At each point the  $r = n(n-1)/2$  linear simulations are performed to compute lumped capacitances  $C_r(q_1, q_2, \dots, q_m)$  in the deformed electrostatic domain, where  $n$  is the number of conductors.

The operating range of each mode is proportional to their mode contribution factors taking into account the total deflection range:

$$q_i = \frac{D_{\max/\min}}{\omega_i^2} \left( \sum_{j=1}^m \omega_j^{-2} \right)^{-1}. \quad (2.7)$$

It should be noted, that mesh-morphing based on a Laplacian smoothing does not allow large transformations of the mesh.

The ROM macromodels capture the complex nonlinear dynamics inherent in MEMS due to highly nonlinear electrostatic forces, residual stresses, stress stiffening and supports multiple electrode systems and mechanical contact phenomena at system level [59]. The resulting ROM model has a good scalability. E.g., the ROM model is able to capture nonlinear squeeze film phenomena, such as deflection dependent damping and stiffening as reported in [60].

Nowadays, the ANSYS ROM tool has become the industry standard for macromodels extracting of MEMS components [61-67]. The MEMS suppliers like IC ones can provide model libraries for their electromechanical components. The ROM technology based on mode superposition method is very effective technique for fast transient simulation of MEMS component and for export macromodels to external system simulators. The most common simulation tools at system level are signal flow graphs system Simulink; PSPICE circuit simulators and VHDL-AMS, VERILOG-AMS simulators. The extracted macromodel can be automatically export to VHDL-AMS language. The description of ROM macromodels in PSPICE is presented in [4].

### 2.3.1 Reduced Order Modeling of Fluid-Structural Interactions

The goal of the FSI modal projection procedure is to find an equivalent damping and stiffness matrix representation which captures the true dependency between structural velocities  $v$  and fluid pressure  $P(v)$  but is written in modal coordinates.

The coefficients  $c_{ji}$  and  $k_{ji}$  state the dependency between structural wall velocities caused by mode  $i$  and the reacting fluid forces which act on mode  $j$ . The coefficients  $c_{ji}$  and  $k_{ji}$  of such a matrix representation can be obtained from the modal force balance equation

$$c_{ji}\dot{q}_i + k_{ji}q_i = \phi_j^T F_i(\phi_i, \dot{q}_i), \quad (2.8)$$

where  $F_i$  is the complex nodal force vector. The complex nodal damping force vector caused by a unit modal velocity of the source mode  $i$  is given by

$$F_i(\phi_i, \dot{q}_i) = \phi_j^T \int N^T P(\phi_i, \dot{q}_i) dA, \quad (2.9)$$

where  $N$  is the vector of the FE shape functions.

In contrast to the quasi-static FE simulations, which are necessary to extract capacitance information of electrostatic-structural interactions, the modal projection approach requires a series of harmonic response analyses to capture the dynamic nature of fluid-structural interactions. In practice one can analyze just five frequencies which are regular spaced around the cut-off frequency or eigenfrequency of each mode [60]. The analysis based on linearized Reynolds equation known from Lubrication theory is widely used in MEMS to determine the fluid pressure  $P(v)$  with regard to frequencies. A modal decomposition of damping effects becomes admissible since the Reynold's squeeze film equation is linear. It is possible to assess the damping properties of individual modes for a unit velocity according (2.8) and later, when using the ROM, the modes are scaled to the current velocities.

One should keep in mind that the linearized Reynold's equation describes dissipative effects at the initial position. A repeated use of the numerical squeeze film analyses, similar to the electrostatic-structural data sampling, allows us to gather damping information at various points of operation. The behavior between data points can be interpolated by analytical functions which are obtained by a least square fit [60].

Small and large signal capabilities of the discussed damping models are implemented in a beta-test element ROM140 in the ANSYS program. It allows up to nine shape functions and can directly be attached to the existing electrostatic-structural ROM144 element [43] for harmonic and transient coupled domain simulations (see Figure 2.4).

### 2.3.2 Package-Transducer Interactions

The cost of packaging, assembly and test of those new devices may be decreased through the increased use of simulation. The problem is the lack the appropriate tools to simulate the package model at system level. Because of size and functional aspects it is more efficient to create two separate FE-models, one for the package with a dummy block of silicon at the transducer's location and one model for the transducer, capturing the electromechanical response of the sensor [36, 68]. Package simulations are coupled thermal-mechanical analyses with the goal to determine the influence of mechanical stress and structural deformation on the transducer cell. After package simulations have been finished the obtained interface data are applied as displacement and temperature constrains on the substrate of the MEMS device. In a subsequent finite element run one computes the equilibrium position of the seismic mass and related capacitances of the transducer cell.

Packaging interactions are usually unidirectional couplings to the transducer. Environmental and operating conditions of the sensor cause thermal and mechanical effects in the package. In particular parameters such as chip temperature, curvature radiuses and in-plane strains at the bonding face must be passed to the transducer cell.

The ROM algorithm based on MSM was recently extended to account for package-transducer interactions [7, 36]. It turned out that modal shape functions  $\phi^E$  are not appropriate to map the mechanical deformation of MEMS caused by packaging stress. In many cases an excessive number of modes have to be chosen to guarantee accurate results for prestressed micromechanical components. A few additional basis functions  $\phi^A$  which describe the deformation states at snapshots of typical environmental conditions overcome the problem. Thermal-mechanical effects in MEMS caused by the package can efficiently be represented by

$$u(x, y, z, t, T) = u(T_{ref}) + \sum_{i=1}^m \phi_i^E(x, y, z) q_i^E(t) + \sum_{i=1}^n \phi_i^A(x, y, z) q_i^A(T). \quad (2.10)$$

The  $u(T_{ref})$  maps displacements at reference temperature, the second term the dynamic response over time  $t$  and the third one improves accuracy for loads varying with temperature  $T$ .

A single additional shape function is sufficient to capture linearly varying temperature and stress profiles caused by the package [36].

### 2.3.3 Assumptions and Restrictions

The existed ANSYS ROM tool uses only polynomial types for fit procedures [43]. Polynomials are very convenient since they can capture smooth functions with high accuracy. The strain energy functions are inherent polynomials. In the case of linear systems, the strain energy can be exactly described by a polynomial of order two since the stiffness is constant.



But for accurate approximation by means of a least squares method, the number of FE data points must be larger than the polynomial order. To get best polynomial fit it is an important to scaling and centering at zero mean the data. It is essential that the fitting function of capacitances must provide not only capacitance data but also the first and second derivatives needed for Maxwell force and electrostatic softening computations. The first and second derivatives of strain energy describe force and stiffness terms.

The fitted functions must be evaluated faster to increase the efficiency of the ODE time integrator at system simulation. Essential speed up for the existed ROM tool at generation and uses passes is achieved since the deformation state of the mechanical system is represented by a weighted combination of a few eigenmodes. Moreover, modes considered for use in the ROM are classified as dominant or relevant, what allow a reduction of the set of polynomial coefficients. In ANSYS ROM tool, it turned out that two dominant modes are sufficient for most applications. The polynomials can then be described by the series representation of functions with three variables [4].

Modes used for ROM can either be determined automatically from the results of the test load or based on their modal stiffness at the initial position. In these matters, ANSYS ROM tool is limited to systems moving primarily in one direction. Separating the generation of ROM models for different operation directions circumvents current limitations of the used ANSYS ROM tool method. Two separate ROMs have to be generated for the angular rate sensor: one representing the in-plane movement of the rotor and the other the out-of-plane movement [65].

Some type of MEMS (e.g. RF switch) requires an excessive number of modes to accurately describe its shape. Increase of the number of considered modes is a way to extend the considered effects within the ROM methods. Unfortunately, the memory and computational costs of the process grow exponentially with the order of the model. The grid-like data sampling process is expected to grow as  $n^k$ , where  $n$  is the number of design parameters and  $k$  is the number of states for each design parameter.

In order to overcome drawbacks of polynomial approximation, one needs the robust algorithms for multivariate data fitting. Rational interpolation sometimes gives better approximations than polynomial interpolation [4]. Rational models are defined as ratios of polynomials and in multivariate case are given by

$$R_{\mu(r_{\max})/\mu(s_{\max})} = \frac{\sum_r a_r \prod_{i=1}^n x_i^{\mu_i(r)}}{\sum_s b_s \prod_{i=1}^n x_i^{\mu_i(s)}}, \quad (2.11)$$

where  $r$  is the degree of the numerator polynomial and  $s$  is the degree of the denominator polynomial,  $n$  is the number of parameters. Polynomial coefficients  $a_r(b_s)$  are arranged in suc-



cessive order, whereby the multi-index  $\mu$  corresponds to the line location index  $r(\mu)$  (see Section 4.6 for details).

The disadvantage of rational is that they become unstable when the denominator has poles. In the multivariate case the issues of unique and convergence of solution is much more delicate than in the univariate case. To start a minimization, one needs to provide an initial guess and algorithms converge only if the initial guess is already somewhat close to the final solution.

The Spellucci-Wittmeyer algorithm, that is more robust than the Gauss-Newton and Levenberg-Marquardt algorithms, is proposed for ROM in [69]. The SWA is an iterative and very fast procedure [70].

The ROM generation pass from the series of FE runs is a computationally expensive. The classical RSM, needed for the behavioral model extraction, is based on an orthogonal sampling scheme. More valuable approach is based on spreading points over the design space. This can be done by a number of methods: random, Monte Carlo, Latin-Hypercube scheme. Alternatively to the data sampling techniques, power expansion approach for behavioral model extraction and building response surfaces was investigated in [71]. Like polynomial fitting, the power expansion is also using a polynomial form for the response surface, but the polynomial represents a Taylor expansion at the initial point of the variation range of the parameters, Figure 2.6. Padé approximants can be used to transform of a Taylor series into a rational function. In particular, the time consuming data sampling process in the static and frequency response domains has been replaced by a single FE run on the basis of the structural, electrostatic and squeeze film analyses with regard to modal amplitudes [71]. More details on derivatives based approach algorithm are given in Section 6.

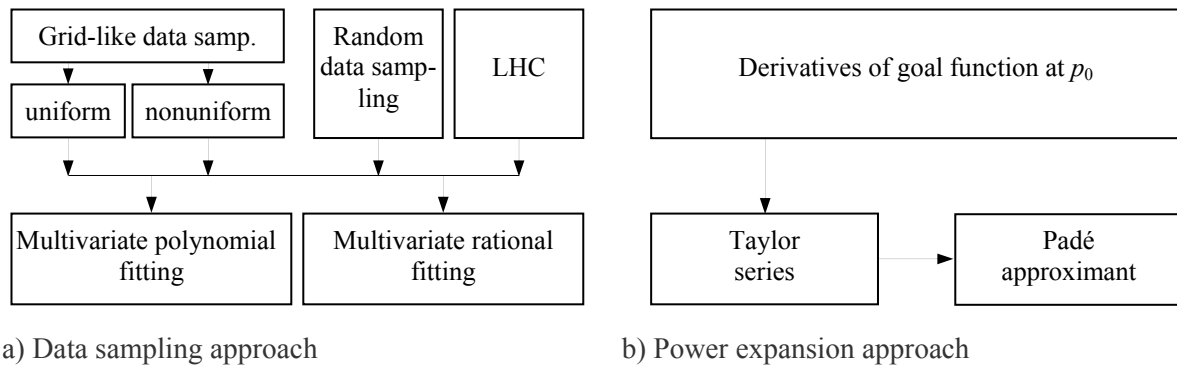


Figure 2.6 Response surface method to the behavioral model extraction

Drawback of the existing ROM techniques is that those algorithms can only analyze a single model configuration with specified dimensions and physical parameters. In practice, there is necessity to know the influence of parameter variations on the structural response in order to optimize the entire system and to assess the effect of tolerances or changed material. In this context the paper compares different techniques which are applied to parametric tasks.

Recently, parametric ROM using data sampling approach and design optimization algorithms has been presented to the angular rate sensor [72]. Parameterization of the reduced order model generation procedure is based on different fitting algorithms which have been compared for an application example.  $K$ -nearest neighbor algorithm, polynomial fitting and Gaussian models have been applied to fit the generated sampling data [72]. This approach is not computationally efficient, but can be used as a reliable method. The result is strongly dependent on excellent fit procedures. Therefore, an optimized approach to generate parameterized ROMs is challenge task yet. Beyond the commercial software the thesis deals with advanced computational approaches required to extend the considered effects within the ROM procedures. Two problems are highlighted: effective model extraction and parameterization of macromodel based on based on mode superposition method.

## 3. Theoretical Background of HODM

*This chapter describes the mathematical basis of HODM for parameterization of the overall analysis procedures. In the standard matrix methods of analysis, based on lumped element idealization, as well as mesh-methods, the structure being analyzed is approximated as an assembly of discrete elements connected at nodes. By using HODM, a parametric solution is extracted as a power series with regard to the required parameter. To demonstrate the theory of the proposed method and its possibilities, two simple, easy to check examples are presented. The first example is the model of a Duffing resonator as the non-linear system. The second example is a 2-DOF mass-spring system with modal and harmonic responses.*

### 3.1 Power Series Expansion of a Function

In many engineering problems a closed form solution of the problem cannot be obtained and one is content with using the power series expansion of the solution. The power series expansion is a possibility to represent an arbitrary function in the form of an infinite sum of power functions. The three main generalizations of power series expansion of a function such as Taylor series, Padé approximant and Gevrey series are discussed here. Such approximations give faithful representations of the function near the point of expansion. Some recent works on two-point or multi-point approximants can be found in [73].

#### 3.1.1 Taylor Series

Taylor expansion is a common engineering approach to estimate the structural response versus parameter variation:

$$f(p) = T_m(p) + R_m(p). \quad (3.1)$$

The coefficients of the Taylor series depend only on the derivatives of the function at the initial point  $p_0$ :

$$T_m(p) = \sum_{i=0}^m \frac{f^{(i)}(p_0)}{i!} (p - p_0)^i. \quad (3.2)$$

The Lagrange form of the remainder is given by

$$R_m(p) = \frac{f^{(m+1)}(\xi)}{(m+1)!} (p - p_0)^{m+1}, \text{ where } p_0 < \xi < p. \quad (3.3)$$

There is a possibility on the representation of function in generalized orthogonal polynomials, for example the Legendre, Chebyshev, Jacobi, Hermite or Laguerre polynomials. According

to the theorems of the approximation theory, the Chebyshev polynomials gives a best approximation to a continuous function over all possible.

The Taylor series is convergent in a neighborhood of  $p_0$ , if the function is analytic. In general, the Taylor series may not convergent to the original function  $f$ . Some functions with singularities on the real axis, with singularities in the complex plane or with branching point cannot be presented as Taylor series. When a pole in the Taylor expansion closes to the value of the parameters the convergence of the Taylor expansion can be slow even through a high derivation order (e.g. capacitance vs. gap between two electrodes, see Chapter 5 for details).

### 3.1.2 Padé Approximant

The  $[n/d]$  Padé approximant of a function  $f(p)$  is denoted as

$$R_{[n/d]}(p) = \frac{A_n(p)}{B_d(p)}, \quad (3.4)$$

where  $A_n(p)$  and  $B_d(p)$  are polynomials of degree  $n$  and  $d$ , respectively. For different values of  $n$  and  $d$  expression (3.4) form a table which called the table of Padé approximants [74, 75].

A Padé tries to extend the extrapolation domain over the poles. The zeros of denominator are the poles of the Taylor expansion. Using the rational function that includes the poles can make convergence faster than a polynomial approximation and it still work where the Taylor series does not converge.

Padé approximant can be compute from a Taylor expansion by means algebraic manipulation, i.e. a transformation the coefficient array in some way without choosing any particular argument. The  $b_0$  must be normalized to unity and the other coefficients  $\mathbf{a}$  and  $\mathbf{b}$  are then related by matching terms in (3.2) and (3.4):

$$c_0 + c_1x + c_2x^2 + \dots + c_mx^m = \frac{a_0 + a_1x + a_2x^2 + \dots + a_nx^n}{1 + b_1x + b_2x^2 + \dots + b_dx^d}, \quad n + d \leq m. \quad (3.5)$$

Firstly, the vector  $\mathbf{b}$  is computed by solving the linear system:

$$\begin{bmatrix} c_0 & c_1 & \dots & c_{d-1} \\ c_1 & c_2 & \dots & c_d \\ \dots & \dots & \dots & \dots \\ c_{d-1} & c_d & \dots & c_{2d-2} \end{bmatrix} \begin{bmatrix} b_d \\ b_{d-1} \\ \dots \\ b_1 \end{bmatrix} = \begin{bmatrix} c_d \\ c_{d+1} \\ \dots \\ c_{2d-1} \end{bmatrix}. \quad (3.6)$$

The vector  $\mathbf{a}$  is calculated by

$$\begin{aligned}
a_0 &= c_0 \\
a_{n+1} &= c_1 + b_1 c_0 \\
&\dots \\
a_{n-1} &= c_{n-1} + b_1 c_{n-2} + \dots + b_{n-1} c_0.
\end{aligned} \tag{3.7}$$

Although the entries in the Padé approximant can be always generated by solving the system of equations (3.6) and (3.7), that approach is computationally expensive. More efficient methods have been devised, including the epsilon algorithm [76].

It would be important for multiparametric analysis to construct a multivariate Pade approximation. During the few last decades much research has been done which try to apply the techniques developed for the univariate Padé approximants to the multivariate case and to find a generalization with good convergence properties [77, 78]. In contrast to the univariate case, the concept of degree is not clear and many choices are possible for developing the multivariate Padé approximants. The systematic developments on the subject are known as the Chisholm approximant (bivariate case) or Canterbury approximant (general multivariate case). For bivariate test functions, authors [79] find that the Levin-like transforms yield better approximants over a wide range of the two variables. However, as in the case of a function of one variable, the Padé approximants are better at reproducing the poles of the function. The multivariate representation can be consisting of a series of nested graphs. More details on how to build a Padé approximation from the derivatives of a function can be found in [78].

### 3.1.3 Gevrey Series

An interesting alternative to Padé approximation is suggested in [80]. In contrast to Padé which tries to extend the extrapolation domain over the poles, the basic idea is to use Gevrey series, which avoid the singularities. A *formal power series* with complex coefficients

$$f(z) = \sum_{m=0}^{\infty} a_m z^m \tag{3.8}$$

is the Gevrey of order  $s$ , if the associated series

$$f^{[s]}(z) = \sum_{m=0}^{\infty} \frac{a_m}{m!^s} z^m \tag{3.9}$$

has a non-zero radius of convergence, i.e. if  $\exists C > 0$  such that  $\forall m > 0, |a_m| < C^m \cdot m!^s$  [81]. Gevrey series of order  $s > 0$  are general divergent. For  $s < 0$ , Gevrey series define entire functions. Gevrey series are widely used for describing solutions of differential equations near singular points and, in particular, for representations of elementary and special functions near their singular points. Using Gevrey series avoid the singularities by the mean of a variable

change. The singularities are rejected out of the convergence domain. The approximation is calculated by a Laplace transform [82].

## 3.2 Parameterization of a Static Analysis

### 3.2.1 Linear Case

The solution of an overall linear static system depending on a parameter  $p$  is described by

$$\mathbf{u}(p) = \mathbf{K}(p)^{-1} \mathbf{F}(p). \quad (3.10)$$

The first derivative of the  $\mathbf{u}$  with respect to  $p$  is given by implicit differentiation of the (3.10)

$$\mathbf{u}(p)^{(1)} = \mathbf{K}(p)^{-1} (\mathbf{F}(p)^{(1)} - \mathbf{K}(p)^{(1)} \mathbf{u}(p)). \quad (3.11)$$

The first order derivatives are commonly used in structural optimization [1]. Haftka [83] pioneered in the application the second order derivatives. Consequently, the second derivative of the  $\mathbf{u}$  with regard to  $p$  is

$$\mathbf{u}(p)^{(2)} = \mathbf{K}(p)^{-1} (\mathbf{F}(p)^{(2)} - 2\mathbf{K}(p)^{(1)} \mathbf{u}(p)^{(1)} - \mathbf{K}(p)^{(2)} \mathbf{u}(p)). \quad (3.12)$$

Higher order derivatives can be computed from the recursive formula

$$\mathbf{u}(p)^{(n)} = \mathbf{K}(p)^{-1} \left( \mathbf{F}(p)^{(n)} - \sum_{i=1}^n C_n^i \mathbf{K}(p)^{(i)} \mathbf{u}(p)^{(n-i)} \right), \quad (3.13)$$

where  $C_n^i = \frac{n!}{i!(n-i)!}$  is the binomial coefficient.

Finally the Taylor series expansion of the unknown displacement vector becomes in terms of derivatives at the evaluation point  $p_0$

$$\mathbf{u}(p) = \mathbf{u}(p_0) + \sum_{i=1}^n \frac{\mathbf{u}(p_0)^{(i)}}{i!} (p - p_0)^i. \quad (3.14)$$

It is important to note that the Taylor series needs just the value of the function and its derivatives at a single point  $p_0$ . The entire approach requires one factorization of the matrix  $\mathbf{K}(p_0)$  and all other operations for computing of the displacement vector derivatives are time efficient matrix-vector products.

### 3.2.2 Non-linear Case

The possibility to apply the HODM to the static non-linear structural analysis is discussed here. In this case, the displacement  $\mathbf{u}$  is the solution of a non-linear equation:

$$\mathbf{R}(\mathbf{u}(p), p) = 0. \quad (3.15)$$

Only the differentiable non-linearity is considered. Using of the chain rule to differentiate implicitly defined functions, the first derivative of  $\mathbf{u}$  with respect to a structural parameter  $p$  is given by

$$\mathbf{u}(p)^{(1)} = -\frac{\partial \mathbf{R}}{\partial p} \bigg/ \frac{\partial \mathbf{R}}{\partial \mathbf{u}}, \quad (3.16)$$

where  $\frac{\partial \mathbf{R}}{\partial \mathbf{u}} \neq 0$  is the tangent matrix, Jacobian in the last iteration of Newton-Raphson's algorithm; the term  $\frac{\partial \mathbf{R}}{\partial p}$  is the partial derivative of the residual term with respect to the structural

parameter  $p$ . Writing  $\mathbf{J}^{(n)} = \frac{\partial^n}{\partial p^n} \left( \frac{\partial \mathbf{R}}{\partial \mathbf{u}} \right)$  is the Jacobian matrix derivatives, and  $\mathbf{R}^{(n)} = \frac{\partial^n \mathbf{R}}{\partial p^n}$  is the residual term derivatives, the second derivatives of  $\mathbf{u}$  can be obtained by continue the derivation process

$$\mathbf{u}(p)^{(2)} = -\mathbf{J}^{-1} \left( \mathbf{R}^{(2)} + \mathbf{J}^{(1)} \mathbf{u}(p)^{(1)} \right). \quad (3.17)$$

The computation of the second derivative of  $\mathbf{u}$  needs only the first derivative of Jacobian  $\mathbf{J}$ , which could be computed with the variation of  $p$  and the corresponding variation of  $\mathbf{u}$ . The right hand-side residual term  $\mathbf{R}$  is an explicit function of  $\mathbf{u}$  and  $p$ .

Higher order derivatives can be computed from the recursive formula

$$\mathbf{u}(p)^{(n)} = -\mathbf{J}^{-1} \left( \mathbf{R}^{(n-1)} + \sum_{i=1}^{n-1} C_{n-1}^i \mathbf{J}^{(i)} \mathbf{u}(p)^{(n-i)} \right). \quad (3.18)$$

The HODM applied to differentiable non-linear analysis has a high efficiency due to the fact that the cost needed to get all derivative displacement vectors is similar to the cost to get the derivatives of displacement vectors in linear case, and smaller than the cost to get the non-linear solutions of (3.15).

### 3.2.3 Secondary Results

In the structural based FE formulation, unknown displacements are computed in first. Derived results, like stresses or reaction forces are then obtained from nodal displacements. For example, elastic strain and stress are computed at element level by

$$\boldsymbol{\varepsilon} = \mathbf{B}\mathbf{u} \quad (3.19)$$

and

$$\boldsymbol{\sigma} = \mathbf{D}\boldsymbol{\varepsilon}. \quad (3.20)$$

Potential energy is obtained by

$$W = \frac{1}{2} \mathbf{u}^T \mathbf{K} \mathbf{u}. \quad (3.21)$$

Rewriting equation for linear analyses by separating out the matrix and vectors into those DOF with and without imposed values:

$$\begin{bmatrix} \mathbf{K}_{FF} & \mathbf{K}_{FS} \\ \mathbf{K}_{SF} & \mathbf{K}_{SS} \end{bmatrix} \begin{Bmatrix} \mathbf{u}_F \\ 0 \end{Bmatrix} = \begin{Bmatrix} \mathbf{F}_F \\ \mathbf{R}_S \end{Bmatrix}. \quad (3.22)$$

Reaction forces at suppressed DOF are obtained by

$$\mathbf{R}_S = \mathbf{K}_{FS}^T \mathbf{u}_F. \quad (3.23)$$

Naturally, the Taylor expansion of derived results is straightforwardly obtained by multiplication of the primary Taylor series of  $\mathbf{B}$ ,  $\mathbf{u}$ ,  $\mathbf{D}$  and  $\mathbf{K}$ . Automatic differentiation, which is numerically manipulating with the derivatives of  $\mathbf{B}$ ,  $\mathbf{u}$ ,  $\mathbf{D}$  and  $\mathbf{K}$ , is the another efficient way to compute Taylor series of secondary results, since the Taylor coefficients are simply scaled derivatives.

## 3.3 Parameterization of a Modal Analysis

The equation of motion for an undamped system, which using for natural frequency and mode shape determination, is

$$\begin{cases} (\mathbf{K} - \lambda_i \mathbf{M}) \phi_i = 0 \\ \phi_i^T \mathbf{M} \phi_i = 1 \end{cases}, \quad i = 1, \dots, n. \quad (3.24)$$

The first equation in (3.24) is singular, and to fully define system, one adds an additional mass normalization equation. The pair  $(\lambda_i, \phi_i)$  is the solution of (3.24), where  $\lambda_i = \omega_i^2$  is an eigenvalue and  $\phi_i$  is a corresponding non-zero eigenvector of mode  $i$ . The eigenfrequencies



and mode shapes of the systems are completely identified dynamic responses of the mechanical systems. Variations in parameters lead to changes in dynamic responses of the system. Using the eigenpair derivatives in large systems can reduce the cost of reanalyzes. The derivatives of the mode shapes with respect to design parameters are particularly useful for approximating a new mode shape due to a variation in a design parameter, estimated the influence of design changes on the dynamic behavior of systems [84-89].

Consider non-repeated eigenvalue  $i$ , the first derivative of the system (3.24) with respect to the design parameter  $p$  writes:

$$\begin{cases} \mathbf{K}\phi_i^{(1)} - \lambda_i \mathbf{M}\phi_i^{(1)} - \lambda_i^{(1)} \mathbf{M}\phi_i = -\mathbf{K}^{(1)}\phi_i + \lambda_i \mathbf{M}^{(1)}\phi_i \\ 2\phi_i^T \mathbf{M}\phi_i^{(1)} = -\phi_i^T \mathbf{M}^{(1)}\phi_i \end{cases} \quad (3.25)$$

Pre-multiplying the first equation in (3.25) by  $\phi_i^T$  leads to

$$-\lambda_i^{(1)} \phi_i^T \mathbf{M}\phi_i = -\phi_i^T (\mathbf{K}^{(1)} - \lambda_i \mathbf{M}^{(1)})\phi_i. \quad (3.26)$$

Finally, the first derivative of eigenvalue  $\lambda_i^{(1)}$  is obtained by

$$\lambda_i^{(1)} = \phi_i^T \mathbf{K}^{(1)}\phi_i - \lambda_i \phi_i^T \mathbf{M}^{(1)}\phi_i. \quad (3.27)$$

Then the mode shape derivative  $\phi_i^{(1)}$  is obtained by solving

$$(\mathbf{K} - \lambda_i \mathbf{M})\phi_i^{(1)} = -\lambda_i^{(1)} \mathbf{M}\phi_i - (\mathbf{K}^{(1)} - \lambda_i \mathbf{M}^{(1)})\phi_i. \quad (3.28)$$

The eigenvector sensitivity  $\phi_i^{(1)}$  cannot be calculated directly from (3.28), because the matrix  $(\mathbf{K} - \lambda_i \mathbf{M})$  is singular. Nelson presented an algorithm for computing the eigenvector derivatives of general real matrices with non-repeated eigenvalues and requires knowledge of only those eigenvectors that are to be differentiated [90]. He proposed that the  $i$ -eigenvector derivative can be written as

$$\phi_i^{(1)} = \mathbf{v}_i + c_i \phi_i. \quad (3.29)$$

Unknown vector  $\mathbf{v}_i$  is calculated from

$$(\mathbf{K} - \lambda_i \mathbf{M})\mathbf{v}_i = \mathbf{F}_i, \quad (3.30)$$

with  $\mathbf{F}_i = -(\mathbf{K}^{(1)} - \lambda_i^{(1)} \mathbf{M} - \lambda_i \mathbf{M}^{(1)})\phi_i$ . The  $k^{\text{th}}$  component of  $\mathbf{v}_i$  must be set to zero, where  $k$  is the location at which the eigenvector  $\phi_i$  has the maximum absolute value. Scalar constant  $c_i$  is determined by differentiating the mass normalization condition in (3.24):

$$c_i = -0.5 \phi_i^T \mathbf{M}^{(1)}\phi_i - \phi_i^T \mathbf{M}\mathbf{v}_i. \quad (3.31)$$

However, this latter value can be obtained with

$$2\phi_i^T \mathbf{M} \phi_i^{(1)} = -\phi_i^T \mathbf{M}^{(1)} \phi_i. \quad (3.32)$$

Higher order eigenvalue and eigenvector sensitivities for non-repeated eigenvalues can be calculated by extending this method and provides iterative computation for  $n^{\text{th}}$  order sensitivities. The  $n^{\text{th}}$  order derivatives are expressed by

$$\begin{cases} \left( \mathbf{K} \phi_i^{(1)} \right)^{(n)} - \left( \lambda_i \mathbf{M} \phi_i^{(1)} \right)^{(n)} - \left( \lambda_i^{(1)} \mathbf{M} \phi_i \right)^{(n)} = - \left( \mathbf{K}^{(1)} \phi_i \right)^{(n)} + \left( \lambda_i \mathbf{M}^{(1)} \phi_i \right)^{(n)} \\ 2\left( \phi_i^T \mathbf{M} \phi_i^{(1)} \right)^{(n)} = - \left( \phi_i^T \mathbf{M}^{(1)} \phi_i \right)^{(n)} \end{cases}, n \geq 0. \quad (3.33)$$

The system (3.33) can be rewritten in the form [38]

$$\begin{cases} (n+1) \mathbf{K} \phi_i^{(n+1)} - (n+1) \lambda_i \mathbf{M} \phi_i^{(n+1)} - (n+1) \lambda_i^{(n+1)} \mathbf{M} \phi_i = \mathbf{S}_\phi^{(n)} \\ (n+1) \phi_i^T \mathbf{M} \phi_i^{(n+1)} = \mathbf{S}_\lambda^{(n)} \end{cases}, \quad (3.34)$$

where  $\mathbf{S}_\phi^{(n)}$  and  $\mathbf{S}_\lambda^{(n)}$  are right terms depending on the previous derivative order.

Multiple eigenfrequencies are expected for the symmetric structure. Difficulties are arising when the matrix is close with repeated eigenvalues. A treatment of the repeated eigenvalues can be found in [1].

### 3.4 Parameterization of a Harmonic Analysis

The steady-state response of a linear system to sinusoidally varied loads at the frequency  $f$  is determined by

$$\mathbf{u}(f, p) = \left( \mathbf{K}(p) + j(2\pi f) \mathbf{C}(p) - (2\pi f)^2 \mathbf{M}(p) \right)^{-1} \mathbf{F}(f, p), \quad (3.35)$$

or

$$\mathbf{u}(f, p) = \left( \mathbf{A}(f, p) \right)^{-1} \mathbf{F}(f, p). \quad (3.36)$$

The matrix of linear system is denoted  $\mathbf{A}(f, p) = \mathbf{K}(p) + j(2\pi f) \mathbf{C}(p) - (2\pi f)^2 \mathbf{M}(p)$ .

Concerning the harmonic analysis, there are three cases, as illustrated in Figure 3.1:

- standard frequency sweep
- parameter sweep at  $f_0$
- parametric frequency sweep

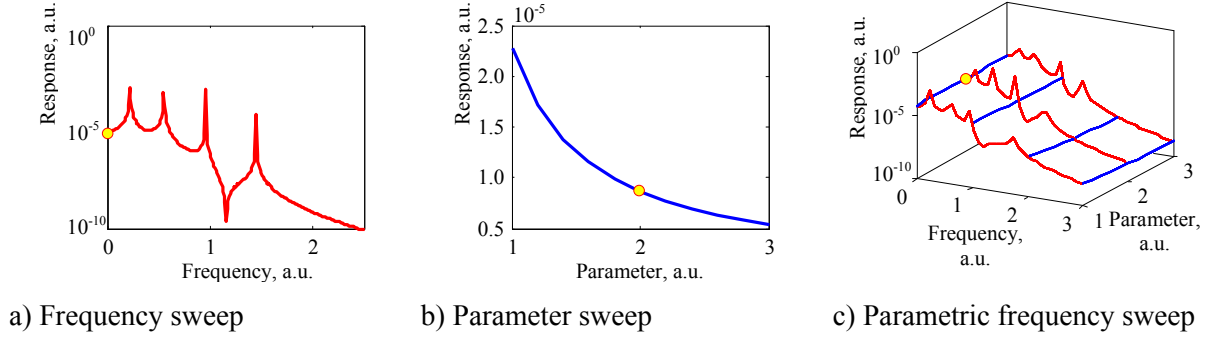


Figure 3.1 Parametric harmonic response

### 3.4.1 Frequency Sweep

In order to solve a standard frequency sweep, a linear system needs to be solved for each frequency  $f_i$ . The cost of frequency response procedure increases significantly with the mesh density and the complexity of the problem. When frequency response must be obtained for large frequency intervals, the computational cost becomes so high that the calculation cannot realistically be made for an industrial problem. It is thereby possible to solve Equation (3.35) for additional load cases, i.e. several right hand sides, without much additional computational effort. An alternative to this frequency sweep procedure is to approximate the frequency response function by a Padé approximant based on high order derivatives. Like linear problem, the Taylor expansion of the response  $\mathbf{u}$  with regard to  $f$  at  $p_0$  is given by the Taylor expansion of  $\mathbf{A}$ :

$$\mathbf{u}(p_0, f)^{(n)} = \mathbf{A}(p_0, f)^{-1} \left( \mathbf{F}(p_0, f)^{(n)} - \sum_{i=1}^n C_n^i \mathbf{A}(p_0, f)^{(i)} \mathbf{u}(p_0, f)^{(n-i)} \right). \quad (3.37)$$

Neglecting frequency dependent viscous damping, the derivatives of  $\mathbf{A}$  matrix with regard to frequency are given by

$$\begin{aligned} \mathbf{A}(p_0, f)^{(1)} &= 8\pi^2 \mathbf{M}(p_0) f, \\ \mathbf{A}(p_0, f)^{(2)} &= 8\pi^2 \mathbf{M}(p_0), \\ \mathbf{A}(p_0, f)^{(3)} &= 0. \end{aligned} \quad (3.38)$$

The second derivative of  $\mathbf{A}$  is constant and the higher order ones are zeros. Notice however that zeros higher order derivative of  $\mathbf{A}$  do not implies zeros higher order derivative of  $\mathbf{u}$  in (3.37).

Proposed algorithm is a different version of the asymptotic waveform evaluation method [91] to approximate the solution by explicitly calculating the truncated Taylor series and the converting the new transfer function to an ODE system. Usually, the procedure of calculating the

model from the transfer function is limited to about eight poles due to round-off errors. Note that this approximates the transfer function only locally around the expansion point of the series; however, multiple expansion points can be used and the subspace generated as the union of the individual subspaces [73].

### 3.4.2 Parameter Sweep

The computation of the harmonic response at the frequency  $f_0$  with respect to the design parameter  $p$  will be based on the derivation of the  $A(p, f_0)$  with regard to the  $p$ .

### 3.4.3 Parametric Frequency Sweep

As the coefficients of the matrix  $A$  depend on the frequency and design parameters, it must be calculated and factorized for each frequency of interest. The parameterization is provided by the crossed high order derivatives with an order  $n$  for frequency and an order  $m$  for parameter:

$$\begin{aligned} \mathbf{u}(p, f)^{(n)(m)} &= \mathbf{A}(p, f)^{-1} \times \\ &\times \left( -n \sum_{j=0}^m C_m^j \mathbf{A}(p, f)^{(1)(j)} \mathbf{u}(p, f)^{(n-1)(m-j)} - n \sum_{j=1}^m \mathbf{A}(p, f)^{(0)(j)} \mathbf{u}(p, f)^{(n)(m-j)} \right). \end{aligned} \quad (3.39)$$

## 3.5 Parameterization of a Transient Analysis

### 3.5.1 Full Method

A discussion on the transient problem solution is provided before going into the details of the parameterization of transient analysis. The basic equation of motion solved by a transient analysis in the time domain is

$$\mathbf{M} \mathbf{a}(t) + \mathbf{C} \mathbf{v}(t) + \mathbf{K} \mathbf{u}(t) = \mathbf{F}(t), \quad (3.40)$$

where  $\mathbf{a}(t)$  is the nodal acceleration vector,  $\mathbf{v}(t)$  is the nodal velocity vector.

These equations can be thought of as a set equilibrium equations that also take into account inertia forces  $\mathbf{M}(p)\mathbf{a}(t)$  and damping forces  $\mathbf{C}(p)\mathbf{v}(t)$ . The response at the current time is calculated using the time integration method with the following initial conditions:  $\mathbf{v}(0) = \mathbf{v}_0$  and  $\mathbf{u}(0) = \mathbf{u}_0$ . The Newmark family of time integration methods is discussed here. The velocity and displacement at time  $t_{n+1}$  can be integrated by

$$\begin{aligned} \mathbf{v}_{n+1} &= \mathbf{v}_{pr} + \gamma \Delta t \mathbf{a}_{n+1}, \\ \mathbf{u}_{n+1} &= \mathbf{u}_{pr} + \beta \Delta t^2 \mathbf{a}_{n+1}, \end{aligned} \quad (3.41)$$

where  $\mathbf{v}_{pr} = \mathbf{v}_n + (1 - \gamma)\Delta t \mathbf{a}_n$  and  $\mathbf{u}_{pr} = \mathbf{u}_n + \Delta \mathbf{v}_n + (1/2 - \beta)\Delta t^2 \mathbf{a}_n$  are the velocity and displacement vector predictors,  $\beta$  and  $\gamma$  are the integration parameters.

Then, Equation (3.40) can be expressed in terms of acceleration vector at time  $t_{n+1}$ , as

$$(\mathbf{M} + \gamma\Delta t \mathbf{C} + \beta\Delta t^2 \mathbf{K})\mathbf{a}_{n+1} = \mathbf{F}_{n+1} - \mathbf{K}\mathbf{u}_{pr} - \mathbf{C}\mathbf{v}_{pr}. \quad (3.42)$$

After solution (3.42), the velocity and displacement vector are again corrected.

The explicit integration method corresponds to the case in which  $\beta = 0$  and  $\gamma = 1/2$  with diagonal matrices of  $\mathbf{K}$  and  $\mathbf{C}$ .

Now, HODM can be extending to the time domain analysis. By assuming the time interval is independent of design parameter, differentiation of (3.40) yields the following equation:

$$(\mathbf{M} + \gamma\Delta t \mathbf{C} + \beta\Delta t^2 \mathbf{K})\mathbf{a}_{n+1}^{(1)} = \mathbf{F}_{n+1}^{(1)} - \mathbf{K}\mathbf{u}_{pr}^{(1)} - \mathbf{K}^{(1)}\mathbf{u}_{n+1} - \mathbf{C}\mathbf{v}_{pr}^{(1)} - \mathbf{C}^{(1)}\mathbf{v}_{n+1} - \mathbf{M}^{(1)}\mathbf{a}_{n+1}. \quad (3.43)$$

The derivatives of displacement and velocity are updated in a manner similar to (3.41), after solving for the acceleration derivative. In addition to the derivatives of stiffness and mass matrices, Equation (3.40) requires the derivative of displacement at the previous time step, which makes the sensitivity equation history dependent. The factored coefficient matrix from the response analysis can be reused in solving the sensitivity equation efficiently. In the explicit method, the sensitivity analysis becomes more expensive because calculating the right-hand side of (3.43) is more computationally expensive than that of (3.42) and the sensitivity analysis cannot take advantage of the factored coefficient matrix from the response analysis.

### 3.5.2 Modal Superposition Method

Linear structural dynamics may be effective solve using a modal superposition method [43]. One needs to start a parametric modal analysis in order to obtain the eigenfrequencies and the eigenshapes as explicit functions of the parameters  $p$ . After selection the parametric modal basis  $\Phi_m$ , one can to build the reduced matrices  $\tilde{\mathbf{K}}$  and  $\tilde{\mathbf{M}}$  with

$$\tilde{\mathbf{K}}(p) = \Phi_m^T(p) \mathbf{K}(p) \Phi_m(p) = \omega_m^2(p) \quad (3.44)$$

and

$$\tilde{\mathbf{M}}(p) = \Phi_m^T(p) \mathbf{M}(p) \Phi_m(p) = \mathbf{I}. \quad (3.45)$$

The damping matrix  $\tilde{\mathbf{C}}$  is defined by a linear combination of  $\tilde{\mathbf{K}}$  and  $\tilde{\mathbf{M}}$  [43]. When the natural modes are used as basis vectors the reduced mass and stiffness matrices are diagonal, and the reduced damping matrix can also be diagonal for proportional damping. This allows un-

coupled solution of the reduced equations of motion. The reduced forces vector is defined as  $\tilde{\mathbf{F}}(t, p) = \Phi_m^T(p) \mathbf{F}(t, p)$ . The modal displacement vector is written as  $\mathbf{q}(t, p) = \Phi_m^T(p) \mathbf{u}(t, p)$ .

The design parameters-time domain equations of motion are then reduced to

$$\tilde{\mathbf{M}}(p) \ddot{\mathbf{q}}(t, p) + \tilde{\mathbf{C}}(p) \dot{\mathbf{q}}(t, p) + \tilde{\mathbf{K}}(p) \mathbf{q}(t, p) = \tilde{\mathbf{F}}(t, p). \quad (3.46)$$

The differentiation of (3.46) can proceed as for the original full equations (3.40). On the other hand, the reduced system (3.46) can be also solved directly for each set  $p$ , because the modal reduction has greatly lower the computational cost of the time domain analysis.

## 3.6 Examples

It is interesting to consider how the HODM work for a simple lumped system. The purpose of this subsection is to use two simple examples to explain the basics of how derivatives of matrices are formulated and how different parametric analyses are performed.

### 3.6.1 Duffing Oscillator

The Duffing oscillator, which is an odd nonlinearity system, is chosen as an application example to illustrate the HODM approach, Figure 3.2a. The static non-linear equilibration equation of a Duffing oscillator is

$$(\alpha u^2 + \beta)u = F, \quad (3.47)$$

where  $\alpha$  and  $\beta$  are the nonlinear and linear spring parameters respectively.

Computer Algebra Systems software such as MathCAD or MATLAB Symbolic Toolbox [92] can be used to solving (3.47) in analytical form. The displacement of this oscillator under load  $F$  is expressed as

$$u(\alpha, \beta) = \gamma - \frac{\beta}{3\alpha} \gamma^{-1}, \text{ where } \gamma = \sqrt[3]{\frac{F}{2\alpha} + \sqrt{\left(\frac{F}{2\alpha}\right)^2 + \left(\frac{\beta}{3\alpha}\right)^3}}. \quad (3.48)$$

This solution is valid for hardening case  $\alpha > 0$ . The nonlinearity  $\alpha$  is selected as design parameter. Other parameters are given as:  $\beta = 1, F = 1$ .

From Equation (3.18) follows that  $u^{(n)}(p) = f(u^{(1)}, \dots, u^{(n-1)}, R, \dots, R^{(n-1)}, J, \dots, J^{(n)}, J^{-1})$ . Consider the precomputed derivatives of residual force vector and Jacobian:

$$\begin{aligned}
R(u) &= (\alpha u^2 + \beta)u - F, & J(u) &= 3\alpha u^2 + \beta, \\
R^{(1)}(u) &= u^3, & J^{(1)}(u) &= 3u^2 + 6\alpha u u^{(1)}, \\
R^{(2)}(u) &= 3u^2 u^{(1)}, & J^{(2)}(u) &= 12uu^{(1)} + 6\alpha u(u^{(1)})^2 + 6\alpha u u^{(2)}, \\
R^{(3)}(u) &= 6u(u^{(1)})^2 + 3u^2 u^{(2)}, & J^{(3)}(u) &= 18(u^{(1)})^2 + 18\alpha u^{(1)}u^{(2)} + 18uu^{(2)} + 6\alpha u u^{(3)}.
\end{aligned} \tag{3.49}$$

After that, the derivatives of displacements can be assembled from the (3.18). It should be noted that the analytical derivatives of (3.48) are more complicated than the function itself. The results of the parametric study are presented in Figure 3.2.

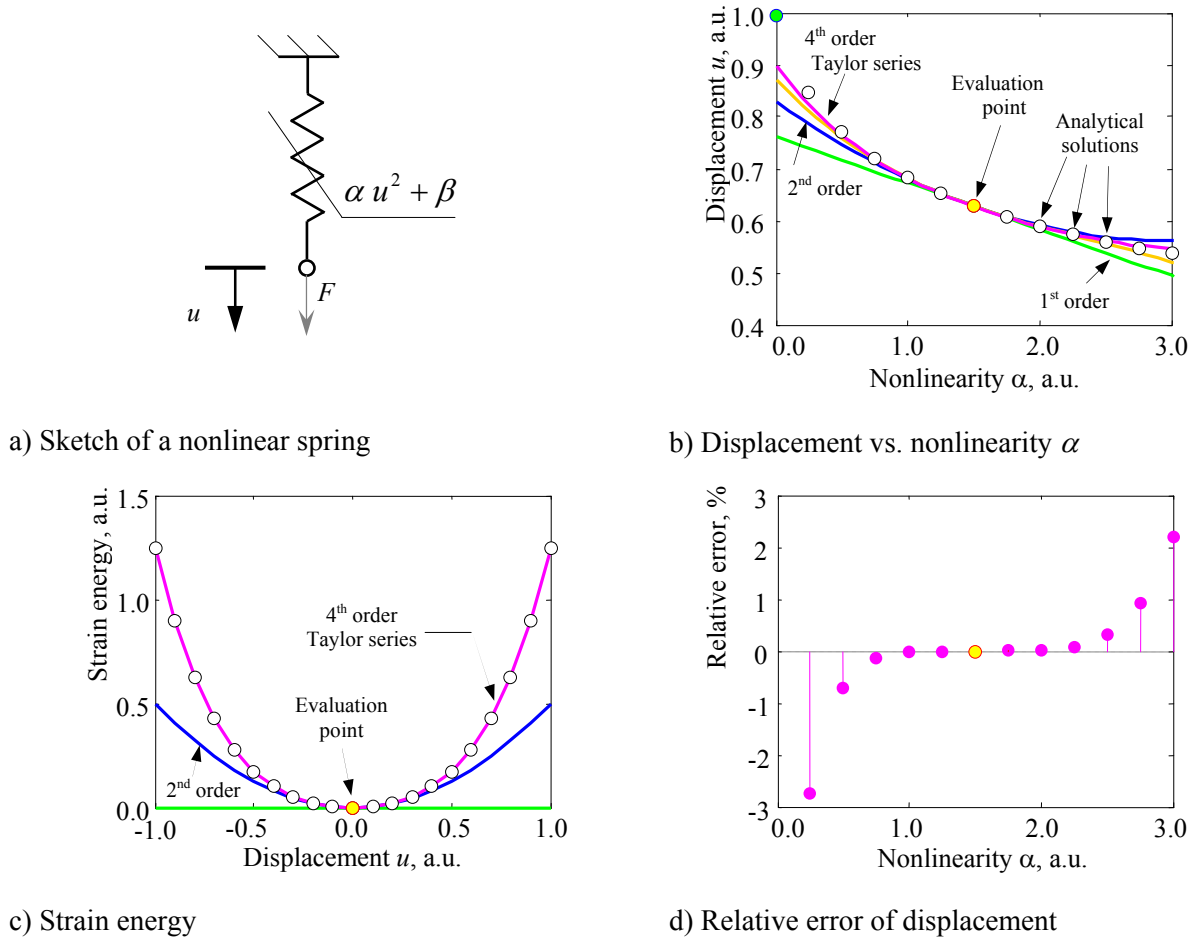


Figure 3.2 Static behavior of a Duffing oscillator

The displacement is closely approximated by its Taylor polynomial of degree 4 (magenta curve) for an interval  $\alpha \in [0 \dots 3]$ . So in this case ( $\alpha_0 = 1.5$ ,  $m = 4$ ), the remainder (3.3) is given by

$$R_4(\alpha_0) = \frac{1}{5!} f^{(5)}(\xi)(3 - \alpha_0)^5. \tag{3.50}$$

Since  $\alpha_0 < \xi < \alpha$ , or  $1.5 < \xi < 3.0$ , the error is bound between:  $-0.0205 < R_4(1.5) < -0.0008$ . The absolute relative error on the interval  $[0.3 \dots 3]$  is no more than 2.2%.

The Taylor series has infinite terms and only in special cases such as a finite polynomial does it have a finite number of terms. In the case of linear systems, the strain energy can be described by a polynomial of order two since the stiffness is constant. In a nonlinear case, the strain energy is exactly captured by polynomials of order four, Figure 3.2c.

### 3.6.2 Mass-Spring System

The mass-spring systems are wide used for describe the mechanical systems by lumped elements. To illustrate the results of the HODM analysis, consider a 2-DOF mass-spring system (e.g. cascaded micromirror, folded flexure resonator, housing to hold the PCB) with a rigid body mode and no damping. The mass and stiffness matrices for this system are, respectively:

$$\mathbf{M} = \begin{bmatrix} m_1 & 0 \\ 0 & m_2 \end{bmatrix} \text{ and } \mathbf{K} = \begin{bmatrix} k_1 + k_2 & -k_2 \\ -k_2 & k_2 \end{bmatrix}. \quad (3.51)$$

The components of the mass matrix  $\mathbf{M}$  of the system are

$$m_1 = 15\text{mg} \text{ and } m_2 = 15\text{mg}. \quad (3.52)$$

The components of the stiffness matrix  $\mathbf{K}$  are given as

$$k_1 = 20\text{kN/m} \text{ and } k_2 = 60\text{kN/m}. \quad (3.53)$$

#### Modal analysis

Solving the eigenproblems for the (3.51), the eigenvalues and eigenvectors of a 2-DOF mass-spring system are given as

$$\begin{aligned} \lambda_{1,2} &= \frac{\beta \mp \sqrt{\beta^2 - 4\alpha}}{2}, \text{ where } \beta = \frac{k_1}{m_1} + \frac{k_2}{m_1} + \frac{k_2}{m_2} \text{ and } \alpha = \frac{k_1 k_2}{m_1 m_2}, \\ \phi_{1,1} &= \sqrt{\frac{(k_2 - m_2 \lambda_1)^2}{m_1 (k_2 - m_2 \lambda_1)^2 + k_2^2 m_2}}, \quad \phi_{1,2} = \frac{k_1 + k_2 - m_1 \lambda_1}{k_2} \phi_{1,1}, \\ \phi_{2,1} &= \sqrt{\frac{(k_2 - m_2 \lambda_2)^2}{m_1 (k_2 - m_2 \lambda_2)^2 + k_2^2 m_2}}, \quad \phi_{2,2} = \frac{k_1 + k_2 - m_1 \lambda_2}{k_2} \phi_{2,1}. \end{aligned} \quad (3.54)$$

The results were obtained by use of a symbolic algebra program. First the eigenproblem of Equations (3.54) is solved for (3.52) and (3.54) to yield the eigenvalues and the mass-normalized eigenvectors:

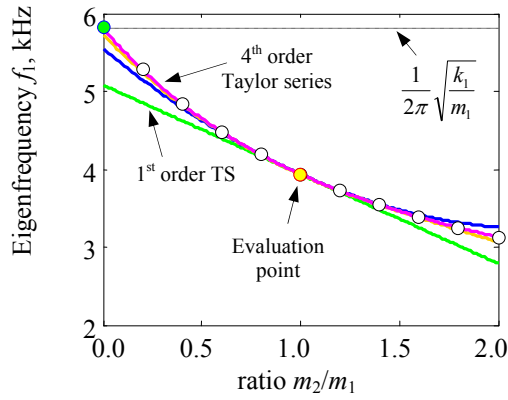
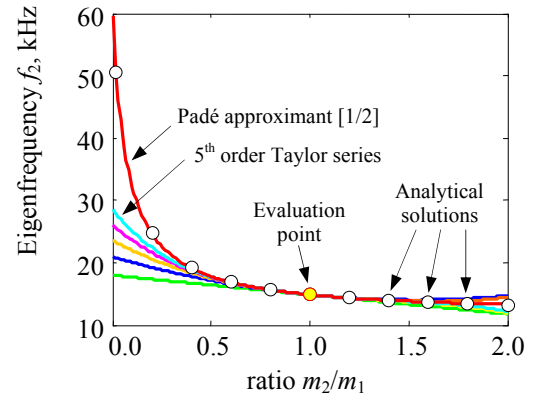
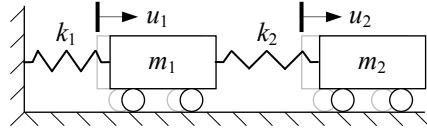


$$\lambda_1 = 0.61 \times 10^9, \phi_1 = \begin{Bmatrix} 166.89 \\ 197.01 \end{Bmatrix},$$

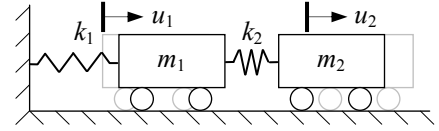
$$\lambda_2 = 8.72 \times 10^9, \phi_2 = \begin{Bmatrix} 197.01 \\ -166.89 \end{Bmatrix}. \quad (3.55)$$

Two eigenmodes are observed, one in which the two springs on either side are in phase (symmetric) and the other mode in which the two springs are out-of-phase (anti-symmetric).

The design parameter selected in this example is  $p = m_2/m_1$ , which is a mass ratio of the system. Fixing the parameter  $m_1$ , the second mass is  $m_2 = pm_1$ .

a) Mode 1 eigenfrequency vs. ratio  $p$ b) Mode 2 eigenfrequency vs. ratio  $p$ 

c) Mode 1 shape plot



d) Mode 2 shape plot

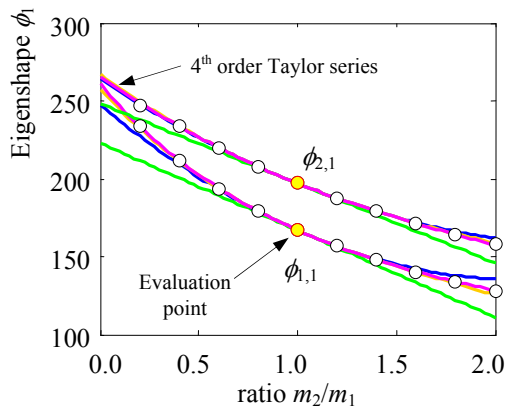
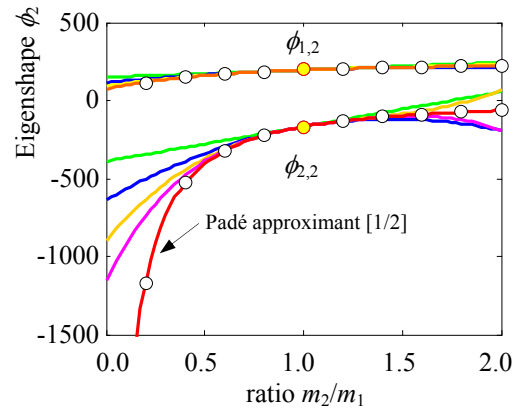
e) Mode 1 eigenshape vs. ratio  $p$ f) Mode 2 eigenshape vs. ratio  $p$ 

Figure 3.3 Parametric modal analysis of a 2-DOF spring mass system

The parametric technique was applied in order to extract the eigenvalues and the mass-normalized eigenvectors due to a perturbation in a design parameter. The variations of exact eigenfrequencies and eigenvectors are plotted in Figure 3.3.

To prepare for building the derivatives of the eigenvalues and eigenvectors, the derivatives of mass and stiffness matrices for this system are expressed:

$$M(p)^{(1)} = \begin{bmatrix} 0 & 0 \\ 0 & m_1 \end{bmatrix} \text{ and } M(p)^{(2)} = \begin{bmatrix} 0 & 0 \\ 0 & 0 \end{bmatrix},$$

$$K(p)^{(n)} = \begin{bmatrix} 0 & 0 \\ 0 & 0 \end{bmatrix}.$$
(3.56)

Considering the difference between the exact value and the Taylor expansion, the errors of the approximated eigenvalue  $\lambda_1$  computed by using derivatives of the eigenvalue given by the proposed HOD method are relatively quite small, Figure 3.3a. A typical example, using the rational function that includes the poles, is illustrated in Figure 3.3b. Obviously eigenvalue  $\lambda_2$  tends to infinity as  $m_2 \rightarrow 0$ , the limit of this system is  $\lim_{m_2 \rightarrow +0} \lambda_2 = +\infty$ . The use of a Padé approximant makes it possible to compute an accurate approximation of  $f_2(m_2/m_1)$  even at values of frequency for which the Taylor series of  $f_2(m_2/m_1)$  diverges.

### Harmonic analysis

The spring mass system is also studied in the frequency domain by sweeping frequencies. The closed form solution of the harmonic problem, representing the steady state response of the undamped system to a sinusoidal input, is given as

$$u_1(\omega) = \frac{F_1(k_2 - m_2\omega^2) + F_2k_2}{k_1k_2 - (k_1m_2 + k_2m_1 + k_2m_2)\omega^2 + m_1m_2\omega^4},$$

$$u_2(\omega) = \frac{F_2(k_1 - m_1\omega^2 + k_2) + F_1k_2}{k_1k_2 - (k_1m_2 + k_2m_1 + k_2m_2)\omega^2 + m_1m_2\omega^4}.$$
(3.57)

The load vector for this problem is  $\mathbf{F} = \{0 \ 1\}^T$ . The harmonic response of a 2-DOF mass-spring system is presented in Figure 3.4. It can be easily seen that the Padé method will provide an exact solution of this problem, whereas a Taylor series solution will require an infinite order to converge. Note that all the expressions (3.57) have the same denominator. The roots of a denominator are the eigenfrequencies and Padé correctly evaluated the response at these frequencies. The convergence radius of the Padé approximation is limited to the distance between the initial frequency and the first pole not included in denominator. Poles show the frequencies where the system will amplify inputs. Unlike the poles, which are a characteristic of the system and depend only on the distribution of mass and stiffness, zeros can be different and some transfer functions may have no zeros. The zeros are defined by the roots of its numerator. Zeros show the frequencies where the system will attenuate inputs. Comparison of exact solutions and Padé approximant shows excellent numerical agreement.

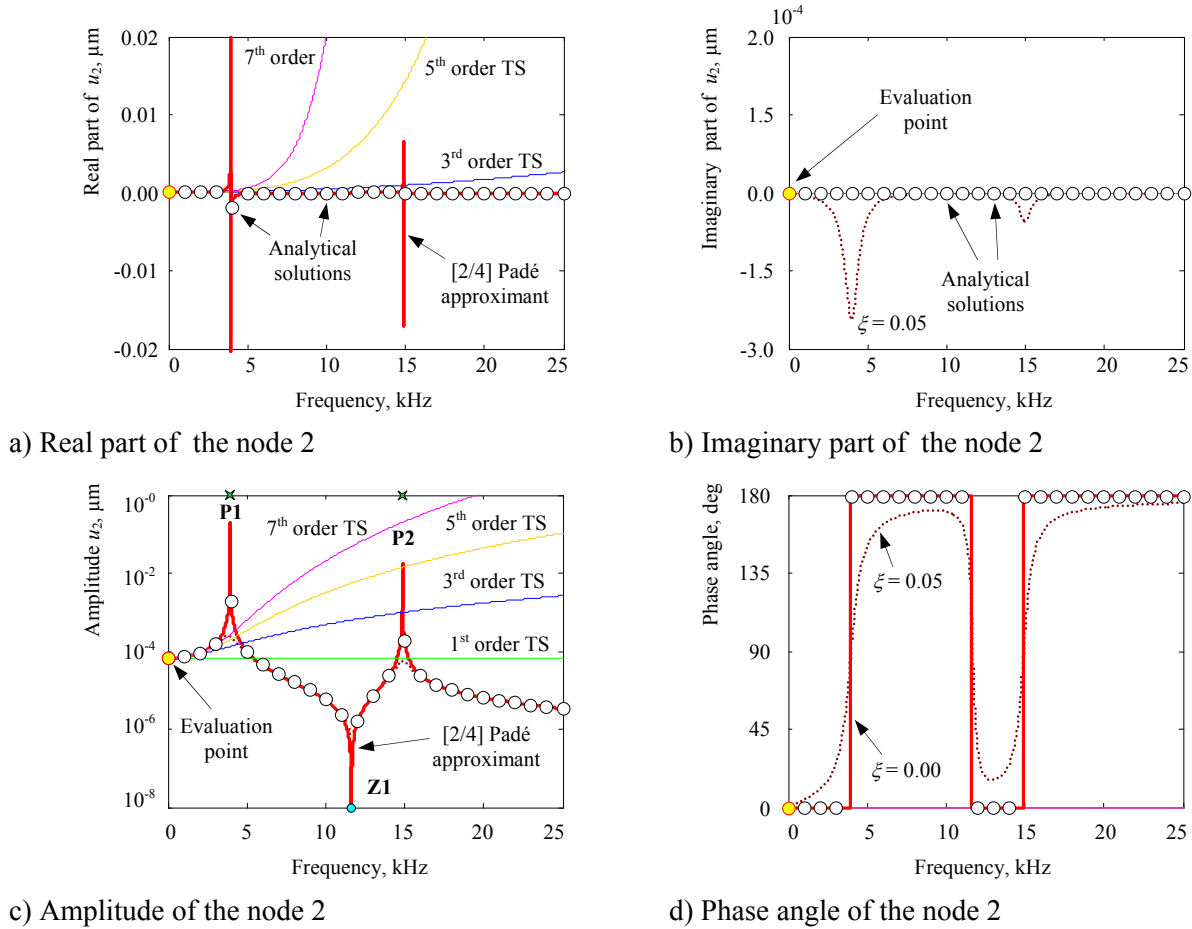


Figure 3.4 Frequency sweep response of a 2-DOF spring mass system

It is necessary to remember that polynomial of high degrees are extremely unstable and can inadequately describe the goal function. In presented examples, Taylor polynomial up to 5<sup>th</sup> degree was used in static and modal analyses. This order is quite enough for many applications. Thus, these HOD techniques can be considered reliably in obtaining parametric solutions of the system in static, modal and harmonic analyses. The proposed method will be applied to FE analysis in the next Chapter 4.



## 4. Implementation of HODM in FEA

In this chapter the implementation issues of the HODM in FEA are presented. The parametric FE-technique has been prototyped in MATLAB, because this is a good prototyping tool for quickly development and test of numerical algorithms. For solid modeling and mesh generation the commercial software can be used. A brief introduction to automatic differentiation is given. The implemented algorithms support static, modal and harmonic analyses of structural, electrostatic, thermal and fluidic domains. It is necessary to point out the need for additional system memory, for parametric mesh-morphing procedures and for having access to the source code. HOD algorithms capabilities are restricted to MATLAB performance and Windows memory management on 32 bit x86 systems.

### 4.1 Global Architecture

The overall schematic of parametric FE technique is flowcharted in Figure 4.1. The software concept of the parametric FE-tool consists of forth main blocks. The preprocessing includes three substeps: parametric solid modeling and mesh-morphing what captures the influence of geometric design variables on a FE-mesh. Initial solid modeling and mesh generation can be realized within external tool. The second step is a FE-model importation into the parametric environment. Most CAD tools support this feature (e.g. NWRITE, EWRITE commands in ANSYS).

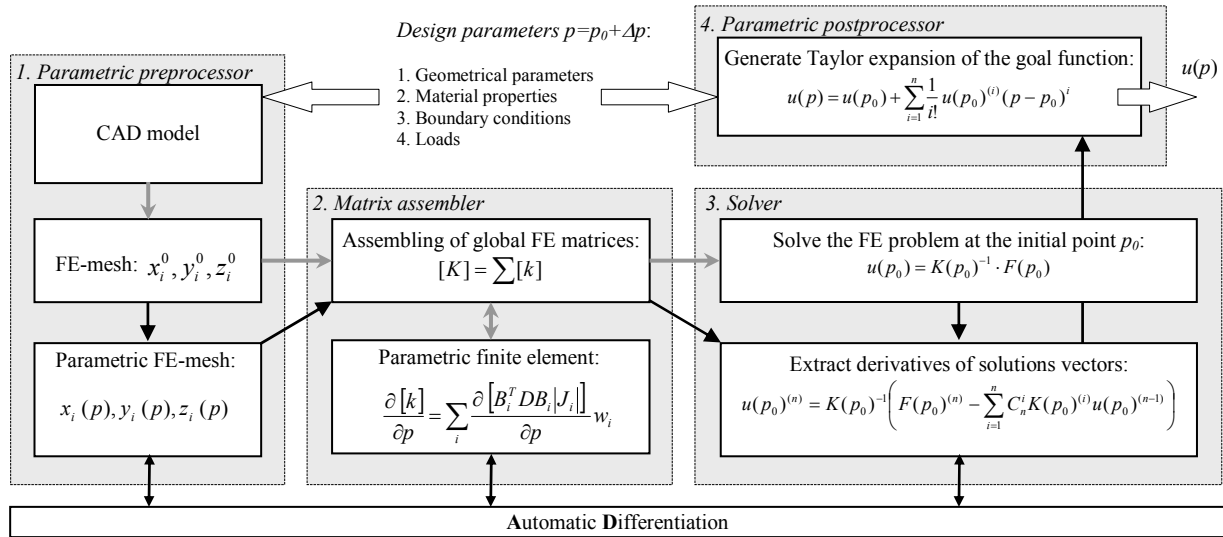


Figure 4.1 Block scheme of parametric FE technique

Parametric FE-mesh means that the nodal table does not only contain a single value for each spatial direction, rather each coordinate will be described by a polynomial with regard to global parameter. Especially geometrical parameter must carefully be mapped to the nodal table since local distortions affect the accuracy of the mesh discretization. A convenient way

to transform global parameter to polynomial nodal coordinates is a Laplacian smoothing algorithm known from mesh-morphing of FEM [93].

The whole idea of the HOD approach is to compute not only the governing system matrix but also HOD with regard to design parameters. The system FE matrix  $\mathbf{K}$  is obtained from a superposition of the elementary matrices  $\mathbf{k}$ . Therefore, calculations of the derivatives of the system matrix need to be coupled with the assembling procedures. The derivatives can be calculated by the techniques including symbolic differentiation, divided difference, and automatic differentiation. Difficulties arose from the fact that extraction of high order partial derivatives becomes numerically unstable and time consuming. In contrast to the symbolic differentiation, which propagates mathematical functions, AD algorithms operate on the numerical values. Efficiency of AD relies on the fact that every function is nothing else than a sequence of arithmetic operations and elementary functions. Remarkable is that AD gives an exact (up to the machine precision) representation of high order derivatives. AD technique utilizes the generalized differentiation rules, which give the exact representation of derivatives combining derivatives of the arguments with binomial coefficients [94].

Taylor expansion of the FE solution can be obtained by differentiation corresponding FE problem (static, modal, harmonic or transient) as described in Chapter 3. Direct methods are more expensive for factorization of large matrix  $\mathbf{K}(p_0)$  in (3.10). For linear static analysis the expression (3.10) can be rewritten as a system of linear equations in the following form:

$$\left\{ \begin{array}{l} \mathbf{K}(p_0)\mathbf{u}(p_0)^{(1)} = \mathbf{F}(p_0)^{(1)} - \mathbf{K}(p_0)^{(1)}\mathbf{u}(p_0) \\ \dots \\ \mathbf{K}(p_0)\mathbf{u}(p_0)^{(n)} = \mathbf{F}(p_0)^{(n)} - \sum_{i=1}^n C_n^i \mathbf{K}(p_0)^{(i)}\mathbf{u}(p_0)^{(n-i)} \end{array} \right., \quad (4.1)$$

where  $\mathbf{F}(p_0)^{(n)} - \sum_{i=1}^n C_n^i \mathbf{K}(p_0)^{(i)}\mathbf{u}(p_0)^{(n-i)}$  is the pseudo load vector.

All linear systems (4.1) have the same matrix  $\mathbf{K}(p_0)$  but different right hand vectors. Such form avoid direct computation of the inverse matrix  $\mathbf{K}(p_0)$ , but require the  $n$  solution of the linear system in order to obtain  $\mathbf{u}(p_0)^{(n)}$ . Iterative methods are superior for a single solution, both in terms of storage requirements and computational efficiency. But derivatives computations are need just one factorization of matrix  $\mathbf{K}$  at  $p_0$ , and then all operations only cost a forward and backward substitution each. In that case, the high order derivatives have very low cost when using a factorization. As result, Taylor vectors of the model response can be expanded in the vicinity of the initial position capturing parameters.

Commercial FE software provides users with a programming language (e.g. APDL in ANSYS) that allows some manipulation of stiffness matrices and displacement vector without access to the source code. It holds the promise of derivatives of the system matrix with little

implementation effort. For example, Chang [95] implemented the sensitivity calculation module that can connect with FE programs as ANSYS, ABAQUS and NASTRAN.

In contrast to design sensitivity analysis, HOD calculations cannot be carried out outside existing finite element codes, using postprocessing data only. In order to have a general approach, capable of treating large size problem, all terms are saved in files instead of managing them all in the memory. Commonly, the derivatives of FE matrix have the same structure as original FE matrix. The FE matrices are naturally sparse. The derivatives of FE matrix may be sparser as the derivatives order increases. So, specific file format for sparse structures and access to the source code is need.

A special topic of this chapter is the discussion and explanation of the automatic differentiation algorithm, which is applied to all FEA stages (preprocessing, element stiffness matrices, finite element equations and postprocessing).

MATLAB was chosen for prototyping of HODM algorithms. The input data to parametric solver are the parametric FE-mesh and parameters definitions. The output data is polynomial coefficient set of the solution vector (displacement) and the goal function (secondary results). In practice, the derivatives of solution vector are stored in a database for each degree of freedom of the structure. Evaluation and visualization can be interfaced with parametric postprocessing stage. The parametric postprocessing will explore the parametric result in order to perform sensitivity curves or response surfaces.

## 4.2 Derivatives of the FE Matrices

The global FE matrix  $\mathbf{K}$  is a superposition of the elementary matrices  $\mathbf{k}$ :

$$\mathbf{K} = \sum_{el} \mathbf{k}. \quad (4.2)$$

So the derivatives of a global FE matrix  $\mathbf{K}^{(n)}$  are obtained from a superposition of derivatives of the elementary matrices  $\mathbf{k}^{(n)}$ . The stiffness matrix of the isoparametric finite element can be computed according to the general relationship [96]

$$\mathbf{k} = \int_V \mathbf{B}^T \mathbf{D} \mathbf{B} dV. \quad (4.3)$$

Evaluation of the integrals is done by Gauss integration

$$\mathbf{k} = \sum_{i=1}^{ngp} \mathbf{B}_i^T \mathbf{D} \mathbf{B}_i |J_i| w_i, \quad (4.4)$$

where  $|J_i|$  is the determinant of the Jacobian matrix  $\mathbf{J}$  of the isoparametric transformation from local  $(\xi, \eta, \zeta)$  to global  $(x, y, z)$  coordinates,  $w_i$  is the weighting factor. Generally, the expressions of Jacobian matrix depend on the FE element type (through the shape functions) and the nodal coordinates of the element. The shape functions for different elements are given in Appendix A.3.

Consider brick element having three degrees of freedom at each node: translations in the nodal  $x$ ,  $y$  and  $z$  directions, the element is mapped to a cube of size 2 in the local coordinate system  $(\xi, \eta, \zeta)$  (see Figure 4.2a). The strain-displacement matrix  $\mathbf{B}$  is determined by operating on the shape functions  $N_i(\xi, \eta, \zeta)$ , and it is found that

$$\mathbf{B} = [\mathbf{b}_1 \mathbf{b}_2 \dots \mathbf{b}_i \dots \mathbf{b}_8], \quad (4.5)$$

where the submatrix  $\mathbf{b}_i$ , which is associated with the nodal point  $i$  of the finite element, has the form

$$\mathbf{b}_i = \begin{bmatrix} \frac{\partial}{\partial x} N_i & 0 & 0 \\ 0 & \frac{\partial}{\partial y} N_i & 0 \\ 0 & 0 & \frac{\partial}{\partial z} N_i \\ \frac{\partial}{\partial y} N_i & \frac{\partial}{\partial x} N_i & 0 \\ 0 & \frac{\partial}{\partial z} N_i & \frac{\partial}{\partial y} N_i \\ \frac{\partial}{\partial z} N_i & 0 & \frac{\partial}{\partial x} N_i \end{bmatrix}. \quad (4.6)$$

Here, the derivatives of the shape functions  $N_i(\xi, \eta, \zeta)$  with respect to global  $(x, y, z)$  coordinates are given by

$$\begin{Bmatrix} \frac{\partial}{\partial x} N_i \\ \frac{\partial}{\partial y} N_i \\ \frac{\partial}{\partial z} N_i \end{Bmatrix} = \begin{bmatrix} \frac{\partial x}{\partial \xi} & \frac{\partial x}{\partial \eta} & \frac{\partial x}{\partial \zeta} \\ \frac{\partial y}{\partial \xi} & \frac{\partial y}{\partial \eta} & \frac{\partial y}{\partial \zeta} \\ \frac{\partial z}{\partial \xi} & \frac{\partial z}{\partial \eta} & \frac{\partial z}{\partial \zeta} \end{bmatrix} \begin{Bmatrix} \frac{\partial}{\partial \xi} N_i \\ \frac{\partial}{\partial \eta} N_i \\ \frac{\partial}{\partial \zeta} N_i \end{Bmatrix} = \mathbf{J}^{-1} \begin{Bmatrix} \frac{\partial}{\partial \xi} N_i \\ \frac{\partial}{\partial \eta} N_i \\ \frac{\partial}{\partial \zeta} N_i \end{Bmatrix}. \quad (4.7)$$

The Jacobian matrix at integration point is computed according to (4.8). Note that  $\mathbf{J}$  is expressed in terms of the derivatives of shape functions  $N_i(\xi, \eta, \zeta)$  with respect to the local element coordinates evaluated at gauss points and of the global coordinates of nodal points of the element. The shape functions  $N_i(\xi, \eta, \zeta)$  of the finite element depend only on the local coordinates within the element and thus are independent of the actual geometry of the element:



$$\mathbf{J} = \begin{bmatrix} \frac{\partial N_1}{\partial \xi} & \frac{\partial N_2}{\partial \xi} & \frac{\partial N_3}{\partial \xi} & \frac{\partial N_4}{\partial \xi} & \frac{\partial N_5}{\partial \xi} & \frac{\partial N_6}{\partial \xi} & \frac{\partial N_7}{\partial \xi} & \frac{\partial N_8}{\partial \xi} \\ \frac{\partial N_1}{\partial \eta} & \frac{\partial N_2}{\partial \eta} & \frac{\partial N_3}{\partial \eta} & \frac{\partial N_4}{\partial \eta} & \frac{\partial N_5}{\partial \eta} & \frac{\partial N_6}{\partial \eta} & \frac{\partial N_7}{\partial \eta} & \frac{\partial N_8}{\partial \eta} \\ \frac{\partial N_1}{\partial \zeta} & \frac{\partial N_2}{\partial \zeta} & \frac{\partial N_3}{\partial \zeta} & \frac{\partial N_4}{\partial \zeta} & \frac{\partial N_5}{\partial \zeta} & \frac{\partial N_6}{\partial \zeta} & \frac{\partial N_7}{\partial \zeta} & \frac{\partial N_8}{\partial \zeta} \end{bmatrix} \begin{bmatrix} x_I & y_I & z_I \\ x_J & y_J & z_J \\ x_K & y_K & z_K \\ x_L & y_L & z_L \\ x_M & y_M & z_M \\ x_N & y_N & z_N \\ x_O & y_O & z_O \\ x_P & y_P & z_P \end{bmatrix}. \quad (4.8)$$

Like  $\mathbf{J}$ , the strain-displacement matrix  $\mathbf{B}$  depends on coordinates of the nodal points, whereas the constitutive matrix  $\mathbf{D}$  depends only on the constitutive parameters. The derivatives of an elementary stiffness matrix  $\mathbf{k}$  can be done with respect to material properties, to geometrical parameters or to load and boundary conditions. These expressions for derivatives of an elementary stiffness matrix  $\mathbf{k}$  are explained below.

#### 4.2.1 Element Derivatives versus Material Properties

All types of material properties like Young's modulus, mass density, conductivity coefficients, shear modulus, and components of the constitutive matrix and orientation of anisotropy for a silicon material can be chosen as design parameters.

The derivatives of an elementary stiffness matrix  $\mathbf{k}$  with regard to material properties are obtained by equation

$$\frac{\partial^n}{\partial p^n} \mathbf{k}(p) = \sum_{i=1}^{ngp} \mathbf{B}_i^T \frac{\partial^n \mathbf{D}(p)}{\partial p^n} \mathbf{B}_i | \mathbf{J}_i | w_i. \quad (4.9)$$

Linear material properties can be constant or temperature-dependent, and isotropic or orthotropic. Material matrix for a linear elastic and isotropic material is given by

$$\mathbf{D}(E, \nu) = \frac{E}{(1+\nu)(1-2\nu)} \begin{bmatrix} 1-\nu & \nu & \nu & 0 & 0 & 0 \\ \nu & 1-\nu & \nu & 0 & 0 & 0 \\ \nu & \nu & 1-\nu & 0 & 0 & 0 \\ 0 & 0 & 0 & \frac{1-2\nu}{2} & 0 & 0 \\ 0 & 0 & 0 & 0 & \frac{1-2\nu}{2} & 0 \\ 0 & 0 & 0 & 0 & 0 & \frac{1-2\nu}{2} \end{bmatrix}. \quad (4.10)$$

The material parameters  $E$  and  $\nu$  define the modulus of elasticity and the Poisson's ratio, respectively.

The groups of elements (components) can be considering as discrete parameters or Boolean parameters. Typical examples of such features would be ribs or holes. The effects of removing these components from the model can be study by changing their material properties:

$$E(p) = E(0)p . \quad (4.11)$$

Discrete parameter  $p$  corresponds to sets of elements in the model that can be turned **1** or **0**. Then  $p = 0$ , the elements components remains in the model but contributes a near-zero stiffness (or conductivity etc.) value to the global matrix like deactivates the specified element with the birth and death capability.

### 4.2.2 Derivatives of a FE Matrix versus Geometrical Parameters

The derivatives of an elementary stiffness matrix  $\mathbf{k}$  with regard to geometrical parameters  $p$  are obtained by equation

$$\frac{\partial^n}{\partial p^n} \mathbf{k}(p) = \sum_i^{ngp} \frac{\partial^n \mathbf{B}_i(p)^T \mathbf{D} \mathbf{B}_i(p) |\mathbf{J}_i(p)|}{\partial p^n} w_i . \quad (4.12)$$

Thus, the derivatives of elementary stiffness matrix (4.12) can be expressed from the derivatives of analytical functions  $x_i(p)$ ,  $y_i(p)$ ,  $z_i(p)$ , which connect node coordinates of the element with involved geometrical parameters  $p$ .

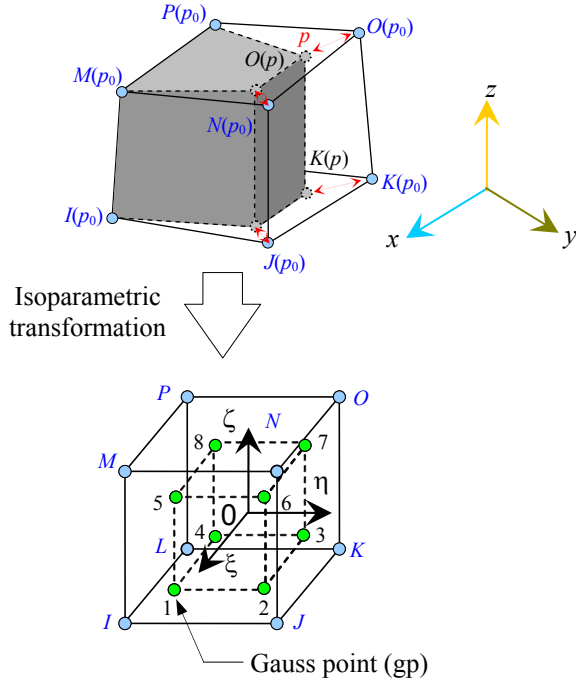
The extraction algorithm of the element matrix and its derivatives for an eight nodes solid element having three translations degrees of freedom at each node (like ANSYS SOLID45 3D structural solid element) is shown in Figure 4.2.

Generally, the strain-displacement matrix  $\mathbf{B}$  is depending on the inverse of the Jacobian matrix. As shown by Guillaume [2] and Perrin [38], the derivatives of  $\mathbf{J}^{-1}$  and  $|\mathbf{J}|$  can be getting using automatic differentiation.

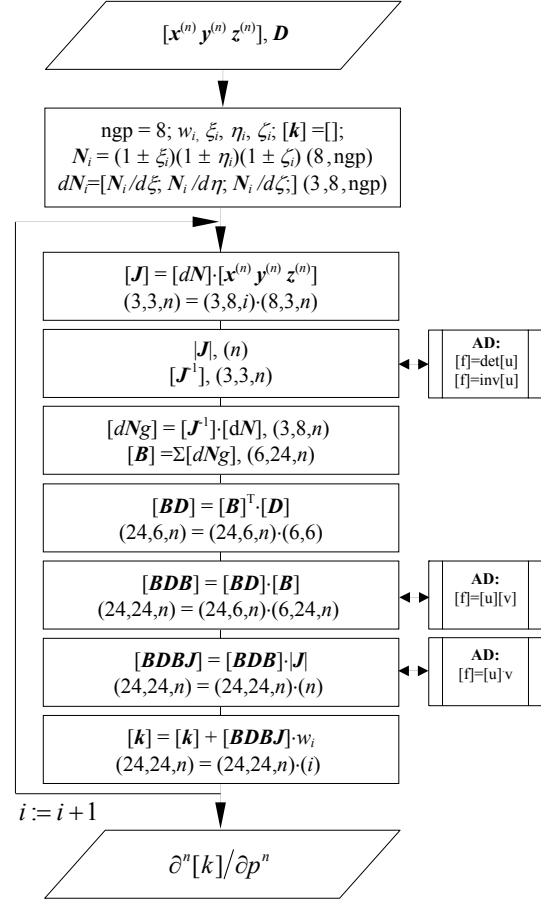
Derivatives of the mass matrix versus geometrical variables can be established using the same approach as above for the mass matrix:

$$\mathbf{m} = \int_V \mathbf{N}^T \rho \mathbf{N} dV . \quad (4.13)$$

Six different 2D/3D parametric finite elements have been implemented as shown in Table A.1.



a) Sketch



b) Flow chart

Figure 4.2 Parametric 3D eight node solid element

### 4.2.3 Derivatives of a FE Matrix versus Boundary Conditions

The matrix  $\mathbf{K}$  is singular after assembling, because the rows and columns of matrix are linear combinations of each other. The system of equations (3.10) can be solved only considering the boundary conditions. If the finite element equations are derived on the basis of variational principle; the natural boundary condition will be automatically incorporated in the formulation, and hence only the geometric boundary condition are to be enforced on the solution. Essential boundary conditions are boundary conditions, which directly involves the nodal freedoms. The simplest essential boundary conditions in mechanical are support and symmetry conditions. To eliminate linear combinations of the columns and render the system nonsingular, the physical support conditions as displacement boundary conditions must be applied.

#### Applying Displacement Boundary Conditions by Static Condensation

The simplest way to account for support conditions is to remove equations associated with known joint displacements from the system. This can be systematically accomplished by deleting rows and columns corresponding to given zero displacements from  $\mathbf{K}$  and the corresponding components from  $\mathbf{F}$  and  $\mathbf{u}$ . The elimination gives the reduced system of rearranging

equations. The matrix rearrangement leads to the non-differentiable problem, because the associativity of the nodes in matrix is not retained.

### Applying Displacement Boundary Conditions by Modification

As there, the main objective is to avoid rearranging the stiffness matrix. To apply support conditions without rearranging the equations, the  $i$ -rows and the  $i$ -columns from  $\mathbf{K}$ , and force components from  $\mathbf{F}$  corresponding to zero displacements are set to zero. Ones are placed on the diagonal to maintain non-singularity:

$$\begin{aligned} K_{ii} &= 1, F_i = 0. \\ K_{ij} &= 0, K_{ji} = 0 \quad \text{for } i \neq j. \end{aligned} \quad (4.14)$$

Solving this modified system produces the complete displacement solution directly.

The group of  $m$ -DOFs with displacement boundary conditions can be considering as discrete parameter. The parameterization of the displacement boundary conditions is described as

$$\begin{aligned} K_{mm}(p) &= K_{mm}(0)(1-p) + p, & F_m(p) &= F_m(0)(1-p). \\ K_{mj}(p) &= K_{mj}(0)(1-p), & K_{jm}(p) &= K_{jm}(0)(1-p) \quad \text{for } i \neq j, \end{aligned} \quad (4.15)$$

where  $p$  is the discrete parameters that can be turned **1** or **0**.

Traditional techniques for applying boundary conditions in FEA like penalty method and Lagrange multiplier can be parameterized using the same approach as above.

## 4.3 Derivatives of the Load Vectors

In practical problems, distributed loads are more common than concentrated loads. Distributed loads may be of surface  $\mathbf{F}^S$  or volume  $\mathbf{F}^B$  type [41]. In FE analysis, distributed loads must be converted to equivalent nodal forces as illustrated in Figures 4.3 and 4.4. The consistent element load vector  $\mathbf{f}^{el}$  is given by

$$\mathbf{f}^{el} = \int_A \mathbf{N}^T \mathbf{F}^S dA + \int_\Omega \mathbf{N}^T \mathbf{F}^B d\Omega. \quad (4.16)$$

Obviously, converted nodal forces depend on the geometrical variations of the element.

### 4.3.1 Surface Load

Pressure in a structural analysis is an example of a distributed load applied over a surface:

$$\mathbf{f}^{el} = \int_A \mathbf{N}^T P dA. \quad (4.17)$$

The derivatives of the nodal force vector versus the geometrical design variable, becomes

$$\frac{\partial^n}{\partial p^n} \mathbf{f}^{el}(p) = \sum_{i=1}^{ngp} \mathbf{N}_i^T P \frac{\partial^n |J_i(p)|}{\partial p^n} w_i. \quad (4.18)$$

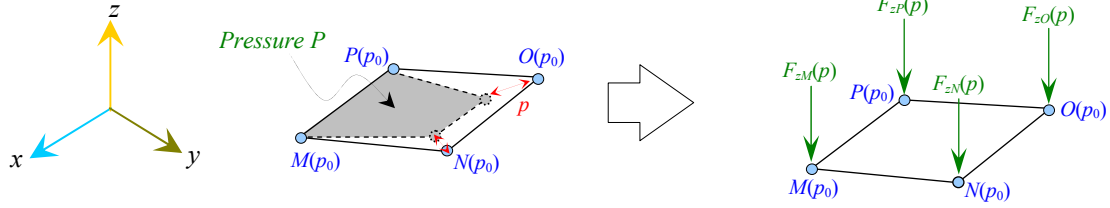


Figure 4.3 Surface load on the element

### 4.3.2 Volume Load

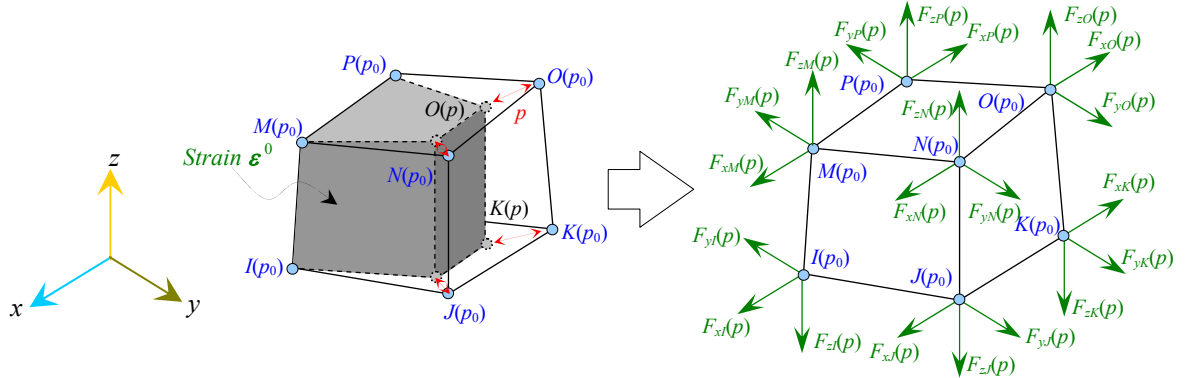


Figure 4.4 Body load on the element

An initial strain is a typical example of a volumetric load in structural discipline. A consistent nodal force vector  $\mathbf{f}^{el}$  due to the initial induced strains at element level is given by

$$\mathbf{f}^{el} = \int_V \mathbf{B}^T \mathbf{D} \boldsymbol{\varepsilon}^0 dV, \quad (4.19)$$

where initial strain has the form

$$\boldsymbol{\varepsilon}^0 = \{\varepsilon_x^0 \ \varepsilon_y^0 \ \varepsilon_z^0 \ 0 \ 0 \ 0\}^T. \quad (4.20)$$

The derivatives of the nodal force vector with respect to geometrical design variable, becomes

$$\frac{\partial^n}{\partial p^n} \mathbf{f}^{el}(p) = \sum_{i=1}^{ngp} \frac{\partial^n \mathbf{B}_i(p)^T \mathbf{D} \boldsymbol{\varepsilon}^0 |J_i(p)|}{\partial p^n} w_i. \quad (4.21)$$

## 4.4 Differentiation

In contrast to symbolic differentiation, novel approaches make use AD algorithms which process numerical values extracted at the initial position. Chain rules of differential calculus describe how to combine partial derivatives and binomial coefficients in order to form elementary mathematical operations and where to store results in arrays.

### 4.4.1 Automatic Differentiation

Research for AD methods has existed as a research topic since the 1980s. Automatic differentiation is having a deep impact in many areas of science and engineering. The capability of automatic differentiation opens up a wide range of applications such as sensitivity analyses; solution of nonlinear systems: Jacobian and Hessian exact estimation for Newton solver; improving the optimization algorithms by computing the relevant derivative information efficiently; inverse problems.

In terms of implementation, there are mainly two ways to implement an automatic differentiation tool. One is source-to-source transformation and the other is operator overloading. AD has two basic modes of operation known as forward and reverse. These modes correspond to a bottom-up and a top-down strategy of derivatives accumulation of elementary functions that define the computational scheme of the function [97, 98].

Source transformation consists in adding into the existed code the new data structures (variables, arrays) that will hold the derivatives and in generation the new subroutines that compute these derivatives. The advantage is that the resulting program can be compiled into an efficient code, and the reverse mode is possible.

Operator overloading is available in computer languages, such as C++, that provide the ability to redefine the meaning of elementary operators for various classes of variables. Each elementary operator is overloaded, i.e. internally replaced by a new one, working on object, which computes the value and its derivatives. The advantage is that the original code is virtually unchanged, i.e. the code can be transformed without increasing its size substantially. E.g., ADOL-C overloads all the mathematical functions contained in the ANSI C standard for the math library are overloaded for active arguments. It is very difficult to implement the reverse mode with overloading. The drawback of the operator overloading approach is that it requires more computing time, compared to explicitly stated code.

Finally, automatic differentiation refers to a differentiation of the computer code itself. Even if the finite element programs are composed of many complicated subroutines and functions, they are basically a set of elementary functions, arithmetic expressions, do-loops and if-then-else constructs. The AD methods define the derivatives of these elementary functions, and then the derivatives of complicated subroutines and functions are computed using propagation

and the chain rule of differentiation. The AD tools have been applied to FLUENT with over a million lines of source code [99]. Although, programs that calculate the derivatives of output of other source codes are now available, the human intervention in the process is required in many cases in order to obtain an acceptably efficient code. The better performance can be achieved by using AD to parts of the source.

The main characteristics are summarized in the Table 4.1 and details are available in [100]. Several tools have been developed to handle the automatic differentiation process. Much AD software tools release under the GNU/GPL license.

Table 4.1 Overview of AD software

Tools	Language	Technique	Order	Comment
ADIFOR	Fortran77	source transformation	1st	1991
ADOL-C	C/C++	operator overloading	up to $n$	1992
ADMIT-1	MATLAB	operator overloading	up to 2 <sup>nd</sup>	1996 / 98
ADIC	C/C++	source transformation	up to 2 <sup>nd</sup>	1997
FFADLib	C/C++	operator overloading	up to $n$	2000
ADiMat	MATLAB	source transformation operator overloading	up to 2 <sup>nd</sup>	2002 Jacobian and Hessian
ADOGEN	C/C++	source transformation	up to $n$	patented, proprietary tools for derivate matrices

The AD tool for parametric FEA must support the differentiation of matrices (including matrix product, inverse and determinant) and matrix-vector operations (sum, product) up to arbitrary order. Only in the last decade have programs begun to appear that compute multivariable Taylor series for any arbitrary number of variables, up to arbitrary order. It can be a massive problem for any complicated expression with several variables. While various AD tools are until under academic research and development, the tool AD, based on [94] and extended on matrix functions, have been prototyped and implemented as a subroutine call.

## 4.4.2 Differentiation Rules

HODM is required for basic arithmetic matrix-vector operations such as addition, multiplication and division. The matrix product is done element by element. E.g., the product of two multivariate scalar functions  $u(\mathbf{p})$  and  $v(\mathbf{p})$  is expressed by

$$D_p^\mu f = \sum_{\alpha_1=0}^{\mu_1} \sum_{\alpha_2=0}^{\mu_2} \dots \sum_{\alpha_n=0}^{\mu_n} C_{\alpha_1}^{\mu_1} C_{\alpha_2}^{\mu_2} \dots C_{\alpha_n}^{\mu_n} D_p^\alpha u D_p^{\mu-\alpha} v, \quad (4.22)$$

where multi-index  $\boldsymbol{\mu} = \{\mu_1, \dots, \mu_n\}$  defines the order of the partial derivatives in multivariate case, the  $n$  is the number of independent arguments. The following notation is used:

$$D_p^\mu f = \frac{\partial^{|\boldsymbol{\mu}|} f}{\partial p_1^{\mu_1} \dots \partial p_n^{\mu_n}}, \quad (4.23)$$

where  $|\boldsymbol{\mu}| = \sum_{i=1}^n \mu_i$ ,  $0 < |\boldsymbol{\mu}| \leq m$  and  $m$  is the order of the highest derivative.

By employing certain concepts in combinatorial analysis [101], one can derive the expressions for the  $m^{\text{th}}$  order derivatives of a matrix inverse from derivatives of a matrix  $\mathbf{J}(p)$ :

$$D_p^m \mathbf{J}^{-1} = m! \left( \sum_{k=1}^m (-1)^k \frac{\mathbf{A}_{i_1}}{i_1!} \frac{\mathbf{A}_{i_2}}{i_2!} \dots \frac{\mathbf{A}_{i_k}}{i_k!} \right) \mathbf{J}^{-1}, \quad (4.24)$$

where the elements of matrix  $\mathbf{J}$  are functions of a parameter  $p$ , the matrix  $\mathbf{A}_i$  is defined as  $\mathbf{A}_i = \mathbf{J}^T D^i \mathbf{J}$ . The summation is taken over all the integers ( $i_1, i_2, \dots, i_k > 0$ ) distinct or otherwise, such that  $\sum_{n=1}^k i_n = m$ .

The  $m^{\text{th}}$  order derivative of a matrix determinant is given by

$$D_p^m |\mathbf{J}| = \sum_{i=0}^{m-1} \sum_{j=0}^{m-1-i} \frac{(m-1)!}{i! j! (m-1-i-j)!} D^i |\mathbf{J}| \text{Trace}(\mathbf{D}^j \mathbf{J}^{-1} \mathbf{D}^{m-i-j} \mathbf{J}). \quad (4.25)$$

The generalized chain rules propagate the partial derivatives in forward mode – from independent to dependent variables. The storage scheme of partial derivatives is the important issue, which affects the efficiency of the algorithm. Several authors suggested arranging the partial derivatives in an array by increasing order of the derivatives [94]. Such scheme rather than pyramidal array guarantees the constant time access to the derivatives via indices. However, the chain rules require the partial derivatives to be addressed through the multi-index  $\boldsymbol{\mu}$ . The mapping of multi-index  $\boldsymbol{\mu}$  to the array index  $R(\boldsymbol{\mu})$  is

$$R(\boldsymbol{\mu}) = \sum_{j=1}^n C_j^{K_j + j}, \quad (4.26)$$

where  $K_j = \sum_{i=0}^{j-1} \mu_{n-i} - 1$ . According to (4.26), the position of the partial derivatives in the array depends not only on its order, but also on the number of independent parameters.



## 4.5 Parametric Mesh-Morphing

A new mesh generation with regard to the varying geometrical parameter provides a mesh that is topologically different from the initial one. This mesh will have a different number of nodes, elements and new element connectivity. Using different meshes to compute Taylor expansion of the solution is impossible. In contrast to ordinary FEM, one needs a special parametric FE-model that captures the variation of geometrical design variables without a re-mesh procedure. Mesh-morphing affects only nodes. The associativity of the nodes and elements is retained with the solid modeling entities. Unlike sensitivity analysis of a shape design variable, where only finite elements situated at the surface are perturbed [1], the HOD approach requires the perturbation of the internal nodes. Parametric mesh-morphing means that the node table contains not only a single numerical value for each spatial direction as it is supported by most CAD tools, rather each node  $i$  will be described by analytical functions  $\{x_i(p), y_i(p), z_i(p)\}$  with respect to geometrical parameters  $p$ .

### 4.5.1 Design Velocity Field

The geometry can be described as a continuous function of the parameters [102]. Consider a structural domain  $\Omega$  with its boundary  $\Gamma$  as a continuous medium at the initial design  $p = 0$  shown in Figure 4.5 (solid line).

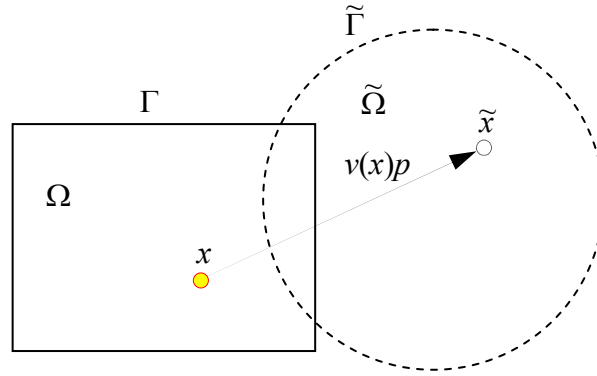


Figure 4.5 Morphing process

Parameter  $p$  defines the transformation  $\mathbf{T}: x \rightarrow \tilde{x}(x)$  that changes the structural domain from  $\Omega$  to  $\tilde{\Omega}$  (dotted lines). Define the design velocity  $v$  with design parameters  $p$  plays the role of time:

$$v(\tilde{x}, p) \equiv \frac{d\tilde{x}}{dp} = \frac{\partial \mathbf{T}(x, p)}{\partial p}. \quad (4.27)$$

In the neighborhood of initial parameters  $p = 0$ , ignoring higher-order terms,  $\mathbf{T}$  can be approximated by

$$T(x, p) = T(x, 0) + \frac{\partial T(x, 0)}{\partial p} p + O(p^2) \approx x + v(x)p, \quad (4.28)$$

where  $x = T(x, 0)$  and  $v(x) = v(x, 0)$ .

The linear approximation (4.28) means that the design velocity  $v(x)$  can be easily computed if the initial and final meshes are known. The crucial aspect of using mesh-morphing is the perturbation of the internal nodes computation after the boundary perturbation with regard to geometrical parameter.

### 4.5.2 Smoothing Technique

A convenient way to transform global parameters to internal nodal coordinates is a Laplacian smoothing used for mesh-morphing in FEA. Generally, internal FE nodes must move smoothly with respect to dimensional modifications, especially in case of large displacements or complicated shape (e.g. perforation holes, sharp notches). Similar problems are widely known from mesh morphing of coupled domain analyses [93]. Especially geometrical parameter must carefully be mapped to the node table since local distortions affect the accuracy of the Taylor series solution. The accuracy of parametric solutions depends mainly on the quality of mesh perturbations caused by mapping of global parameters  $p$  to the nodal table.

There are mainly two types of smoothing methods, namely Laplacian smoothing and optimization-based smoothing. Laplacian smoothing [103] is a technique commonly used for improving finite element meshes by iteratively adjusting node locations to the centroid of their surrounding nodes. It requires a very low computational cost, but it does not guarantee an improvement in the geometric mesh qualities. For example, for node  $k$  at location  $x_k$ , its smoothed location is defined as

$$x_k = \sum_{i=1}^n A_i x_i^c / \sum_{i=1}^n A_i, \quad (4.29)$$

where  $x_i^c$  is the centroid of element  $i$  adjacent  $k$ , and  $A_i$  is the area or volume of element  $i$ . The total number of adjacent elements is given by  $n$ . After applying the structural displacements to the nodes on the boundary, a few iterations of (4.29) can be applied to all nodes of the mesh within proximity of the deformation. Although in most cases Equation (4.29) will improve the surrounding elements, there is no guarantee that the resulting elements will be optimal or on occasions, even better than a previous iteration.

The goal of an optimization based approach is to minimize the mesh modification. The use of the usual strain tensor to measure the modification rate gives good results. This strain tensor is defined on the integration points of each element [38].

### 4.5.3 Automated Mesh-Morphing Algorithm

Two automated the parametric mesh-morphing algorithms are proposed here. The description of the shape change at the outer boundaries is necessary first. Any 3D linear transformation (translation, rotation, scaling and combinations above-mentioned) can be represented by a coordinate transformation matrix  $T$ . A wide variety of configurations can be created with these transformations, as shown in Figure 4.6. Partial derivatives of the transformation matrix  $T$  with regard to design parameters  $p$  can be compute by means of AD. The design velocity for points on the outer boundaries can be calculated by compare the shape before and after the design variable change. After transformation, the topology of the mesh is unchanged but the finite elements are distorted, Figure 4.7d. This is due to the moving of the nodes linked to the parameter. In contract to iterative Laplacian smoothing, the electrical analogy can be effective used to compute design velocities for nodal transformations with regard to geometrical parameter, Figure 4.7b. Using the boundary velocity results as boundary condition for Laplace problem, the design velocity at interior points can be computed. After all design boundary velocity is calculated, the perturbation is extended to the interior domain, Figure 4.7g. In case of the  $n$  design variables, the method requires  $n$  additional analyses.

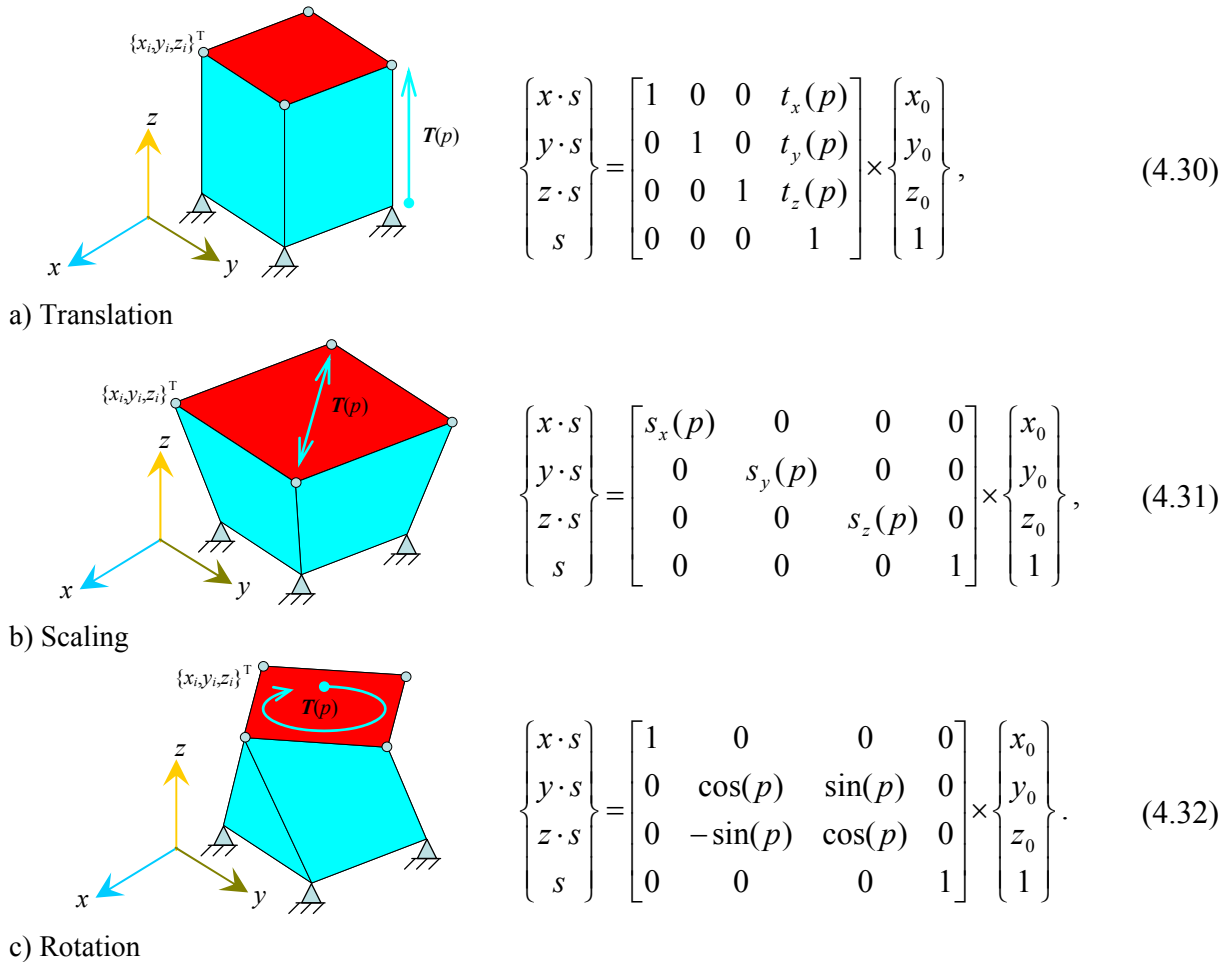


Figure 4.6 Solid transformations

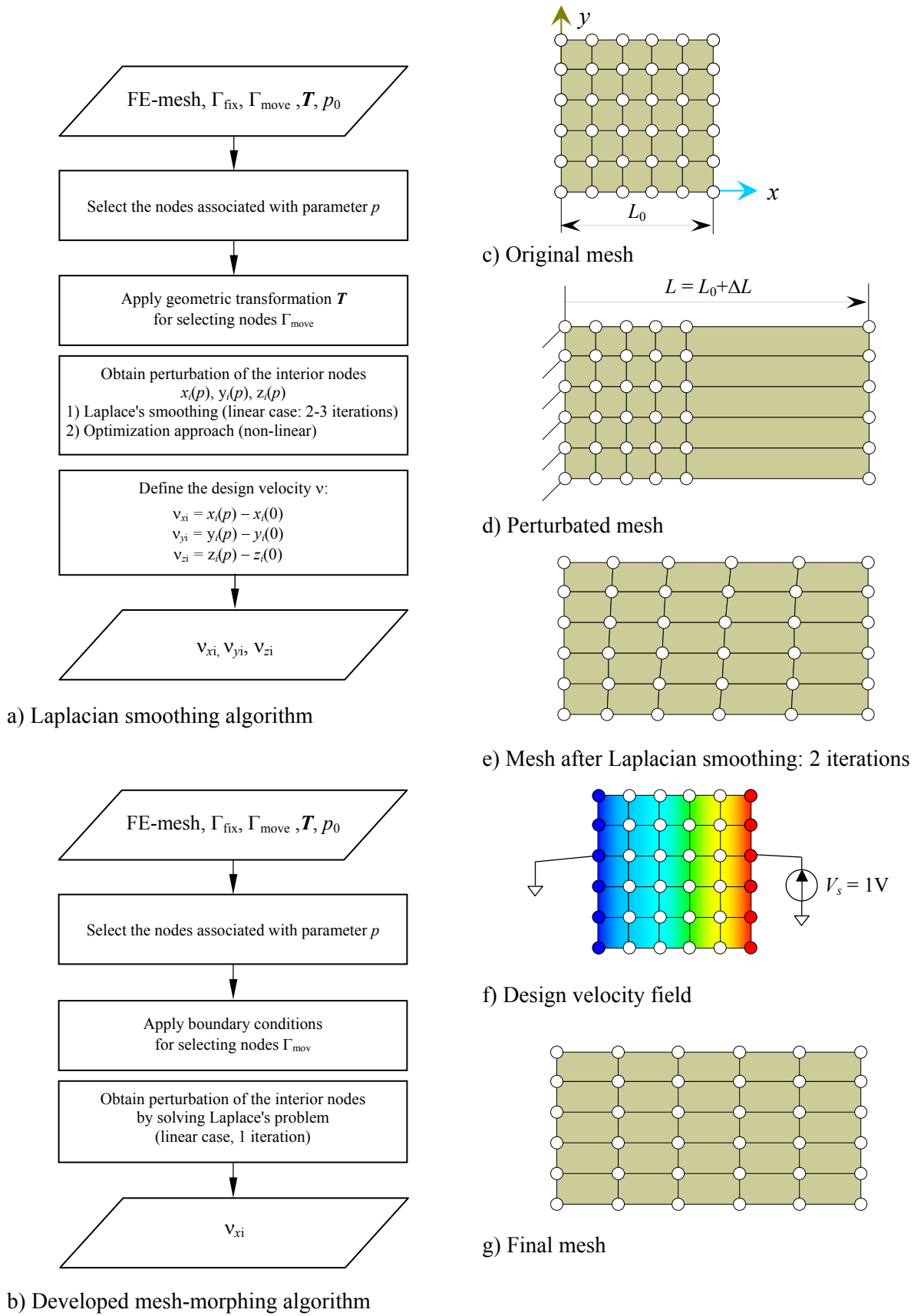


Figure 4.7 Comparison between mesh-morphing algorithms

There are two main situations that cause the proposed design velocity field computation method to fail. First, when dimension is chosen as a design variable for which the variation of a

design surface is not linearly dependent. The second difficulty arises, when the design variables are related to general surfaces, e.g. surface intersection regions or some kinds of surfaces, the parametric representation of the design surfaces may not support natural mapping relations which cause great difficulty for automatic velocity field computation. If the resulting mesh quality is not acceptable, one must utilize nonlinear algorithms for mesh perturbations [38].

## 4.6 Data Structure

A specialized data structure is commonly applied to process and store partial derivatives with given order. Partial derivatives have been arranged in successive planes of matrices in a third dimension as shown in Figure 4.8b.

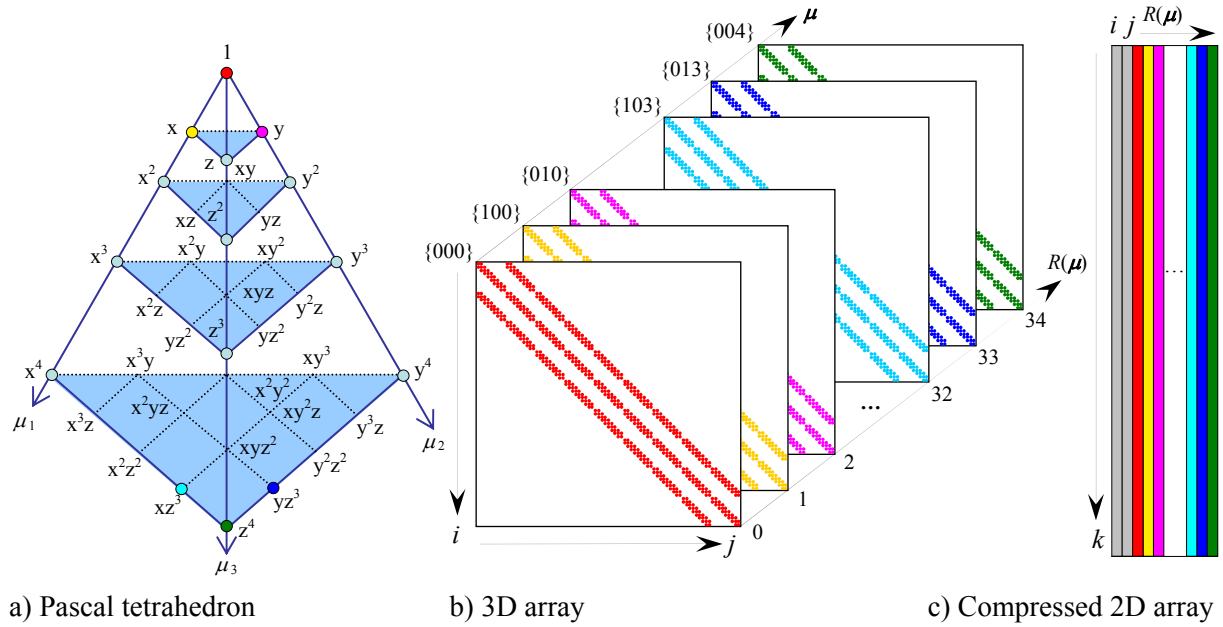


Figure 4.8 3D array ( $n = 3$ ,  $order = 4$ ) and its compressed 2D representation

This allocation scheme simplifies the mapping (4.26) of the multi-index  $\mu$ , which defines the partial derivatives, to the plane location index  $R(\mu)$ . Another important piece of information is the total number of panels. This is an indication of how much memory is needed to complete the calculation. Notation of the Lagrange and Pascal coefficient terms are explained in Appendix B.

The number of matrices planes can be estimate by formula

$$size = \binom{order + n}{n}. \quad (4.33)$$

E.g., three variable Pascal polynomial ( $n = 3$ ) with 4<sup>th</sup> order has 35 coefficients. The six variable Pascal polynomial ( $n = 6$ ) with 4<sup>th</sup> order has 210 coefficients. The apparent drawback is

exponential grown of the data structure with number of parameters and order of the derivatives.

To store nonzero sparse FE matrix elements, a coordinate column-wise format is used. Only nonzero entries are provided, and the coordinates of each nonzero entry is given explicitly. Compressed array is illustrated in the Figure 4.8c.

## 4.7 Substructuring Technique

Parametric technique typically requires large increases in system memory to store system matrix and its derivatives. In order to save system memory, the combine of substructure technique and parametric analysis is proposed. The FE-model can be divided into superelements, which are independent or variable with regard to parameter. The substructure technique uses the Guyan approaches [104] of global matrix transformation to reduce the system matrices to a smaller set. It represents a set of elements that are reduced to act as one superelement. The substructure technique may be used in any linear analysis type: modal, harmonic and transient analyses. This technique belongs to the standard procedures of the FE software. The one superelement may be used to generate more superelements. To reconstruct the solutions (e.g. displacements and stresses) within the superelement, an expansion pass is required.

### 4.7.1 Static Analysis

The stiffness matrix  $\mathbf{K}$  may be partitioned into two groups, the master and the slave DOFs

$$\begin{bmatrix} \mathbf{K}_{mm} & \mathbf{K}_{ms} \\ \mathbf{K}_{sm} & \mathbf{K}_{ss} \end{bmatrix} \begin{Bmatrix} \mathbf{u}_m \\ \mathbf{u}_s \end{Bmatrix} = \begin{Bmatrix} \mathbf{F}_m \\ \mathbf{F}_s \end{Bmatrix}, \quad (4.34)$$

or expanding

$$\begin{aligned} \mathbf{K}_{mm}\mathbf{u}_m + \mathbf{K}_{ms}\mathbf{u}_s &= \mathbf{F}_m \\ \mathbf{K}_{sm}\mathbf{u}_m + \mathbf{K}_{ss}\mathbf{u}_s &= \mathbf{F}_s \end{aligned} \quad (4.35)$$

Solving Equation (4.35) for  $\mathbf{u}_s$ ,

$$\mathbf{u}_s = \mathbf{K}_{ss}^{-1} \mathbf{F}_s - \mathbf{K}_{ss}^{-1} \mathbf{K}_{sm} \mathbf{u}_m. \quad (4.36)$$

Substituting  $\mathbf{u}_s$  into Equation (4.35)

$$(\mathbf{K}_{mm} - \mathbf{K}_{ms} \mathbf{K}_{ss}^{-1} \mathbf{K}_{sm}) \mathbf{u}_m = \mathbf{F}_m - \mathbf{K}_{ms} \mathbf{K}_{ss}^{-1} \mathbf{F}_s, \quad (4.37)$$

or

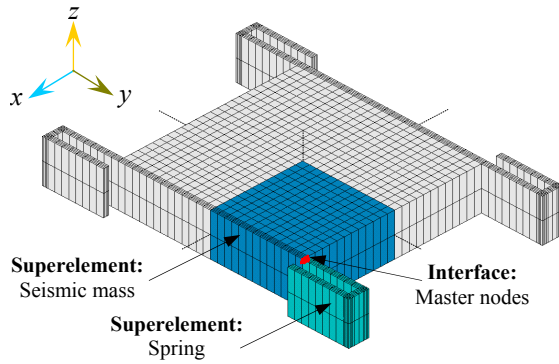
$$\hat{\mathbf{K}}\hat{\mathbf{u}} = \hat{\mathbf{F}}. \quad (4.38)$$

$\hat{\mathbf{K}}$  and  $\hat{\mathbf{F}}$  are the superelement stiffness matrix and load vector, respectively

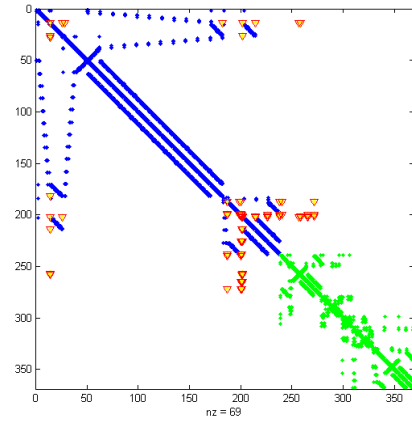
$$\begin{aligned} \hat{\mathbf{K}} &= \mathbf{K}_{mm} - \mathbf{K}_{ms} \mathbf{K}_{ss}^{-1} \mathbf{K}_{sm}, \\ \hat{\mathbf{F}} &= \mathbf{F}_m - \mathbf{K}_{ms} \mathbf{K}_{ss}^{-1} \mathbf{F}_s, \\ \hat{\mathbf{u}} &= \mathbf{u}_m. \end{aligned} \quad (4.39)$$

The factorization of reduced matrices  $\mathbf{K}_{mm}$ ,  $\mathbf{K}_{ss}$ , needing for solution (4.39) is less expensive in compare to factorization of the full matrix  $\mathbf{K}$ . In solving the statics problems, this approach yields the exact solution for the particular FE-model. DOF of master nodes keep their physical meaning and no back transformation needed for master nodes.

The master DOFs will be used to couple the superelement to other superelements as shown in Figure 4.9.



a) FE-model



b) Sparsity pattern of the FE stiffness matrix

Figure 4.9 Substructure of a resonator

## 4.7.2 Component Mode Synthesis

Component Mode Synthesis is a modal analysis of the entire assembly from its superelements. The displacement vector  $\mathbf{u}$  may be represented in terms of component generalized coordinates [105]:

$$\begin{Bmatrix} \mathbf{u}_m \\ \mathbf{u}_s \end{Bmatrix} = \mathbf{T} \begin{Bmatrix} \mathbf{u}_m \\ \mathbf{y}_\delta \end{Bmatrix}, \quad (4.40)$$

where  $\mathbf{y}_\delta$  is the truncated set of generalized modal coordinates. For the fixed-interface method [106], the transformation matrix has the form

$$\mathbf{T} = \begin{bmatrix} \mathbf{I} & \mathbf{0} \\ \mathbf{G}_{sm} & \mathbf{\Phi}_s \end{bmatrix}, \quad (4.41)$$

where  $\mathbf{G}_{sm} = -\mathbf{K}_{ss}^{-1}\mathbf{K}_{sm}$  is the redundant static constraint modes,  $\mathbf{\Phi}_s$  is the fixed-interface normal modes (eigenvectors obtained with interface nodes fixed).

After applying the transformation in Equation (4.41), the reduced mass and stiffness matrices of the CMS substructure will be

$$\begin{aligned} \hat{\mathbf{M}} &= \mathbf{T}^T \mathbf{M} \mathbf{T}, \\ \hat{\mathbf{K}} &= \mathbf{T}^T \mathbf{K} \mathbf{T} = \begin{bmatrix} \hat{\mathbf{K}}_{mm} & \mathbf{0} \\ \mathbf{0} & \mathbf{K}_{\delta\delta} \end{bmatrix}, \end{aligned} \quad (4.42)$$

where  $\hat{\mathbf{K}}_{mm}$  stiffness partition obtained from the Guyan reduction and  $\mathbf{K}_{\delta\delta} = \mathbf{\Phi}_s^T \mathbf{K}_{ss} \mathbf{\Phi}_s$ .

In the modal problems, the Guyan reduction gives an approximate solution [106].

## 4.8 Error Estimation

The parametric solution error  $\delta$  is defined as the difference between its approximation and the ordinary FE-solution, as shown in Figure 4.10.

The three main sources of error in a typical FE-solution are:

- formulation errors (simplifications made in the analysis: geometry, load, boundary condition, material properties; using of elements that do not precisely describe the behavior of the physical problem)
- discretization errors (errors due to insufficient mesh discretization; new mesh lead to a different discretization error; mesh-morphing procedures avoid the meshing errors due to remeshing)
- numerical errors (result of numerical calculation procedures, the loss of precision due to computer rounding of decimal quantities).

In such a way, convergence domain of the Taylor expansion of FE-solution depends on the regularity of the mesh perturbation, order derivatives and parameters range. These parameters are possible to control. Primary, the mesh perturbations must be smooth as possible. If the parameter variation range is bigger than the convergence radius, the range will be reduced to be within the convergence radius, and using a fixed derivative order. Based on the requested



accuracy of the expected results, the necessary order of the approximation can be automatically determined.

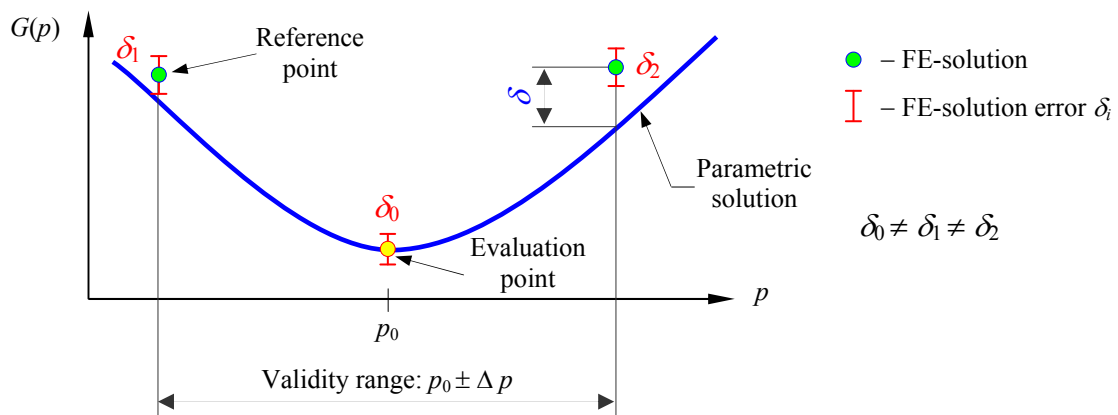


Figure 4.10 Error estimation in parametric analysis



## 5. Application of HODM

The objective of this section is to demonstrate the viability of HOD methods for the parametric FE simulation in the static, modal, frequency response domains on the basis of the structural, electrostatic and coupled field analyses. Two basic issues, which can be viewed as the criteria for reliability and correctness of HOD method are numerical accuracy and computation time. To validate the approach, parameterized solution, using the polynomials is compared to converged FE results, achieved by restarting for each set of parameters. Numerical details, accuracy and observed problems are discussed on several examples, which come from MEMS problems. For solid modeling and mesh generation the ANSYS Academic Research product is used. The perturbation of internal nodes with respect to parameters is obtained by solving Laplace's equation with Dirichlet boundary conditions.

### 5.1 Parametric Structural Analysis

#### 5.1.1 Linear Static Analysis

The first example for which the above described algorithm has been applied is a fixed-fixed beam under uniform load, which is a basic element for many MEMS structures. The beam is assumed to be made of a homogeneous isotropic material with Young's modulus  $E = 169$  GPa, Poisson's ratio  $\nu = 0.066$ , and mass density  $\rho = 2.329$  g/cm<sup>3</sup>. The difficulty for the application of beam element lies in the power law dependences of beam performance specifications on dimensions (see Appendix C). The fabrication process typically involves undercutting the beam structure. These dependences also mean that beam is quite sensitive to variation in process parameters. The length  $L$ , width  $B$  and thickness  $H$  of the beam were used as design parameters, as shown in Figure 5.1a.

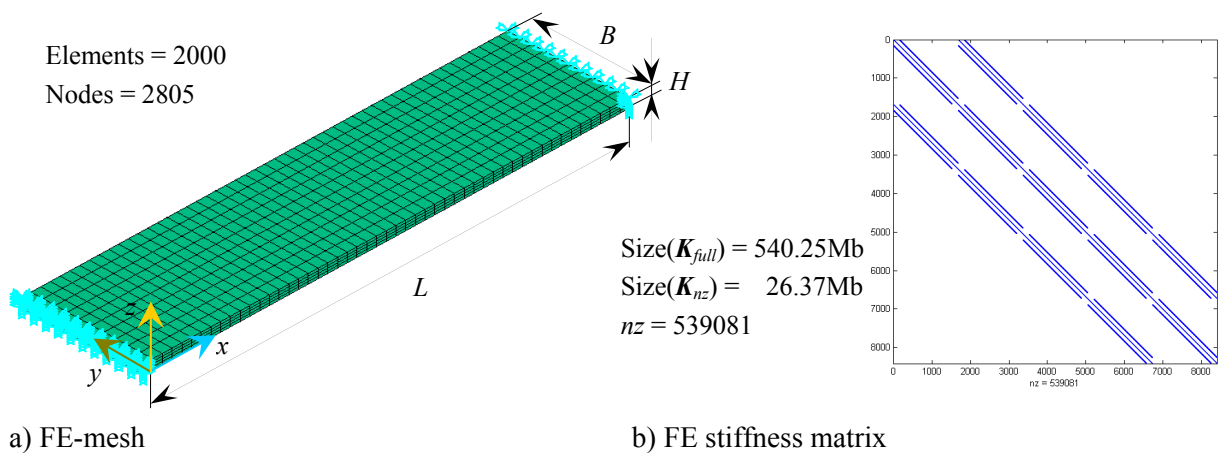


Figure 5.1 FE-model of a fixed-fixed beam

The beam is discretized by a grid of the  $50 \times 10 \times 4$  parameterized eight nodes element having three degrees of freedom at each node (translations in the  $x$ ,  $y$  and  $z$  directions). The stiffness

matrix  $\mathbf{K}$  is of dimension  $8415 \times 8415$  with 539081 nonzeros. For the static analysis, the maximum displacement, the maximum nodal Von-Mises stress and the strain energy are the criteria to be analyzed.

The mesh perturbations are described as

$$\begin{aligned} x_i(p_1) &= x_i(0) + v_{xi}p_1 \\ y_i(p_2) &= y_i(0) + v_{yi}p_2, \\ z_i(p_3) &= z_i(0) + v_{zi}p_3 \end{aligned} \quad (5.1)$$

where  $p_1 = (L-L_0)$ ,  $p_2 = (B-B_0)$ ,  $p_3 = (H-H_0)$  are the length, width and thickness variation, respectively. Design velocity  $v$  for  $i$ -node can be expressed analytically as

$$\begin{aligned} v_{xi} &= x_i(0)/L_0 \\ v_{yi} &= y_i(0)/B_0, \\ v_{zi} &= z_i(0)/H_0 \end{aligned} \quad (5.2)$$

Using AD, the derivatives of the global matrix  $\mathbf{K}^{(n)}$  was assembled up to 4<sup>th</sup> order at the initial configuration. The derivatives of the solution vector  $\mathbf{u}^{(n)}$  has been computed by (3.13). The derivatives of strain energy are extracted from derivatives of  $\mathbf{K}^{(n)}$  and  $\mathbf{u}^{(n)}$  at the evaluated point by means of AD for the product  $\mathbf{u}^T \mathbf{K} \mathbf{u}$  according (3.21). The design curves of a fixed-fixed beam under pressure load  $P = 12.5$  kPa with regard to selected parameters are shown in Figure 5.2. Table 5.1 summarizes the parameters using in the analysis.

Table 5.1 Parameters summary for a fixed-fixed beam

Parameter	Evaluation point	Parameter variation	Approximation method	Maximal relative error of the displacement, %
Length $L$ , $\mu\text{m}$	200	50...400	4 <sup>th</sup> order Taylor series	0.5
Width $B$ , $\mu\text{m}$	50	25...200	1 <sup>st</sup> order Taylor series	0.8
Thickness $H$ , $\mu\text{m}$	2	1...8	[2/2] Padé approximant	1.0

As seen from Figure 5.2, in accordance to the theoretical consideration, the maximum displacement, the maximum stress and the strain energy increase as the length of the beam is increased. Similarly in accordance with the theoretical formula (see Appendix C), the maximum displacement should be independent of the width of the beam. No change in the maximum displacement of the beam was observed on changing the width in the specified range. Only the strain energy increases with increasing the width of the beam. The relationship between the thickness and the maximum displacement of the beam has been plotted in Figure 5.2c. It could be shown that Taylor series of mechanical deflection or strain energy with regard to thickness capture the system behavior only in a very limited circle close the evaluation point. Basic transformation of a Taylor series to a Padé approximant allows extending of the acceptable thickness range to about 300 percent as shown in Figure 5.2c.

The present results indicate a correct implementation of the HOD methods for parametric FE analysis of static problems with respect to geometric design variables.

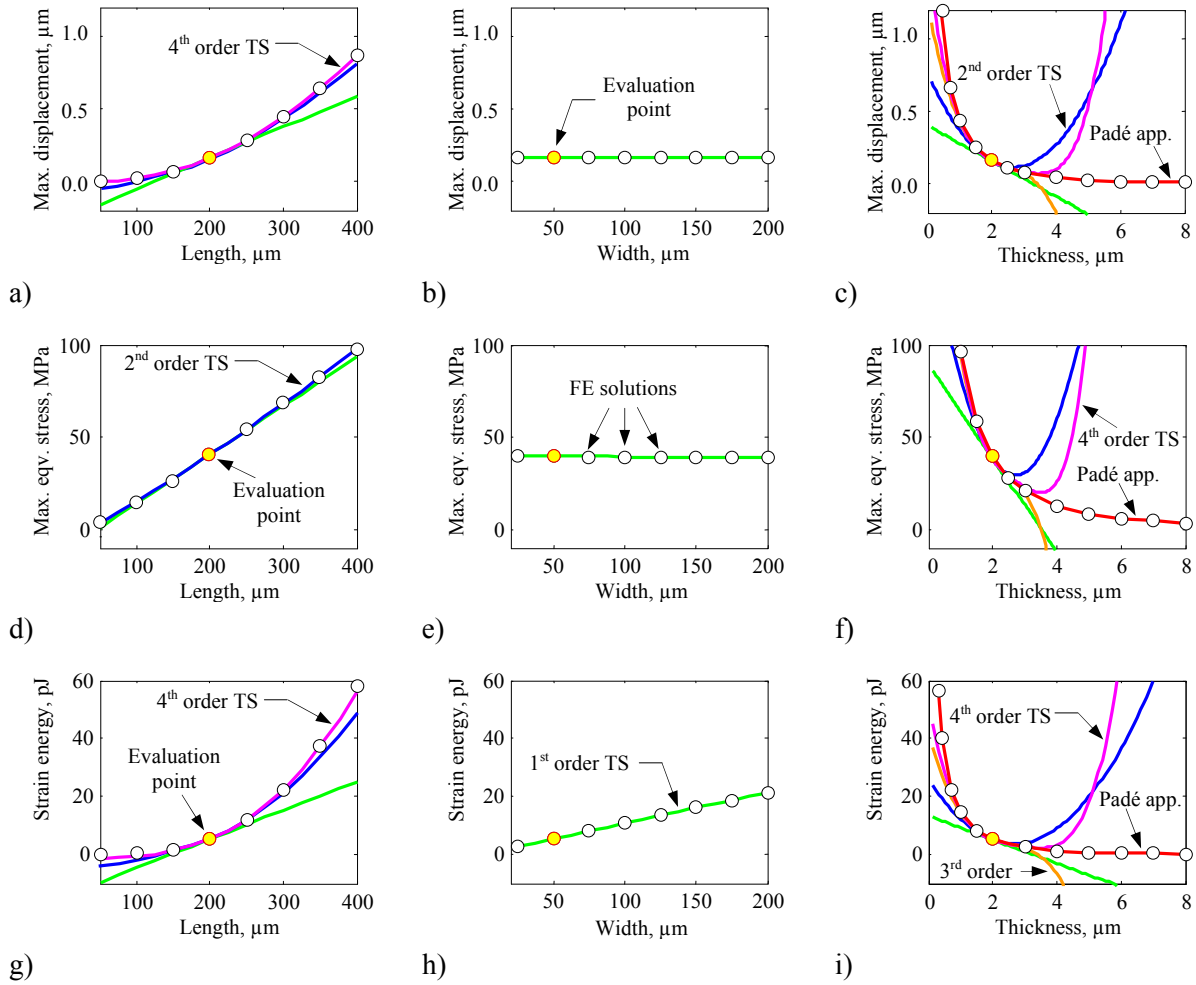


Figure 5.2 Design curves of a fixed-fixed beam under pressure load

Figure 5.3 present the study of time efficiency. The extra time taken for parametric modeling and mesh at the beginning of HODM does not consider. The solution of a system of linear equations is carried out by Cholesky factorization uses the LAPACK subroutines. These results were computed on a desktop PC with Intel® Core™ Duo CPU T2300@1.66GHz and 2.00 Gb RAM running Microsoft® Windows® XP.

The number of partial derivatives needed for a series expansion is comparable with the number of samples required for polynomial fit methods. Sampling procedures are powerful if a low number of sampling points have to be taken into account. Figure 5.3 shows that computing time for four sampling points was still lower compared to parametric FE technique. On the other hand, data acquisition time of sample methods grow exponentially the more variables must be processed. Fortunately, automatic differentiation of additional matrix planes is usually less expensive compared to further FE solution runs needed for sampling.

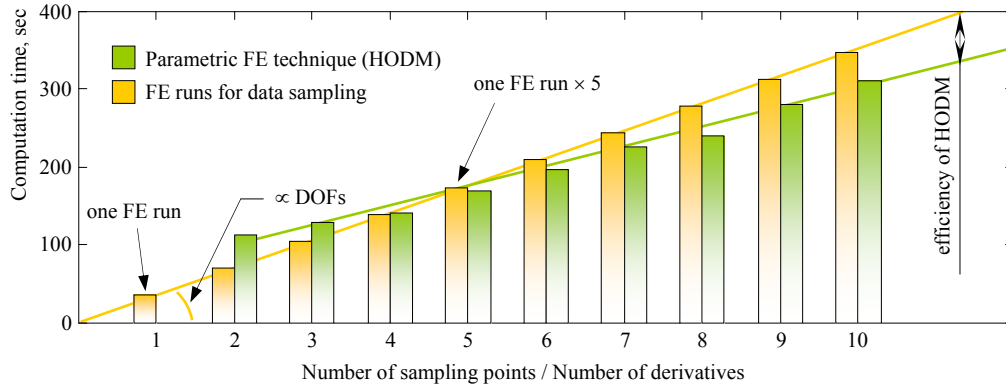


Figure 5.3 Comparison of the time cost between FE-reanalysis and HODM

Benefits of the novel approach compared to ordinary data sampling procedures needed for parametric modeling become obvious for large problems. Hence, the extra time taken for parametric modeling and mesh at the beginning of variational techniques disappears rapidly.

### 5.1.2 Variation in Material Properties

Silicon is an anisotropic material. Dependence of the Young's modulus and Poisson's ratio of the monocrystalline silicon on orientation in (100)-plane can be approximated by equations:

$$E_{(100)}(\theta) = \frac{10^5}{0.768 - 0.704 \cdot \cos^2(\theta) \cdot \sin^2(\theta)}, \quad (5.3)$$

$$\nu_{(100)}(\theta) = \frac{0.214 - 0.708 \cdot \cos^2(\theta) \cdot \sin^2(\theta)}{0.768 - 0.708 \cdot \cos^2(\theta) \cdot \sin^2(\theta)}, \quad (5.4)$$

where  $\theta$  is the orientation angle [12]. It is possible to involve material properties as design parameters taking into account the dependence of a matrix  $\mathbf{D}(E, \nu)$  on the angle  $\theta$ . Dependences of maximal displacement, maximal equivalent stress and strain energy of the uniform loaded silicon beam on crystalline orientation in (100)-plane are shown in Figure 5.4. The difference between the parametric 4<sup>th</sup> order solution and the ordinary FE solution is only 0.5%.

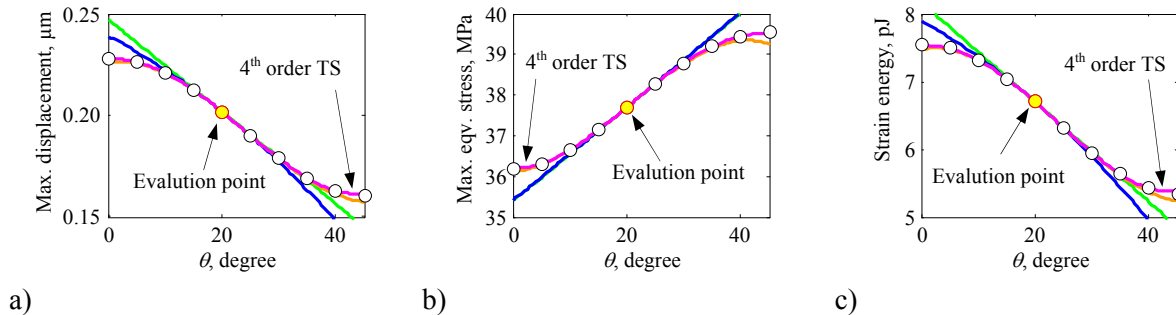


Figure 5.4 Static response: variation in orientation angle

### 5.1.3 Modal Analysis

Parametric modal analysis is important for identification of dimensional parameters by vibration analyses and macromodeling of MEMS [4]. The eigenvectors are  $\mathbf{M}$ -orthonormalized, and the first eigenfrequency of a fixed-fixed beam is considered. Exemplarily, the dependence of first frequency on length of a beam is shown in Figure 5.5a. The analytical solution is described  $f_1(L)$  as  $L^{-2}$  that correspond selected Padé approximant [0/2]. The peak amplitude along of a beam was used for the mode shape estimates, Figure 5.5b. The responses of HODM and ordinary FEA are quite close.

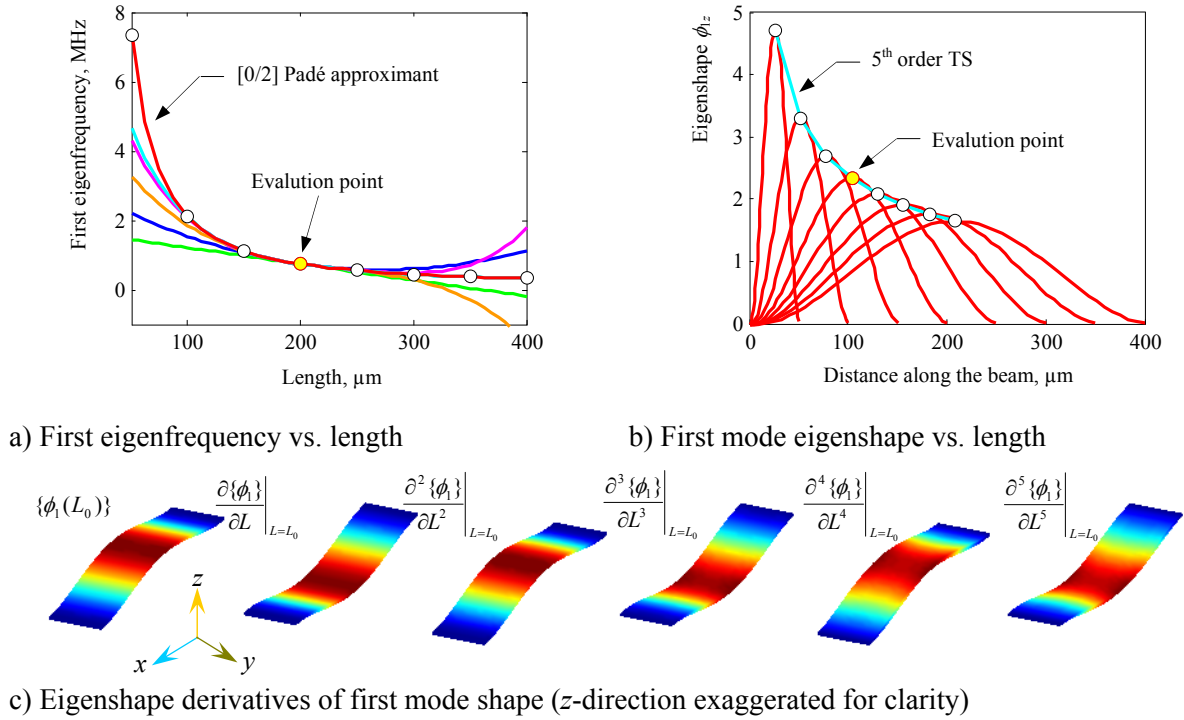


Figure 5.5 Parametric modal study of a fixed-fixed beam

The shape of the mode remains the same whereas the magnitude is different. The eigenvector derivatives of first mode shape are visualized in Figure 5.5c.

### 5.1.4 Harmonic Analysis

The harmonic response analysis is performed over the frequency range [0...15] MHz. The 10 modes have been within this frequency range. The frequency response at the center node along the z direction is presented visualized in Figure 5.6. Results obtained with the FE simulations were compared with the one obtained with HOD method. Padé approximant [8/7] is already sufficient to reproduce the harmonic response of the beam with a relative error smaller than 1%.

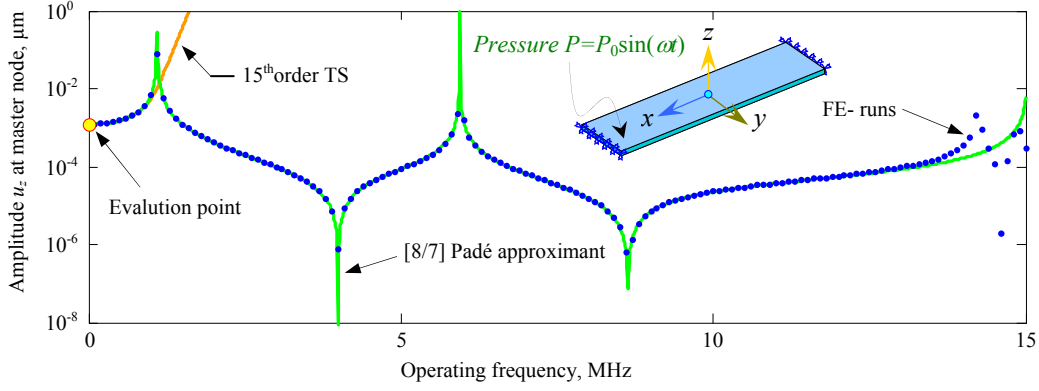


Figure 5.6 Undamped harmonic response of a fixed-fixed beam

## 5.2 Parametric Electrostatic Analysis

The comb-drive consisting of interdigitated fingers is one of the main blocks of MEMS resonators. A comb cell with a large lateral displacement of movable finger was proposed as a benchmark for assessing the accuracy of simulation tool in [4]. Parametric model extraction of the one capacitive cell is selected as an application of the general HOD methodology. Figure 5.7 illustrates the model sketch and FE-mesh of a capacitive cell. The dimensions of the fingers are  $40 \times 4 \times 4 \mu\text{m}$ . The air-gap between the electrodes and the initial electrodes overlap are  $2 \mu\text{m}$  and  $20 \mu\text{m}$ , respectively.

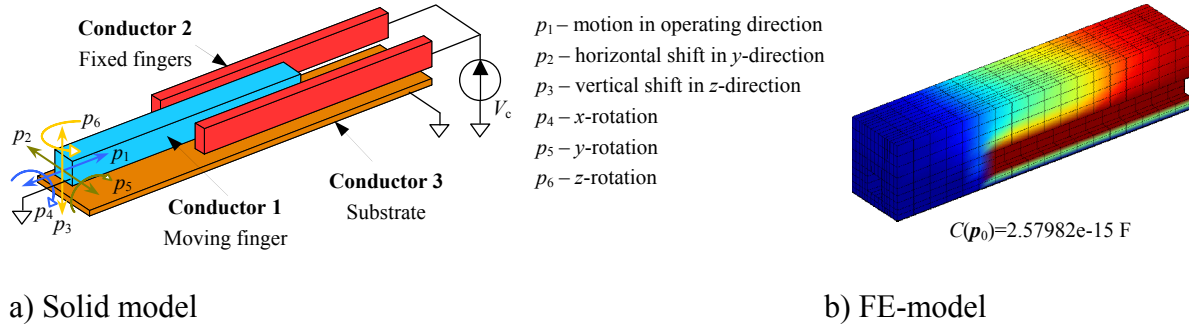


Figure 5.7 Parametric model of a comb cell for computing capacitance stroke functions

The FE-model consists of the 1980 elements and 2682 nodes. Parameterized eight nodes element having one degree of freedom at each node (electrical potential  $\varphi$ ) is used for the analysis. Capacitance stroke functions are directly extracted from the electrostatic field solution based on Laplacian partial differential equation. The system of FE equations can be subdivided into nodes laying on conductor surfaces and nodes in the dielectric region. For capacitance computation, the voltage potential of conductor nodes is entirely constrained and charges on all other nodes become zero. The system of FE equations is written as

$$\begin{bmatrix} \mathbf{K}_{cc} & \mathbf{K}_{ec} \\ \mathbf{K}_{ec} & \mathbf{K}_{ee} \end{bmatrix} \begin{Bmatrix} \mathbf{V}_c \\ \boldsymbol{\varphi}_e \end{Bmatrix} = \begin{Bmatrix} \mathbf{Q}_c \\ \mathbf{0} \end{Bmatrix}, \quad (5.5)$$



where the index  $c$  represents conductor nodes and  $e$  nodes of the electrostatic region (e.g. air). The solution procedure starts with a first step where all unknown potentials are computed:

$$\varphi_e = K_{ee}^{-1}(-K_{ec}V_c). \quad (5.6)$$

A second step the charges on conductor nodes are determined:

$$Q_c = K_{cc}V_c + K_{ec}\varphi_e. \quad (5.7)$$

Note, all vectors and matrices are depended on parameters  $p$ . The six geometrical parameters (motions and rotations of the moving finger) are used to parameterize the cell model. The design velocity field for mesh perturbations is obtained by solving Laplace equation with Dirichlet boundary conditions for outer nodes. The set of matrix derivatives contains the 210 planes, which cover partial derivatives for 4<sup>th</sup> order Taylor expansion with regard to six parameters. The derivatives of electrical potentials vector are extracted at the evaluated point by means of AD according (3.17). Finally, capacitances are extracted from the accumulated charge on conductor surfaces at unit electrical potential  $V_c$ :

$$C(p) = \frac{1}{V_c} \sum_{c \in \text{cond}} \left[ Q_c(p_0) + \sum_{i=1}^n \frac{1}{i!} Q_c^{(i)}(p_0)(p - p_0)^i \right]. \quad (5.8)$$

The capacitance relationships depending on design parameters are illustrated in Figure 5.8.

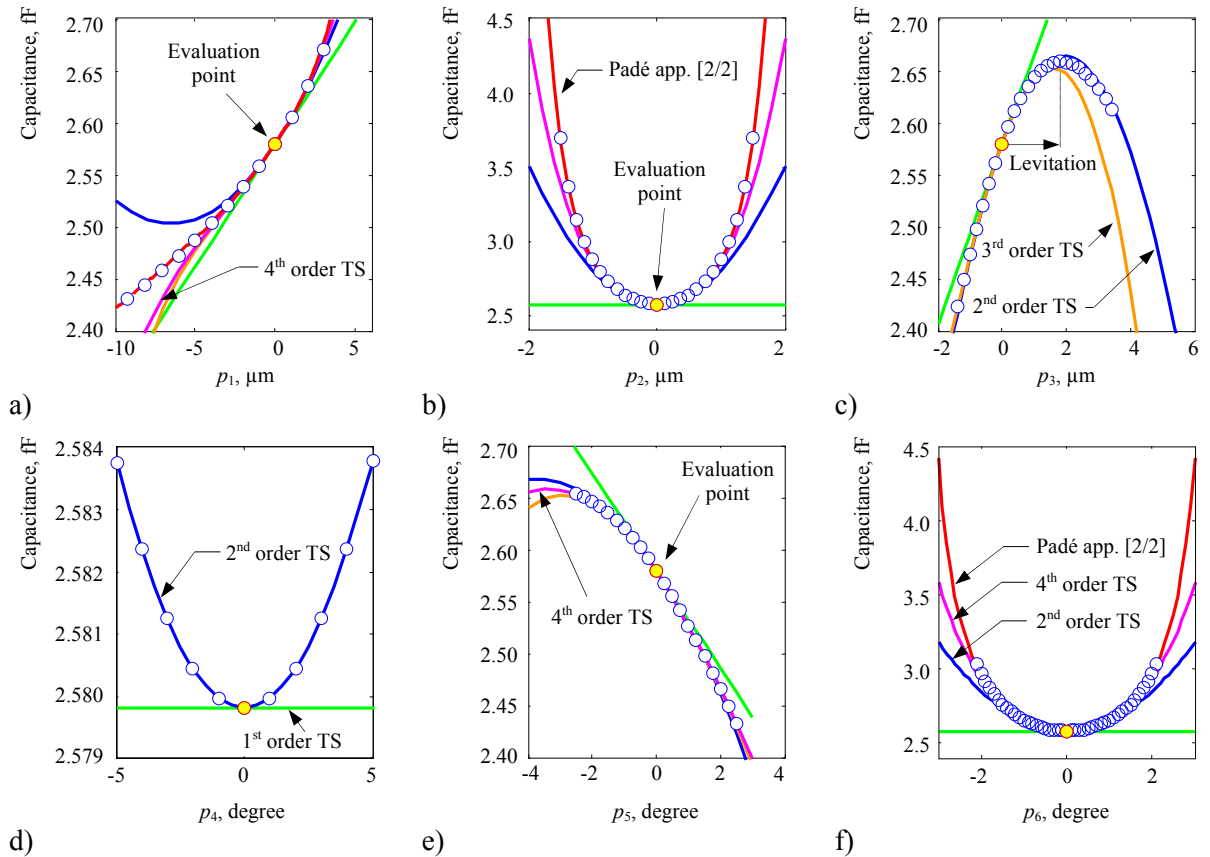


Figure 5.8 Capacitance stroke function of a movable finger with regard to six degrees of freedom

Figure 5.8c shows that the levitation effect of comb cells could be captured well with 2nd order polynomial. The accuracy of parametric results depends mainly on mesh perturbations caused by mapping of global parameter to the nodal table. Figure 5.9 shows the study of the mesh perturbations associated to the design parameter.

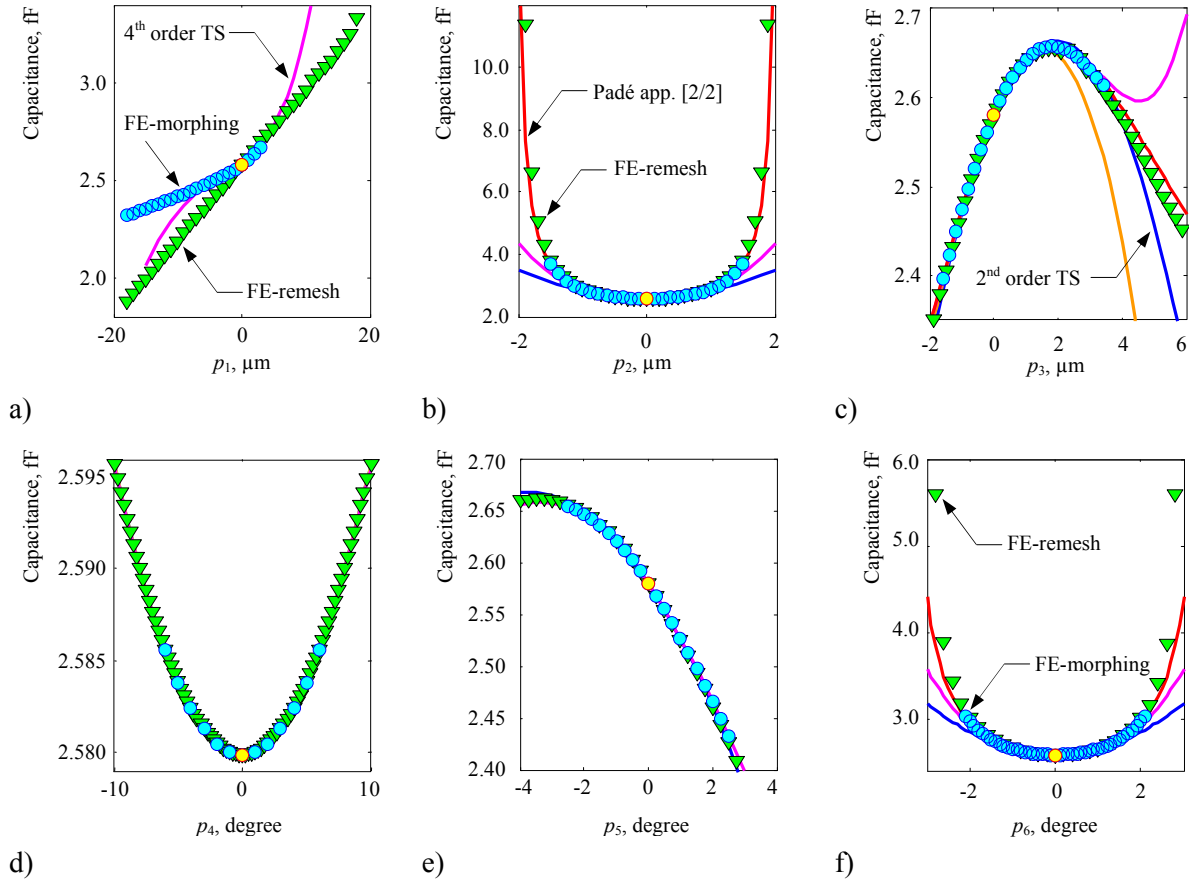


Figure 5.9 Comparison between capacitance functions obtained by different approaches

The obvious disadvantage is that applicable range limited by mesh-morphing procedures. The large mesh perturbation of electrostatic FE mesh is a bottleneck and cannot be applied to parametric analysis, Figure 5.10c.

The domains of practical use, for a reasonable accuracy of 5% with 4<sup>th</sup> order Taylor series, are  $[-2 \dots 2] \mu\text{m}$  in case of the motion in operating direction  $x$ .

It is essential that the obtained parametric solution in polynomial form provides not only capacitance data but also the first and second derivatives needed for Maxwell force and electrostatic softening computations.

The HOD approach can be applied to finger shape optimization with different force profiles.

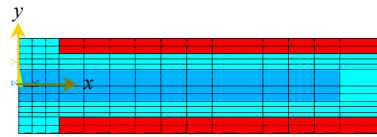
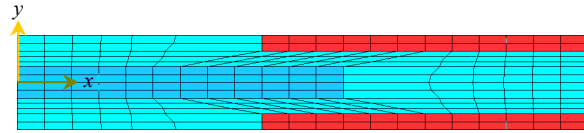
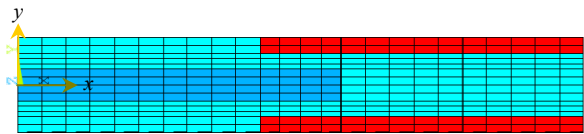
a) Initial FE-mesh  $p_1 = 0 \mu\text{m}$ b) Mesh-morphing  $p_1 = -18 \mu\text{m}$ c) Remesh  $p_1 = -18 \mu\text{m}$ 

Figure 5.10 Comparison between mesh-morphing and remesh approaches

Table 5.2 Parameters summary for a comb cell

Parameter	Eval. point	Parameter variation		Approximation method	Max. relative error of the capacitance, %
		1D variation	6D variation		
motion in operating direction $p_1$ , $\mu\text{m}$	0.0	-10...4	-8.0...8.0	4 <sup>th</sup> order Taylor series	5.0
horizontal shift in $y$ -direction $p_2$ , $\mu\text{m}$	0.0	-1.8...1.8	-1.0...1.0	[2/2] Padé appr.	0.2
vertical shift in $z$ -direction $p_3$ , $\mu\text{m}$	0.0	-1.9...4.0	-1.0...1.0	2 <sup>nd</sup> order Taylor series	0.5
$x$ -rotation $p_4$ , grad	0.0	-5.0...5.0	-1.0...1.0	2 <sup>nd</sup> order Taylor series	0.2
$y$ -rotation $p_5$ , grad	0.0	-2.5...2.5	-1.0...1.0	4 <sup>th</sup> order Taylor series	0.5
$z$ -rotation $p_6$ , grad	0.0	-2.4...2.4	-1.0...1.0	[2/2] Padé appr.	0.2

### 5.3 Parametric Squeeze Film Analysis

Squeeze film analysis simulates the effects of fluid damping of structure moving in small gaps between fixed walls. A harmonic analysis based on linearized Reynolds equation is used to determine the fluid pressure  $P(x,y)$  with regard to frequencies of moving wall [60]. At each frequency step  $\omega_i$ , a following linear system is factorized and solved in order to obtain the complex pressure distribution over the area:

$$\begin{bmatrix} \mathbf{K} & -\omega \mathbf{C} \\ \omega \mathbf{C} & \mathbf{K} \end{bmatrix} \begin{Bmatrix} \mathbf{P}_1 \\ \mathbf{P}_2 \end{Bmatrix} = \begin{Bmatrix} \mathbf{Q} \\ 0 \end{Bmatrix}, \quad (5.9)$$

where  $\mathbf{P}_1$  and  $\mathbf{P}_2$  are the real and imaginary components of the pressure, respectively;  $\mathbf{Q}$  is the nodal volume flow rate vector.

The calculations of the stiffness and damping forces are done by summing the pressure distribution over the area:

$$F_1 = \int_A P_1(x, y) dA. \quad (5.10)$$

$$F_2 = \int_A P_2(x, y) dA. \quad (5.11)$$

The frequency-dependent damping  $c$  and stiffness  $k$  coefficients are extracted by

$$c = \frac{F_1}{v_z}, \quad (5.12)$$

$$k = \frac{F_2 \omega}{v_z}, \quad (5.13)$$

where  $F_1$  is the real part of the pressure force,  $F_2$  is the imaginary part of the pressure force and  $v_z$  is the normal velocity component of the moving structure.

A rectangular plate under transverse motion is modeled by 4-node 3D isoparametric finite element having one degree of freedom at each node (pressure) [107]. The element matrices  $\mathbf{k}$  and  $\mathbf{c}$  are obtained by numerical integration over the element area:

$$\mathbf{k} = \int_A \mathbf{B}^T \mathbf{D} \mathbf{B} dA, \quad (5.14)$$

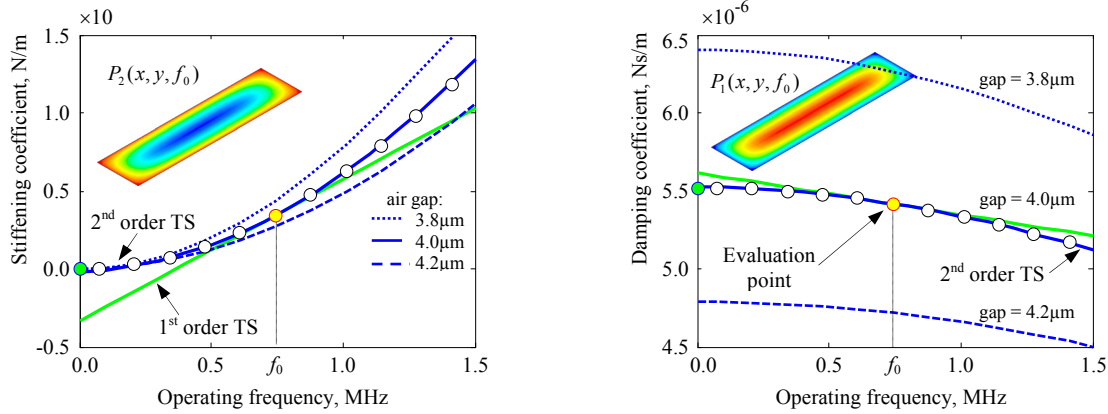
where  $\mathbf{D} = \begin{bmatrix} 1 & 0 \\ 0 & 1 \end{bmatrix} \frac{gap^3}{12\eta}$  is the constitutive matrix, and

$$\mathbf{c} = \int_A \mathbf{N}^T \frac{gap}{P_{amb}} \mathbf{N} dA. \quad (5.15)$$

The element volume flow rate vector is computed from the velocity body loads (wall velocity in normal direction  $v_z$ ) according to Equation (4.17). The pressure at edges  $P_{amb} = 101$  kPa and the fluid dynamic viscosity  $\eta = 18.3 \times 10^{-12}$  kg/ $\mu$ m/s are assumed. The initial air gap height is 4.0  $\mu$ m, which makes the Knudsen number of the air gap flow  $Kn$  to be 0.016 and the conti-

num theory based on a modification of the dynamic viscosity is used [107]. The estimated stiffness and damping coefficients are 3.43 N/m and  $5.4 \times 10^{-6}$  Ns/m, respectively. The computed effective damping and squeeze stiffness coefficients are shown in Figure 5.11. The obtained results and analytical solution according to Blech [108] for a rigid plate moving with a transverse motion are quite close. The HOD approach correctly takes into account the frequency-dependence in a single FE run. The derivatives of the real  $P_1^{(n)}$  and imaginary  $P_2^{(n)}$  parts of the pressure with respect to frequency are extracted from (5.9) by means HODM. In next step, the derivatives of nodal damping force vector  $F_1^{(n)}$  and  $F_2^{(n)}$  are computed from (5.10) and (5.11), respectively.

Figure 5.11 shows that the frequency-dependence of the damping and squeeze stiffness coefficients could be captured well with 2<sup>nd</sup> order TS. First eigenfrequency is used as an evaluation point. The agreement is very good at low frequencies and fair at eigenfrequencies. The difference between the parametric and ordinary FE solutions is 1.8%.



a) Squeeze stiffness coefficient vs. frequency

b) Damping coefficient vs. frequency

Figure 5.11 Squeeze film analysis of a rectangular plate

## 5.4 Advanced Examples

This subsection presents several advanced topics related to MEMS simulation. The first example is a discrete analysis. The next examples are a substructuring technique and a parameterized sequential coupled FE-analysis. Finally, a nonlinear structural FE-analysis is presented.

### 5.4.1 Discrete Analysis: Perforated Beam

Perforations are widely used in MEMS for several reasons. The main purpose is to decrease the damping and spring forces of vibrating structures due to the gas flow in small air gaps. The second goal is to increase eigenfrequency due to reduce the total mass of structures. The following example builds a perforated beam with circular holes having a radius of 25 μm. The five holes are set as discrete variables, allowing simulating the effects caused by removing holes. For  $n$  discrete parameters, the  $2^n$  configurations can be explored at one solution step.

The aim of this example is to illustrate how the results of Sections 5.1 can be used in discrete analysis. The five holes are group into three element components as shown in Figure 5.12. For the present study, the 8 configurations have been explored. The initial point  $p = \{1,1,1\}$  was used for extracting the derivatives of solution vector. The obtained parametric solution is shown in Figure 5.13. Numerical tests have shown that in case of pressure load also needs to correct the pressure for removing area. Then  $p_i \rightarrow 0$ , the surface load applied to the  $i$  elements component must have zero contributes in order to extract a correct parametric solution. Table 5.3 resumes the available configurations found from discrete analysis. The histogram in Figure 5.14 visualizes obtained results. All units are normalized to the maximal values in terms of relative values. Different optimization methods such as Monte-Carlo or genetic algorithms can be used to determine the best configuration using this parametric database.

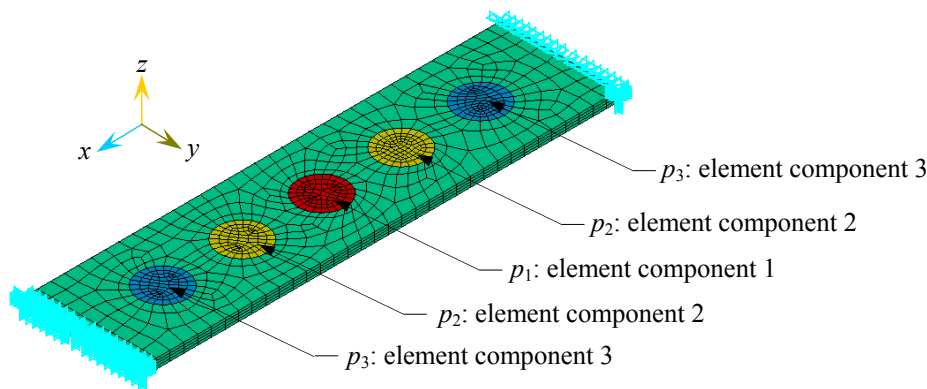


Figure 5.12 FE-model of a perforated beam for discrete analysis

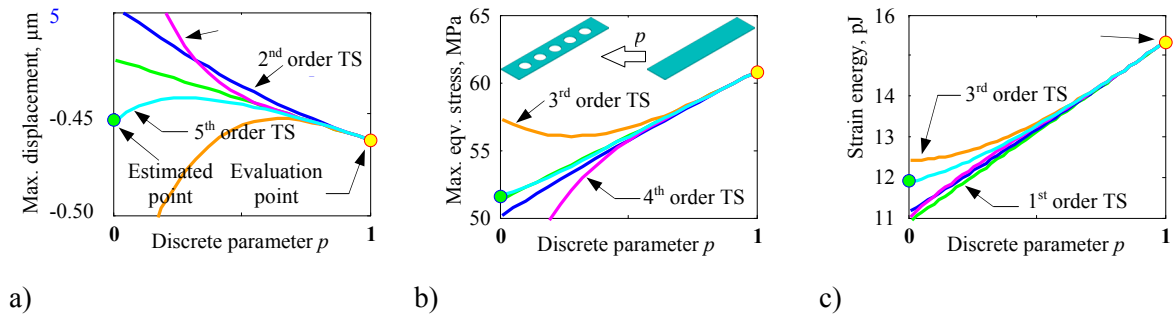


Figure 5.13 Results of a discrete static analysis of a perforated beam

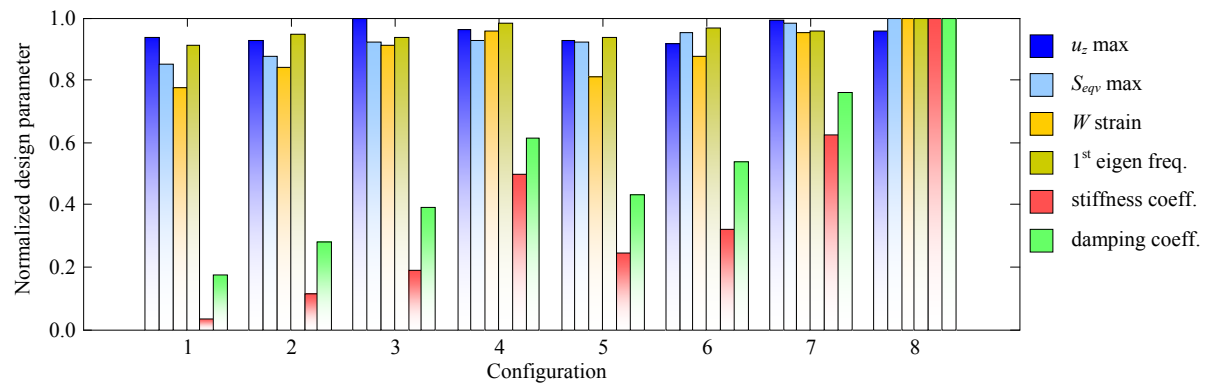
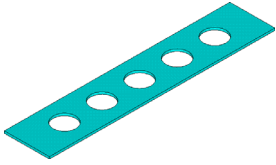
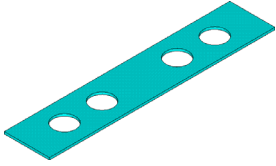
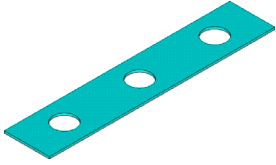
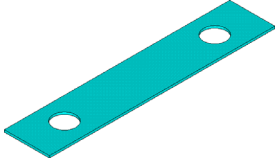
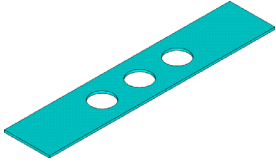
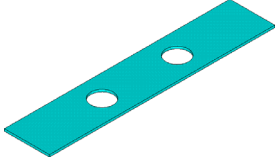
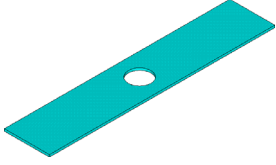
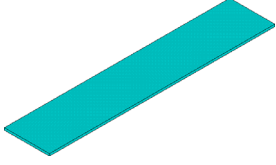


Figure 5.14 Histogram: Discrete analyses of a perforated beam

Table 5.3 Results summary of the discrete analyses of a perforated beam

Configuration	Parameter			Max displacem.	Max eqv. stress	Strain energy	First eigen freq.	Stiffness coeff.	Damping coeff.	Model
	$p_1$	$p_2$	$p_3$							
1	0	0	0	0.94	0.85	0.84	0.91	0.03	0.17	
2	1	0	0	0.92	0.88	0.78	0.95	0.11	0.28	
3	0	1	0	1.00	0.92	0.91	0.94	0.19	0.39	
4	1	1	0	0.96	0.93	0.96	0.98	0.50	0.61	
5	0	0	1	0.93	0.92	0.81	0.94	0.24	0.43	
6	1	0	1	0.92	0.95	0.88	0.97	0.32	0.54	
7	0	1	1	0.99	0.98	0.95	0.96	0.62	0.76	
8	1	1	1	0.96	1.00	1.00	1.00	1.00	1.00	

### 5.4.2 Substructuring Technique: Folded-Flexure Resonator

The objective here is to illustrate that the CMS analysis of eigenfrequencies can be carried out in an accurate way based on the results of parameterized superelements. The resonator is divided into two superelements as depicted in Figure 5.15a. Sensitivity analysis of the folded spring element is performed in order to better understand what will be the real impact for each parameter. Note that sensitivity curves do not require the parametric coupling computations.

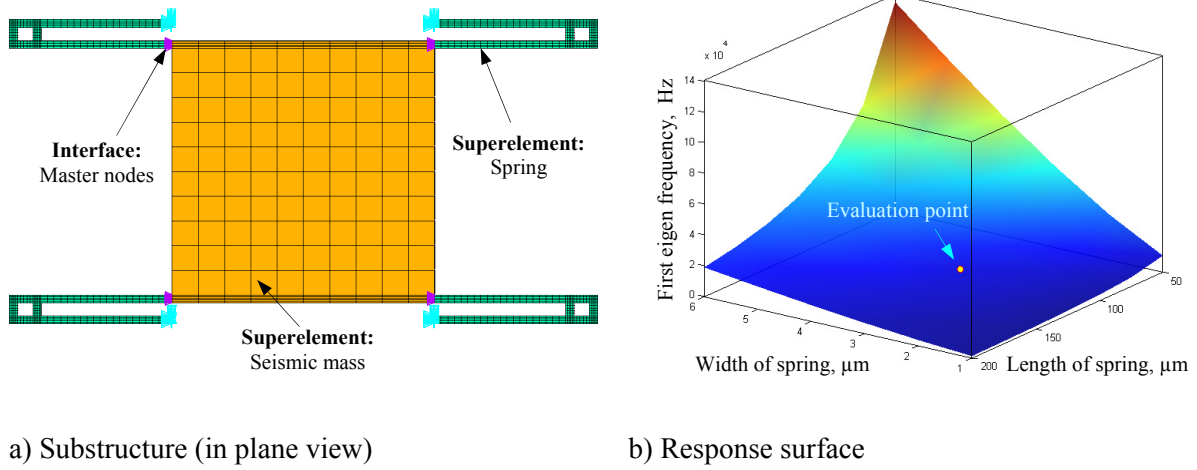


Figure 5.15 Folded-flexure resonator

The length and width of the spring were selected as design parameters. The extracted response surface for the first eigenfrequency by parametric modal FE analysis is shown in Figure 5.15b. The result demonstrates that the eigenfrequency could be captured correctly by polynomial of degree [4,4].

### 5.4.3 Parametric Sequential Coupled Analysis: Piezoresistive Element

The coupled-field FE matrix for the piezoresistive analysis is given by

$$\begin{bmatrix} \mathbf{K}_S & 0 \\ 0 & \mathbf{K}_G \end{bmatrix} \begin{Bmatrix} \mathbf{u} \\ \boldsymbol{\varphi} \end{Bmatrix} = \begin{Bmatrix} \mathbf{F} \\ \mathbf{I} \end{Bmatrix}, \quad (5.16)$$

where  $\mathbf{K}_S$  is the stiffness matrix,  $\mathbf{K}_G$  is the conductivity matrix,  $\mathbf{I}$  is the nodal current vector and  $\boldsymbol{\varphi}$  is the nodal electric potential vector [55].

The piezoresistive coupling problem (5.16) is solved sequential for two iterations. At the first step nodal displacements, under action of external mechanical load are computed:

$$\mathbf{u} = \mathbf{K}_S^{-1} \mathbf{F}. \quad (5.17)$$



Then the elements stress at the gauss points is calculated by (3.16). At the second step a distribution of electrical potentials in the deformed body are calculated:

$$\varphi = \mathbf{K}_G^{-1} \mathbf{I}. \quad (5.18)$$

As sensitive element *p*-type silicon layers on an *n*-type substrate are widely used [109, 110]. In *p*-type silicon, strains cause a change of electric conductivity:

$$\mathbf{G} = \mathbf{G}^0 + \mathbf{G}^1, \quad (5.19)$$

where  $\mathbf{G}^0 = g_0 \{1 \ 1 \ 1 \ 0 \ 0 \ 0\}^T$  is the vector of conductivity matrix components and  $g_0$  is the specific conductivity, and

$$\mathbf{G}^1 = -\mathbf{G}^0 [\pi^1] \boldsymbol{\sigma}, \quad (5.20)$$

where  $[\pi^1]$  is the piezoresistive matrix.

The silicon cantilever  $3000 \times 1000 \times 30 \mu\text{m}$  with the four-terminal piezoresistive element have been used as test object, Figure 5.16. The cantilever is oriented along the crystallographic direction  $[100]$ . The piezoresistive element is a *p*-type layer and is oriented at a  $45^\circ$  angle to the sides of the cantilever. The sensing element is a plate of length  $L$  with four contacts of width  $B$  located at the ends of the plate. A supply voltage  $V_s$  is applied to the electrodes to produce a current in the length direction of the plate. The mechanical stress in the sensing element generates a proportional transverse electric field in the width direction. This signal is detected from the two output conductors.

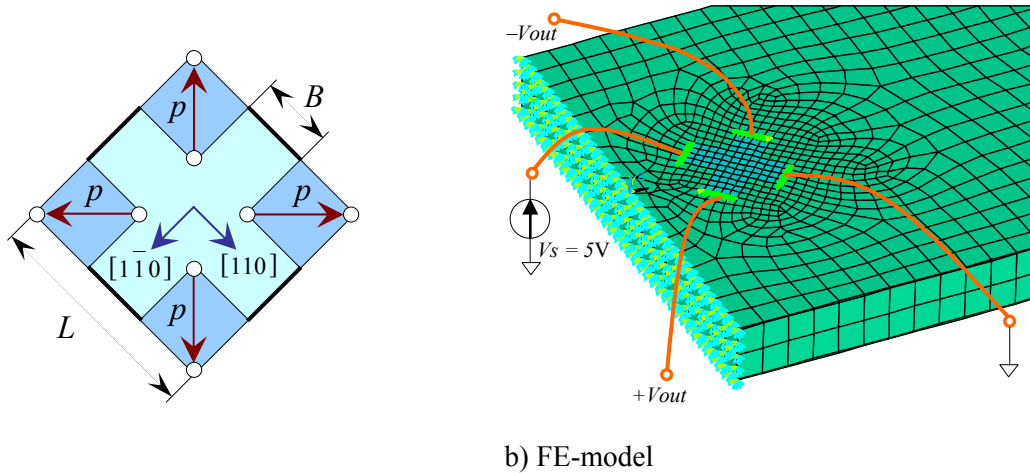


Figure 5.16 Parameterized four-terminal piezoresistive element

Here HOD technique is extended on the sequential coupled problem: calculation the derivatives of secondary variables (strains, stresses) and material properties with regard to design parameters  $p$  under mechanical load. At the second step the derivatives of electrical potentials in the deformed sensitive element are extracted, using the derivatives of conductivity matrix

$\mathbf{G}$  as input data. With the help of developed AD matrix rules, the parametric sequential coupled algorithm is introduced below.

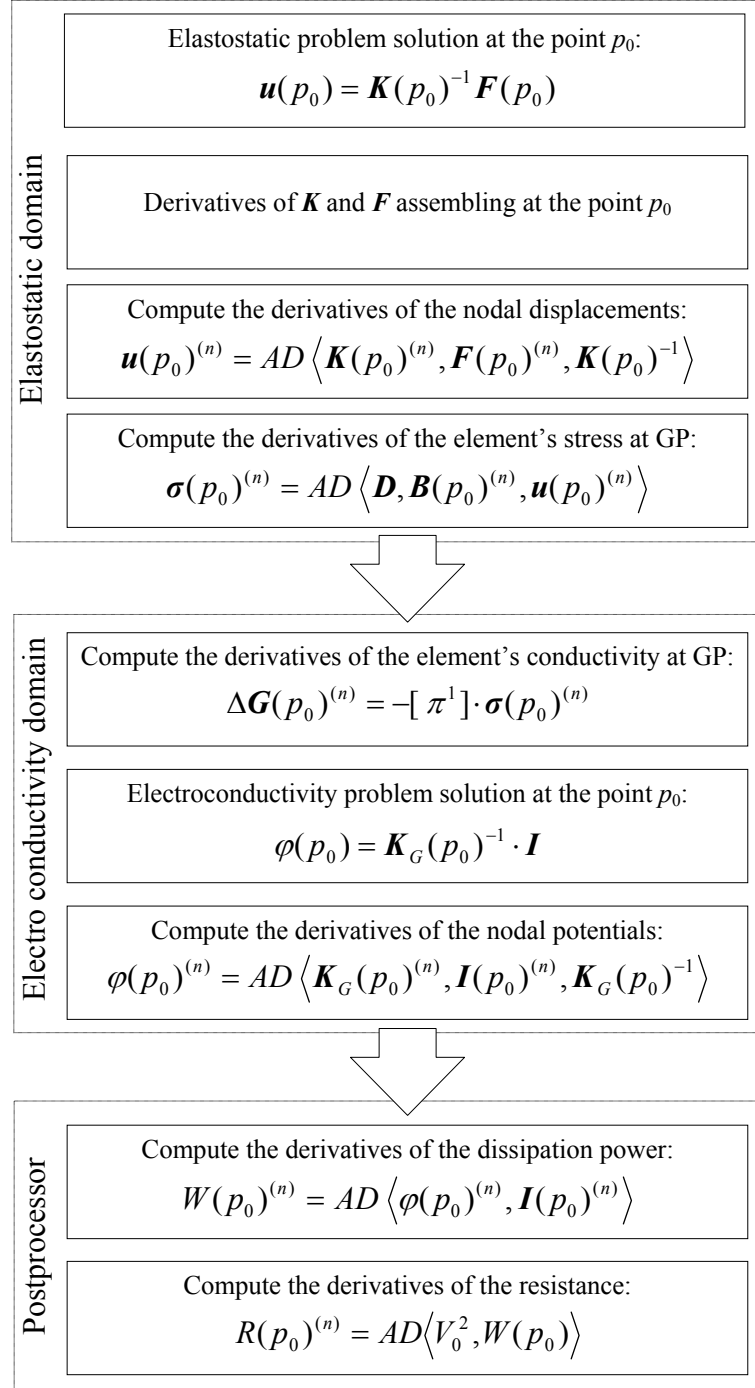


Figure 5.17 Parametric sequential coupled algorithm

The shape of the sensing element is used as design parameter for the optimizations, as shown in Figure 5.16a. Figure 5.18 presents data from numerical studies of problem. First, these results demonstrate that HOD methods are capable of good precision for coupled analysis. Second, the present optimization finds an optimal shape of the sensing element. There are two different optimal shapes of sensing element depend on type of power source. HOD technique allows finding optimum configurations very efficiently.

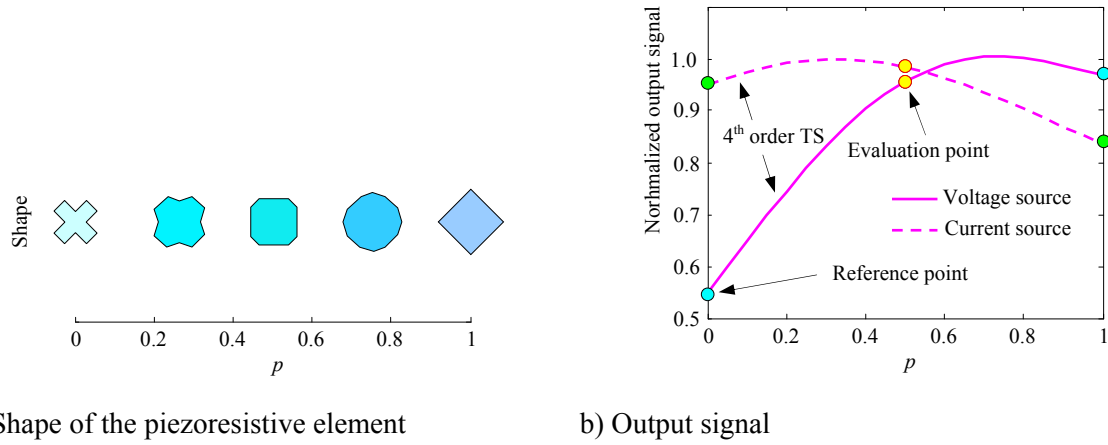


Figure 5.18 Parametric analysis of a four-terminal piezoresistive element

#### 5.4.4 Non-Linear Static Analysis: Semiconductor Microtube

Semiconductor microtubes, fabricated by selective underetching and releasing of a strained bilayer from a substrate, have attracted much attention due to their possible integration into semiconductor technology. The built-in mechanical strain is a driving force of the rolling-up micro- and nanostructures. The residual mechanical strain of the rolled-up microtubes is subject of a number of theoretical and experimental studies [111, 112].

GaAs/ $\text{In}_{0.15}\text{Ga}_{0.85}\text{As}$  bilayer-based structures were grown by molecular beam epitaxy on GaAs substrate. The sacrificial AlAs layer with a thickness of 10 nm was deposited onto substrates before growth of the bilayers. After removing the sacrificial layers by selective etching rolled-up microtubes were formed. A schematic of a microstructure is presented in Figure 5.19a.

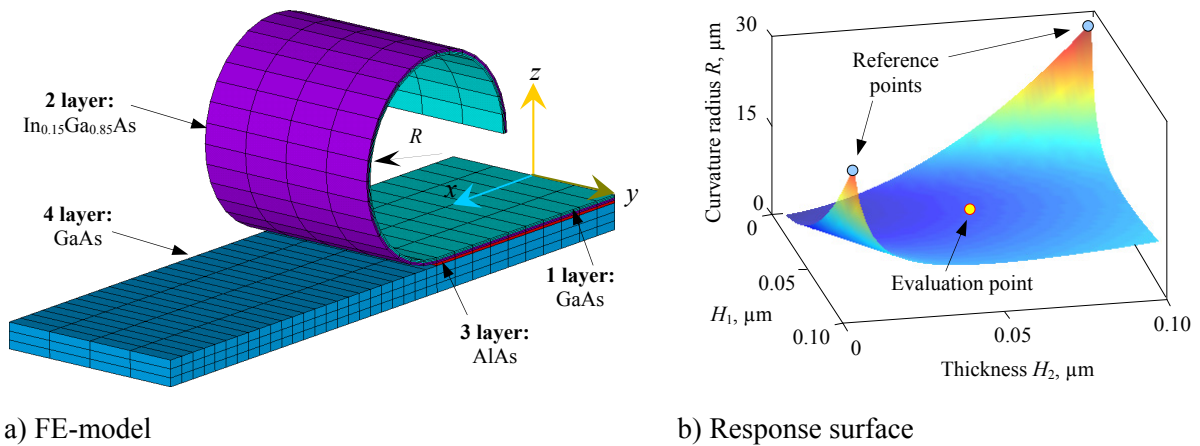


Figure 5.19 Semiconductor microtube

The bilayer structure is modeled with 20-node hexagonal isoparametric elements. Fixed boundary conditions are applied along at the end of the structure. The total number of the elements used in the model is approximately 1000. The material database [113] is used to provide the mechanical properties information for numerical simulation. It is assumed that rotations and translations are large but strains are small. This makes the problem geometrical-

ly nonlinear. Finite element procedures for solution of geometrically nonlinear problems have been considered by Bathe [96]. The nonlinear equation relating load and displacement increments looks like follows:

$${}^i\mathbf{K}_\tau \Delta \mathbf{u} = {}^{i+1}\mathbf{F}_a - {}^i\mathbf{F}_r. \quad (5.21)$$

Here  ${}^i\mathbf{K}_\tau$  is the tangent stiffness matrix at step  $i$ ,  $\Delta \mathbf{u}$  is the nodal displacement increment,  ${}^{i+1}\mathbf{F}_a$  is the applied load vector at next step  $i+1$ , and  ${}^i\mathbf{F}_r$  is the vector of nodal internal forces that correspond to the current stress state at step  $i$ . The tangent stiffness matrix  $\mathbf{K}_\tau$  is a sum of two matrices: the usual linear stiffness matrix  $\mathbf{K}$  and the nonlinear addition  $\mathbf{K}_S$  depending on the stress state:

$$\mathbf{K}_\tau = \mathbf{K} + \mathbf{K}_S. \quad (5.22)$$

The nonlinear element stress stiffness matrix  $\mathbf{k}_S$  is defined in Appendix A.5. Nodal internal forces are obtained by integration of stresses over the current element volume:

$${}^i\mathbf{f}_r^{el} = \int_{{}^iV} \mathbf{B}^T {}^i\boldsymbol{\sigma} dV. \quad (5.23)$$

The difference in lattice constants creates the initial strain in the lower strain layer

$$\boldsymbol{\varepsilon}^0 = (a_2 - a_1)/a_1. \quad (5.24)$$

The initial strain  $\boldsymbol{\varepsilon}^0$  of 1.08% is divided into  $n$  increments. At each step, an increment the nodal stretching forces, which correspond to an increment of the strain were computed by (4.19) and applied to the elements of the lower layer. After that, iteration (5.21) is solved. Coordinate update is performed at each iteration.

The parametric and ordinary analyses for the microstructure with different thickness of layers were performed. The thickness of GaAs/InGaAs layers was varied from 5 to 100 nm. The curvature radius  $R$  of a bilayer tube can be estimated with [111]

$$R = \frac{E_1^2 t_1^4 + E_2^2 t_2^4 + 2E_1 E_2 t_1 t_2 (2t_1^2 + 2t_2^2 + 3t_1 t_2)}{6E_1 E_2 t_1 t_2 (t_1 + t_2)} \boldsymbol{\varepsilon}_2^0. \quad (5.25)$$

The dependence of the curvature radius  $R$  on the thickness of layers is presented in Figure 5.19b where the values of  $R$  determined by the parametric method are compared with FEM data at references points. Equation (5.25) was used to select an appropriate approximation. The results showed excellent agreement. The values obtained by parametric modeling are about 3% lower than correspondent referenced FE values.

## 5.5 Discussion on Examples

The results from numerical case studies of test problems have been presented in this chapter. The examples demonstrate the accuracy of the implemented HOD methods for parametric FE analysis of static, modal, and harmonic problems in structural, electrostatic, fluidic and coupled domains.

As illustrated in the chapter, the HOD parametric FE analysis are a promising alternative to existing data sampling and function fit procedures utilized for MEMS parametric model extraction from ordinary FE analyses. By using the HOD method, the simulation results become directly polynomial or rational functions in terms of design parameters. Polynomials are very convenient since they can capture smooth functions with high accuracy. E.g. the strain energy functions are inherent polynomials. Comparisons with ordinary FE results have been used to validate the accuracy of the parameterized solutions, where up to 5<sup>th</sup> orders polynomials have been computed. Padé approximant allows extending of the acceptable parameter range. The disadvantage is that Padé approximants do not have a global error estimate, and hence it is necessary to select the order manually. It is vital to choose a proper order. From univariate rational approximation theory it is known that for some classes of functions, the most accurate rational models exhibiting the smallest truncation error, are the ones with approximately equal numerator and denominator degree [74].

In cases where the large lateral perturbations of the FE mesh, the HODM method has been shown to be prone to yield erroneous results. This is demonstrated for electrostatics analysis of a capacitive cell in Section 2.2. In this case the solution can be approximate in few subdivided interval by Taylor expansions that must be matched on overlapping intervals. An alternative to the approximation of the solution in the form of a piecewise polynomial in several subintervals is considered in [73] that simplifies the computations.

The benefits of parametric technologies compared to ordinary data sampling procedures become obvious for multi-parametric problems. The method is also very efficient for large matrices, because the factorization of the system increases with the matrix dimensions. It is necessary to point out the need for additional system memory and for parametric mesh-morphing procedures. Further, optimization methods of high order can be applied to parametric results, which have significantly higher convergence speed.

Usually, the design parameters values are randomly scattered and defined by probability distributions. A few thousands MCS are performed to proof the interplay of packages and transducers with the electronic circuit [36]. For this purpose, the profits of using HODM are evident.

The presented approach to parametric analysis based on differentiation of element matrices has been shown to yield accuracy for all studies made and must be recommend a very reliable tool in MEMS design.



## 6. Application of HODM to MEMS Macromodeling

*The objective of this chapter is to demonstrate the viability of HOD method for automated MEMS macromodel generation using a single FE run for ROM data extraction, which allows accelerating the generation of macromodel. In the second part, HOD technique is applied for extraction geometrically parameterized reduced order models model of the MEMS components. The parameterization of the mode superposition based reduced order models in the coupled-physics domains, numerical details, accuracy and observed problems are demonstrated by the macromodel generation procedure of an electrostatically actuated fixed-fixed beam.*

### 6.1 Generation of MEMS Macromodels Using HODM

The ROM generation pass from the series of FE runs is computationally expensive. Alternatively to the data sampling techniques, derivatives based approach for behavioral model extraction and building response surfaces is investigated.

This information is gathered in a so-called ROM model *Generation Pass* [43]. The following diagram explains the generation process, Figure 6.1. A test load is applied to the model to simulate the primary motion of the device. Then a modal analysis is performed to compute the mode shapes  $\phi_i(x,y,z)$ . The test load deflection  $\mathbf{u}(x,y,z)$  is compared with the mode shapes  $\phi_i(x,y,z)$  in order to select modes which become the state variables of the macromodel.

A time consuming FE data sampling process can be replaced by single parametric FE runs in structural, electrostatic and fluid domains. The characterizing parameters of electromechanical system must be captured in modal coordinates. Now the extraction process of the characterizing parameters like strain energy, capacitances and damping parameters is considered in detail.

#### 6.1.1 Extraction of Strain Energy Functions

A set of the higher order derivatives of the reaction force vector  $\mathbf{F}^{(n)}$  at the point  $q_0$  is obtained by performing a parametric linear analysis (small signal case) in structural domain. The nodal displacements  $\mathbf{u}(x,y,z)$  is applied as load. The displacements are given by (2.3). The eigenvector  $\phi_i(x,y,z)$  is normalized with respect to its largest element. The derivatives of the displacements vector  $\mathbf{u}^{(n)}$  with regard to  $q_i$  can be computed from (2.3) analytically. The derivatives of strain energy  $W_{SENE}$  are extracted from the matrix-vector product  $\mathbf{u}^T \mathbf{K} \mathbf{u}$  by means of AD. Taylor series coefficients of strain energy ( $W_{SENE}(q_0)^{(i)} / i!$ ) are store in ROM database for further use.

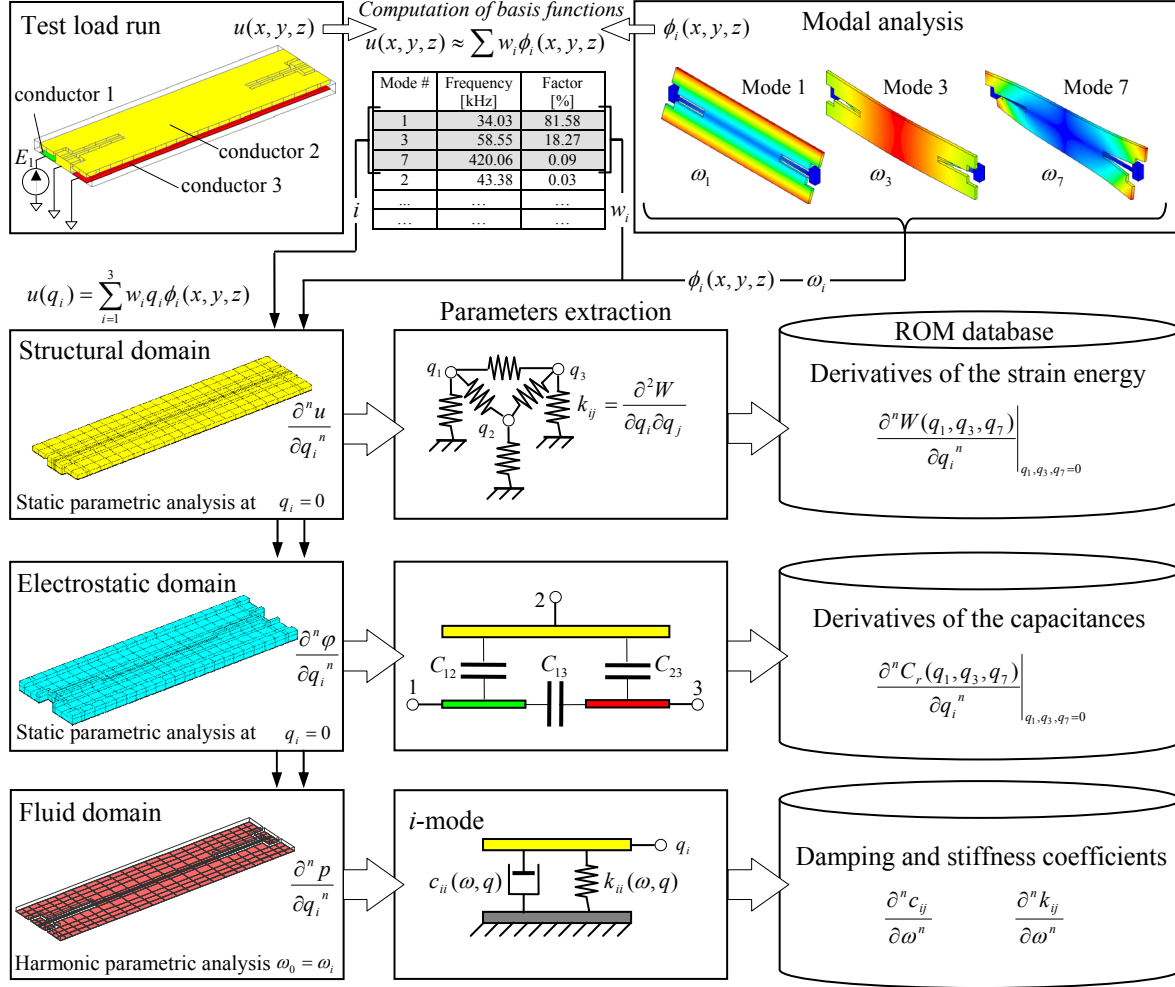


Figure 6.1 Overview of the data generation for MEMS reduced order macromodel by HOD technique

### 6.1.2 Extraction of Capacitance Functions

Capacitance stroke function is directly extracted from the electrostatic field solution based on Laplacian differential equation as described in Section 5.2.

### 6.1.3 Extraction of Modal Damping Parameters for Squeeze Film Problems

A harmonic analysis based on Equation (2.9) is used to determine the fluid pressure  $\mathbf{P}(v)$  with the normal velocity component of the moving structure defined by  $v_z(x, y) = \phi_i(x, y, z_{neut}) \cdot \text{const.}$  The derivatives of the real  $\mathbf{P}_1^{(n)}$  and imaginary  $\mathbf{P}_2^{(n)}$  parts of the pressure with respect to frequency are extracted by (5.9). In next step, the derivatives of nodal damping force vector  $\mathbf{F}^{(n)}$  are computed by means AD from (5.10). Finally, the derivatives of the damping  $c^{(n)}$  and stiffness  $k^{(n)}$  coefficients of each mode can be found on the main diagonal terms:



$$c_{ji}^{(n)}(\omega) = \frac{\phi_j^T}{\dot{q}_i} F_1^{(n)}(\omega) \quad (6.3)$$

and

$$k_{ji}^{(n)}(\omega) = \frac{\phi_j^T}{\dot{q}_i} \frac{\partial^n (\omega F_2(\omega))}{\partial \omega^n}. \quad (6.4)$$

### 6.1.4 Example

An example for assessing the accuracy of reduced order models is a micromirror with two degrees of freedom, the transversal shift and tilt angle [43, 114]. The coupled FE-model consists of the 3844 elements, 5733 nodes. Three conductors with three capacitance functions are involved. The following model considers the three modes: torsion mode, transversal mode in  $z$ -direction and one mode responsible for plate warp, Figure 6.1.

In order to obtain the strain energy and capacitance information in the modal space, the movable structure must be displaced to linear combinations of considered eigenmodes. The perturbations of internal nodes with respect to modal amplitude  $q_i$  as parameter are obtained by solving Laplace equation with Dirichlet boundary conditions for outer nodes [71].

The results from numerical studies of test problems in linear static and harmonic structural domains are presented in Figure 6.1. This results were computed on a desktop PC with Intel® Core™ Duo CPU T2300@1.66GHz and 2.00 Gb RAM running Microsoft® Windows® XP. Comparisons with ordinary FE results have been used to validate the accuracy of the parameterized solutions.

Capacitance stroke functions and strain energy terms have been computed for three modes: 1, 3 and 7 up to order four ( $\mu_1 + \mu_3 + \mu_7 \leq 4$ ). The differential tuples contain  $R = 35$  planes, according to (4.21), which cover partial derivatives for Taylor series expansion. The number of differential planes is comparable with the number of samples required for polynomial interpolation assuming 35 sample points for three modes:

$$C(q_1, q_3, q_7) = c_0(q_1^0, q_3^0, q_7^0) + \sum_{i=0}^R c_i q_1^{\mu_1(i)} q_3^{\mu_3(i)} q_7^{\mu_7(i)}. \quad (6.5)$$

The 125 orthogonal sampling points (5 sample points for each mode) are used for the function fit method. Figure 6.2 shows that the response functions for capacitance and strain energy can be captured correctly with order two. The relative errors are less than 0.8 %.

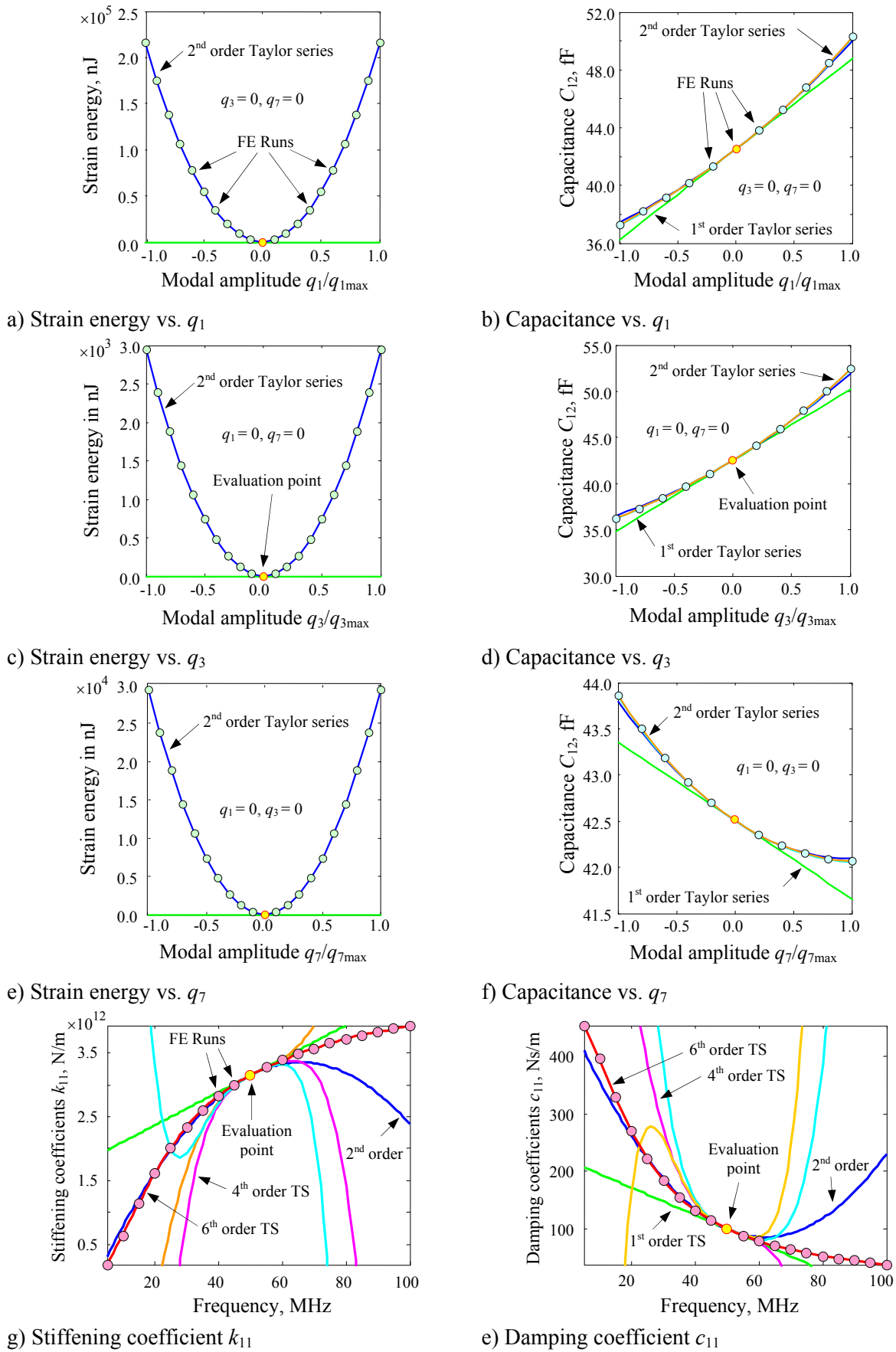


Figure 6.2 Accuracy of HOD method compared to ordinary FE sampling for ROM

In small signal case, the dependence of squeeze parameters on the film thickness can be not taken into account. The HOD approach correctly captures the frequency-dependence of stiffness and damping coefficients in a single FE run. Exemplarily, dependence of damping coefficients  $c_{11}$  on frequency is shown in Figure 6.2e. Numerical results demonstrate that the generated models are highly accurate in a wide range of modal amplitudes.

The computation times are summarized in Table 6.1.

Table 6.1 Summary of computation times: small signal case; number of modes = 3 (1,3,7)

ROM Generation Pass	Type of element	Number of elements	Number of nodes	Time, s		
				Data sampling		HODM
Structural domain Electrostatic domain	8-node solid	624	1197	<i>35 points</i> 1050	<i>125 points</i> 3750	<i>4<sup>th</sup> order</i> 880
	20-node solid	2932	5223	1522	5375	1175
Fluid domain	4-node shell	288	371	<i>8 points</i> 9.1	— —	<i>6<sup>th</sup> order</i> 12
				2581.1	9125	2067
Total	—	3844	5733	2581.1	9125	2067

Table 6.1 shows that computing time for one parameter (squeeze film analysis  $c_{11}(f)$ ,  $k_{11}(f)$ ) was still lower compared to the HOD approach. The reason is the overhead for computing derivatives of functions. On the other hand, data acquisition time of sample methods grows exponentially if more variables are taken into account. For the parametric analysis of linear systems, the reduction in expected computing time is at least a factor of two.

## 6.2 Parameterization of MEMS Reduced Order Models

### 6.2.1 Algorithm Description

The equilibrium equation of an electrostatically actuated flexible structure can be rewritten in parameterized form as follows:

$$m_i(p)\ddot{q}_i(t) + 2\xi_i(q(t), p)\omega_i(p)m_i(p)\dot{q}_i(t) + f_r(q(t), p) = f_{elec}(t, q(t), p) + f_q(t, p), \quad (6.6)$$

where

$$f_r(q(t), p) = \frac{\partial W_{SENE}(q, p)}{\partial q_i} \quad \text{is the internal modal force;}$$

$$f_{elec}(t, q(t), p) = \frac{1}{2} \sum_r \frac{\partial C_{ks}(q, p)}{\partial q_i} (V_k(t) - V_s(t))^2 \quad \text{is the actuated electrostatic modal}$$

force and  $f_q$  is the external modal force. A set of modal coordinates  $q_i(\mathbf{p})$  is define by

$$u(x, y, z, t, \mathbf{p}) = \sum_{i=1}^m \phi_i(x, y, z, \mathbf{p}) q_i(t, \mathbf{p}). \quad (6.7)$$

The basic steps in performing the parametric ROM generation process are as follows:

1. Create the fully-meshed FE-model of coupled-domain device
2. Mesh parameterization  $\{x_i(\mathbf{p}), y_i(\mathbf{p}), z_i(\mathbf{p})\}$  with regard to geometrical design parameters
3. Assembling of the system matrices and its derivatives  $\mathbf{M}(\mathbf{p})^{(n)}$  and  $\mathbf{K}(\mathbf{p})^{(n)}$  with regard to design parameters  $\mathbf{p}$
4. Assembling load force vectors and its derivatives  $\mathbf{F}(\mathbf{p})^{(n)}$  with regard to design parameters  $\mathbf{p}$
5. Perform ordinary modal analysis at the point  $\mathbf{p}_0$ :  $(\lambda_i(\mathbf{p}_0), \phi_i(\mathbf{p}_0))$
6. Selection of the  $m$  appropriate modes and their operating range  $q_{imax}$
7. Parameterization of the eigenvalues  $\lambda_i(\mathbf{p})$  and eigenvectors  $\phi_i(\mathbf{p})$
8. Re-parameterization of the system matrices  $\mathbf{K}(q_1, q_2, \dots, q_m, \mathbf{p})$  with respect to modal amplitude  $q_i$  and design parameters  $\mathbf{p}$
9. Extraction of strain energy  $W_{SENE}(q_1, q_2, \dots, q_m, \mathbf{p})$ , capacitance functions  $C_r(q_1, q_2, \dots, q_m, \mathbf{p})$  and modal damping parameter  $\xi_i(q_i, \mathbf{p})$  with regard to modal amplitude  $q_i$  and design parameters  $\mathbf{p}$ .

As a first step, a solid model of the structure and the electrostatic field surrounding the structure is build. It is assumed that the mode set is not changed during parameter variation. After the data for reduced order model is extracted, the time and parameter dependent simulations can be performed with external simulators.

## 6.2.2 Fixed-Fixed Beam

An example for assessing the accuracy of pROM generation process is an electrostatically actuated fixed-fixed beam [115]. The nominal dimensions of the beam are  $200 \times 20 \times 2 \mu\text{m}$ . Figure 6.3a shows the 3D model of the structure. Three conductors with three capacitance functions are involved. The air-gap separation is  $4 \mu\text{m}$ . The beam length  $L$  is considered as a design variable and all other dimensions are fixed as annotated in the drawing. The analytical models for the important parameters derived below and also reports the dependence on the

beam length of each parameter are summarized in Appendix C. The observed scaling provides important design insight for dimensioning the beam resonators. The beam should be designed for the smallest possible aspect ratio  $L/B$ . However, very small  $L/B$  approximately less than to 10 may cause departure from the assumed mode shape as the long beam assumption breaks down.

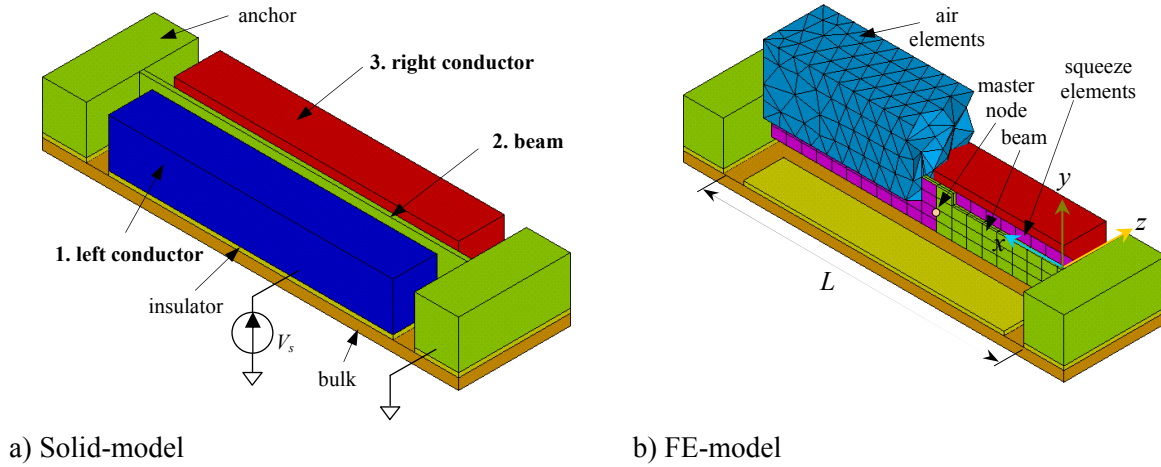


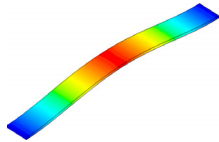
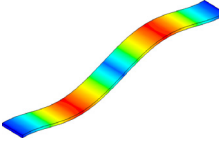
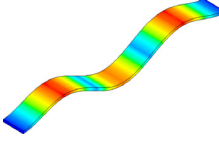
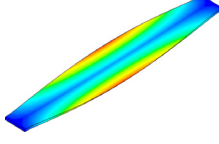
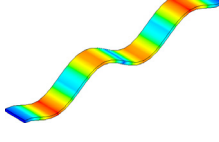
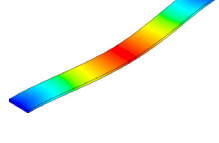
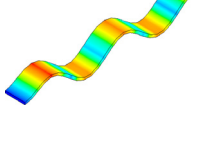
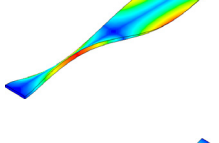
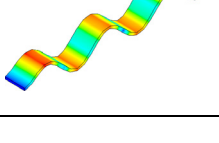
Figure 6.3 Model of an electrostatically actuated fixed-fixed beam

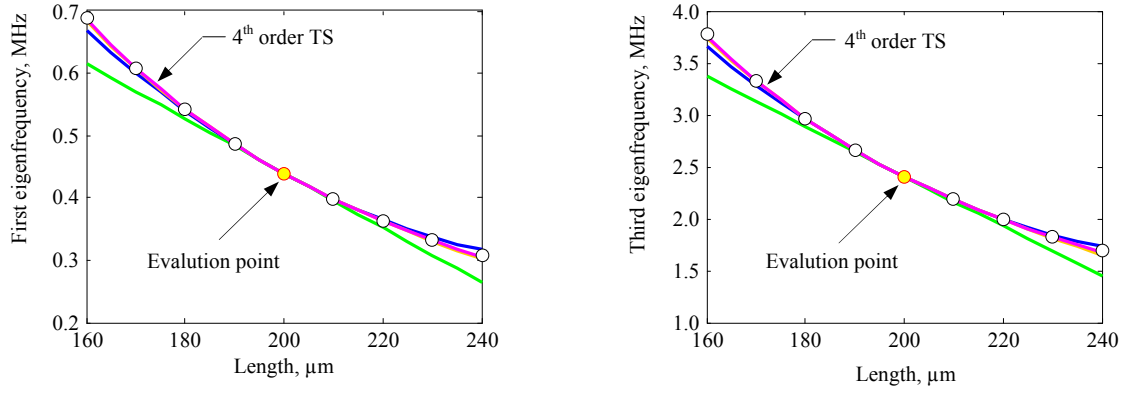
At the same time, the narrow air gap between the moving beam and the substrate will generate back pressure force on the beam due to the squeeze film effect. As the beam becomes shorter, the pull-in voltage of the switch becomes higher [116].

The coupled FE-model consists of the 4294 elements, 7138 nodes. The model uses hexahedral solid elements for the structural domain and tetrahedral elements for the electrostatic domain. Ordinary modal FE analysis at  $L_0 = 200\mu\text{m}$  is performed in order to select appropriate modes for ROM. Table 6.2 illustrates the difference between using different approaches for automated mode selection. Bound for total deflection range is  $4.0\mu\text{m}$ . In first case, the modes and their amplitude range was determined with respect to the linear modal stiffness ratios in the  $z$ -operating direction. The nine lowest modes are considered. In second case, a voltage test load applied on the beam excites only symmetric eigenmodes in the operating direction. In third case, a voltage test load correspond to large displacement is applied. Finally, the beam is driven due to applied voltage greater than pull-in voltage to the ground conductor placed at the center of the structure. The mode contribution factors are determined by LSM [43]. The amount of applied loads is not important for mode selection. The resulting displacements are essential only to evaluate the ratios between modal coordinates. The simplest test load could be recommended for automated mode selection.

The first and third modes were selected as basis functions. Perturbation of the nodes in structural domain with regard to length variation is given by (5.1). The extracted eigenfrequencies dependences on length by parametric modal FE analysis are plotted in Figure 6.4.

Table 6.2 Mode specifications for ROM

Mode	Eigenfrequency at $L_0$ , MHz	Operating range, $\mu\text{m}$ / Modal contribution factor, %				Mode shape
		1 case	2 case	3 case	4 case	
1	0.439469	3.17 81.91	3.92 98.48	3.73 94.27	3.51 88.47	
2	1.217759	0.41 10.67	—	—	—	
3	2.405750	0.11 2.73	0.08 1.38	0.20 4.98	0.42 10.60	
4	3.022455	0.07 1.73	—	—	—	
5	4.017995	0.06 0.98	—	—	—	
6	4.172344	—	—	—	—	
7	6.080111	0.06 0.43	—	0.07 0.75	0.07 0.93	
8	6.103776	0.06 0.42	—	—	—	
9	8.624934	0.06 0.21	—	—	—	



a) First eigenfrequency

b) Third eigenfrequency

Figure 6.4 Eigenfrequencies of a fixed-fixed beam vs. length

Comparisons with ordinary FE results have been used to validate the accuracy of the parametric solutions. The numerical result demonstrates that the dependences  $f_i(L)$  can be captured correctly by 4<sup>th</sup> orders polynomials. The absolute relative error in this approximation on the length interval  $[160 \dots 240] \mu\text{m}$  is no more than 1.4%. It has previously been speculated that accurate approximation of eigenfrequencies is very important for parameterization of ROM model [7]. The  $L^{-2}$  scaling of the resonant frequency is predicted in Appendix C. The use of a Padé approximant makes it possible to represent the dependences  $f_i(L)$  with an accuracy of 0.1%.

Fixed-fixed beam can behave in a highly nonlinear behavior due to deflection dependent stiffening. Application HODM to macromodeling can be expanded in a nonlinear case. In order to obtain the strain energy information for stress stiffened structures, it is necessary to choose nodes on a neutral plane of the beam, which is perpendicular to the operating direction and to apply the appropriate displacement constraints [4]. Perturbations of the nodes on a neutral plane of the structure with respect to modal amplitude  $q_i$  and design parameters  $p$  are given by

$$z(q_1, q_3, p) = z(0, 0, p) + q_1 \phi_{1z}(x, y, z, p) + q_3 \phi_{3z}(x, y, z, p). \quad (6.8)$$

After parametric nonlinear solution in structure domain, the displacement constraints are imposing on all nodes in electrostatic domain:

$$z(q_1, q_3, p) = z(0, 0, p) + u_z(x, y, z, p) \cdot v(x, y, z). \quad (6.9)$$

Figure 6.6 illustrates the parametric ROM database information with regards to modal amplitude  $q_1$  extracted by derivatives based technique. The result demonstrates that the structural energy  $W(q_1, L)$  and capacitance  $C(q_1, L)$  functions could be correctly captured over a wide range of modal amplitudes by rational  $R_{[4 \ 3/0 \ 3]}$  and  $R_{[2 \ 2/2 \ 2]}$  respectively. Figure 6.6a demonstrates nonlinear effects: strain energy  $W_{SENE}(q_1, p)$  of stress-stiffened could be captured correctly by polynomials of order four. The linearized Reynolds equation was used to estimate the squeeze film damping factor and modal damping ratio is shown in Figure 6.6h.

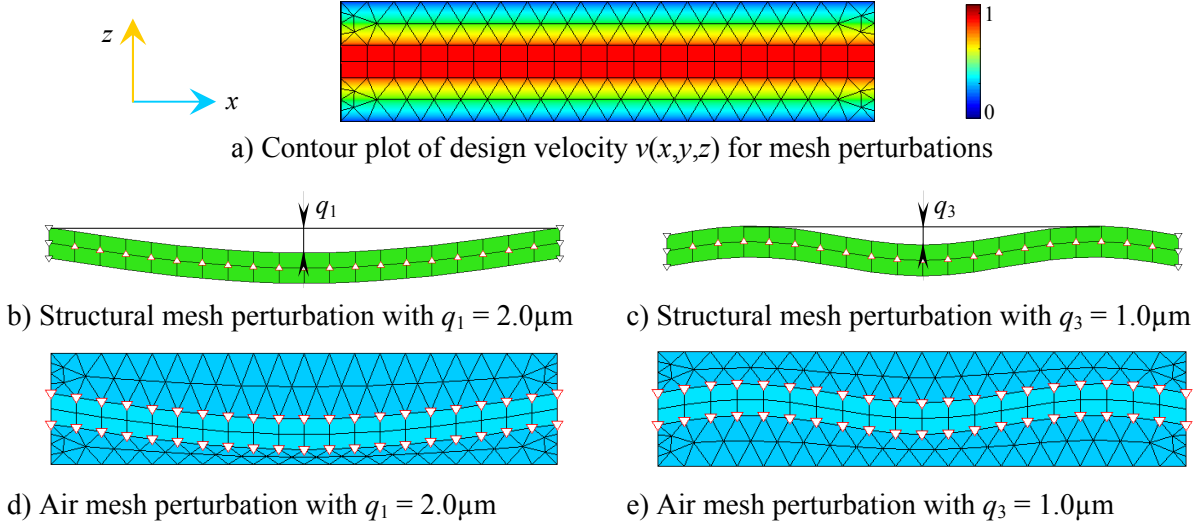


Figure 6.5 Mesh-morphing for parametric macromodeling of a fixed-fixed beam ( $z$ -direction exaggerated for clarity)

Exemplarily, Figure 6.7 shows the accuracy of strain energy capacitance functions with regard to length and modal amplitudes  $q_1$  and  $q_3$ . Calculated data demonstrate that the generated models accurately predict effects over a wide range of modal amplitudes.

A transient dynamic analysis on a beam can be performed using the extracted parameters. There is no procedure that describes the complex nature of the involved energy loss mechanisms in MEMS through a modal projection. The geometrical parameter and deflection dependent modal damping factors based on modal projection procedure for squeeze film damping are assumed for transient analysis [60].

MATLAB/Simulink was used to execute the simulation of the resulting parameterized equations of motion (6.6). The developed parametric ROM model is shown in Figure 6.8. It also defines the functions, which calculates the strain energy and capacitances as well as their first derivatives with respect to the modal amplitudes  $q_1$ ,  $q_3$  and  $L$  using the information of the polynomials defined at the generation step.

A double-step voltage pulse is applied over a short duration ( $20\mu\text{s}$ ) then released as shown in Figure 6.9a. The displacement of the master node near the center of the plate over time for a voltage pulse excitation is plotted in Figure 6.9b. The example illustrates a coupled electrostatic-structural-fluid transient solution. The maximum amplitude of displacement ( $0.07\mu\text{m}$ ) is small enough to ignore large deflection damping effects for short beam. As seen in Figure 6.9b, the damping plays an important role in the behavior of the MEMS resonators.

The phase noise performance of very small MEMS resonators is limited by nonlinear effects, due to fundamental physical phenomena [117]. Based on the parametric dynamic macromodel, the proper scaling to smaller sizes can help to optimize the resonator performance.



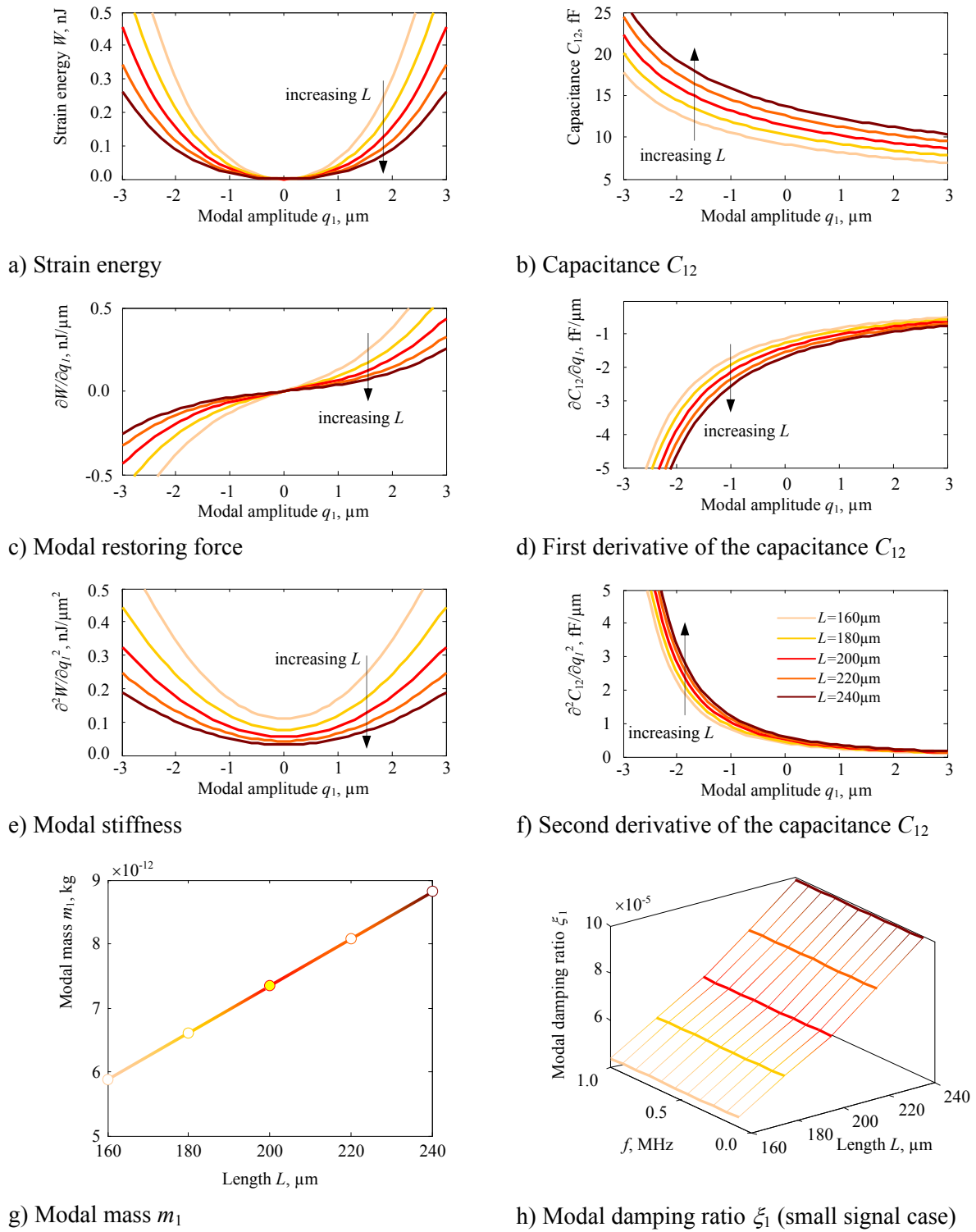


Figure 6.6 Parametric ROM data extracted by HOD technique

In contrast to traditional ROM tool, a new derivatives based technique is proposed for macromodel extraction. The accuracy of the derivatives method is compared to ordinary ROM method. The derivatives technique was found to provide good accuracy in the geometrical and modal space. As a summary it can be concluded that method have been successfully used for macromodel extraction.

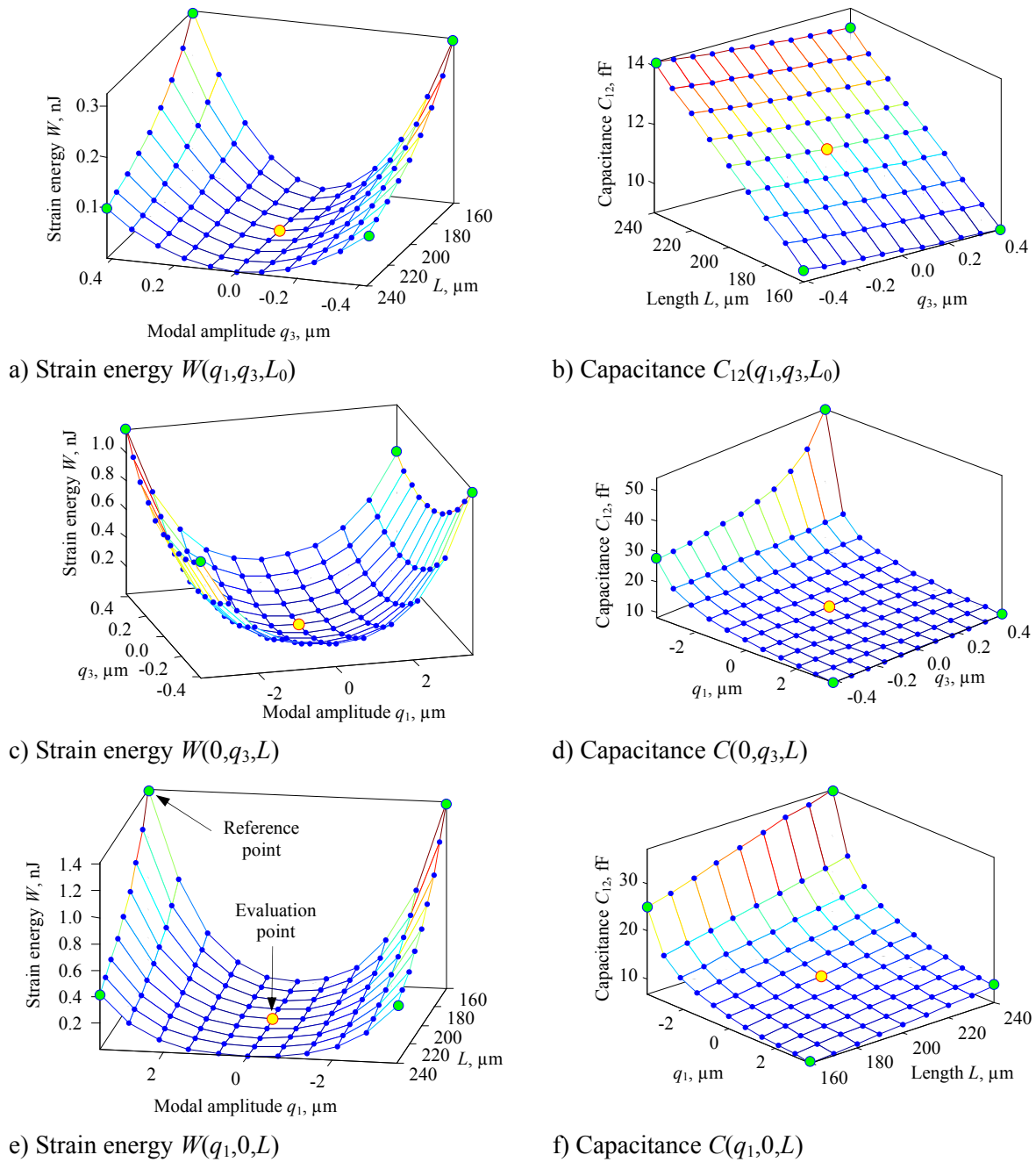


Figure 6.7 Accuracy of HOD technique compared to ordinary FE sampling for parametric ROM

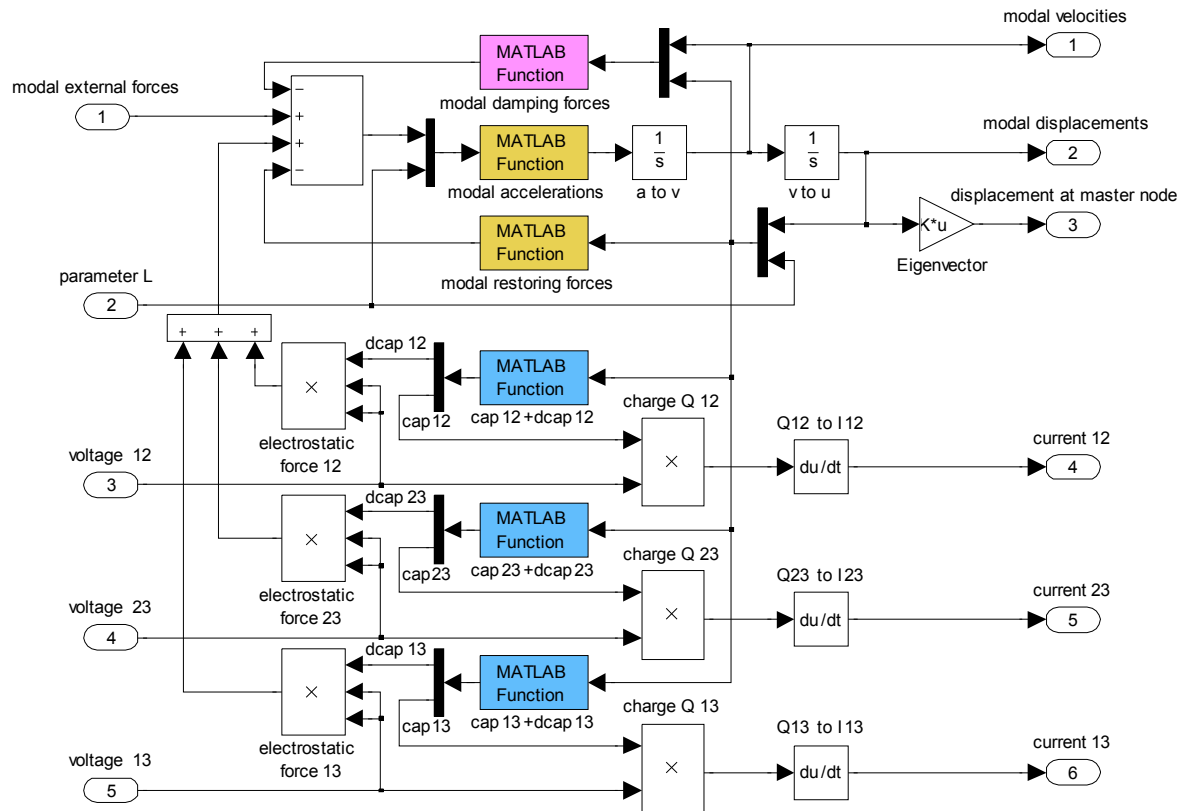
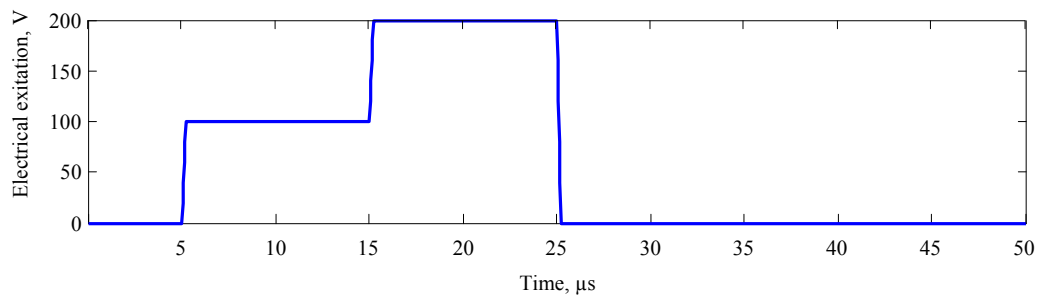
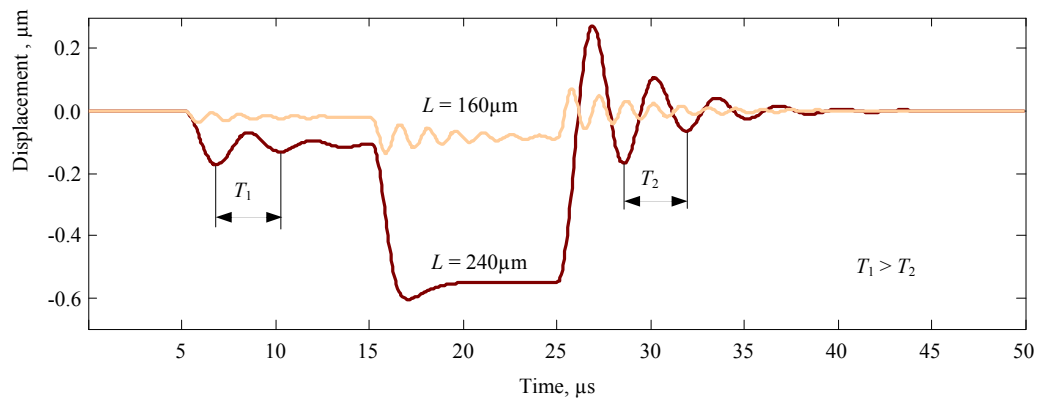


Figure 6.8 Parametric ROM model of a fixed-fixed beam in MATLAB/Simulink



a) Electrical excitation



b) Displacement at master node

Figure 6.9 Simulated transient response of the beams to an electrical excitation

The HOD method is well suited for parametric macromodeling using design changes that can be represented as changes of finite element model parameters, such as material properties and modifications of the geometry. The accuracy achieved with of the HOD method, making it practical for optimize MEMS components at system level in the design phase. HOD technique allows parametric studies of MEMS devices in a cost-effective manner. The method provides a two times to five times speedup for the macromodel generation, depending on the hardware and complexity of the model. The drawback of reduction methods is not a prior computable error bound for the transient analysis. More complicated examples and an experimental comparison of accuracy of developed methods should be performed [118]. Extensions of the presented parametric squeeze film model by full Navier-Stokes equations are suggested for further work. Future developments must address computational issues for improving the efficiency and automation of the prototype tools presented herein.

## 7. Conclusions and Outlook

Many topics in the field of parametric FE analysis and parametric reduced order modeling are covered in this work. A short summary and conclusions of the presented work are given in the following:

- A parametric FE-solver based on the derivation of discretized FE equations and the computation of a Taylor polynomial or Padé approximant of the solution from the high order derivatives has been prototyped
- Automatic differentiations technique for extraction high order derivatives of the FE matrixes, its inverse and determinant has been utilized
- A Library of parameterized finite elements has been developed
- A new mesh-morphing algorithm has been successfully implemented
- A large number of numerical tests have been performed in order to evaluate the accuracy and efficiency.

The microbeam and capacitance cell were used as the benchmarks. The parametric models were compared with the result obtained by the ordinary FE-method. Comparisons with standard FE results have validated the accuracy of the parameterized solutions, when up to six orders were computed to give reasonably engineering accuracy within 2%. For parametric problem with three coupled parameters, presented method is more effective than ordinary FE runs. HODM is a technique to build explicit functions with respect to design parameters. The parametric database allows interactive update of model response for any parameter values. Consequently, HODM is particularly attractive where the number of evaluation point is large. Behavior model extraction and design optimization is a main field of applications of HODM. It has been found that this technique is limited to moderate parameters variations  $\pm 15\%$  due to the mesh-morphing procedures.

The concepts of automatic macromodel generation and parametric macromodeling were well known and have been investigated in the past, but this research makes several advances. For the extension of possibilities for reduced order methods based on mode superposition technique the following investigations were done.

First, this thesis introduces the concept of Taylor expansion or Padé approximant in order to accurately replace computationally cumbersome full three-dimensional simulation. Effective ROM model generation was evaluated by the example of micromirror.

Next, this research introduced and implemented the parametric macromodeling. In the thesis, the successful implementation of a methodology for parameterization of macromodel by the example of microbeam and for exporting these macromodels into MATLAB/Simulink to determine dynamical behavior has been reported.

### **Further Work**

Although a very general approach has been developed, there are still many possibilities for extensions and improvement. Future works will address larger MEMS applications (over  $10^5$  DOF) with a fully automatic approach to parametric mesh generation, and other topics related to the pre- and post-processing facilities. Key remaining issues include: data structure for symmetry sparse matrices, and parallel implementation. Algorithms for functions represented by Fourier-type series can be used to obtain the coefficients of the series expansions, much like what has already been done for Taylor series.

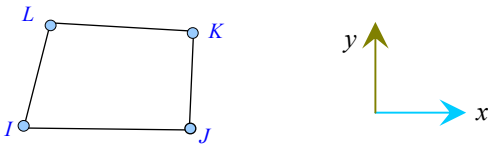
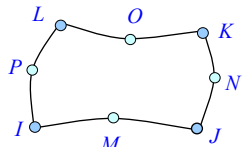
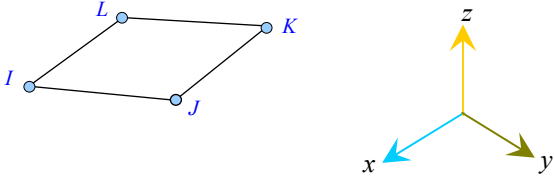
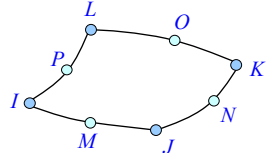
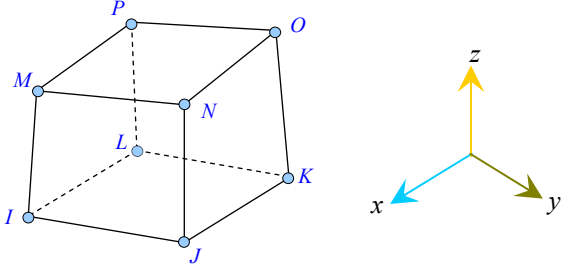
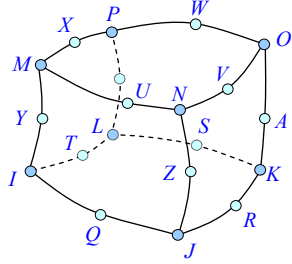
In the future MEMS will get more and more complex so that further research on parametric ROM/MOR methods is required to improve the automation of the model extraction and extend the coverage of considered effects within the macromodel, making it practical for designers to optimize MEMS at the system level. More work should be done in integration of the methods with projection technique based on Krylov subspace and methods based on mode superposition technique.

# Appendix A

## Isoparametric Finite Elements Formulations

### A.1 Element Geometry

Table A.1 Finite element geometry

Type	Linear	Quadratic
2D plane quadrilateral		
3D shell quadrilateral		
3D solid hexahedral (brick)		

### A.2 Interpolation inside the Finite Element

Within the isoparametric formulation of a finite element, the displacement field and coordinates are interpolated inside the finite element from nodal values  $u_i$  and  $x_i, y_i, z_i$  using shape functions:

$$u(x, z, y) = \sum_{i=1}^n N_i u_i . \quad (\text{A.1})$$

$$x = \sum_{i=1}^n N_i x_i , \quad y = \sum_{i=1}^n N_i y_i , \quad z = \sum_{i=1}^n N_i z_i . \quad (\text{A.2})$$

Shape functions for the 2D/3D isoparametric finite elements are given in Section A.3.

### A.3 Shape Functions

The shape functions for the 4-node 2D/3D elements are given

$$\begin{aligned} N_1 &= (1 - \xi)(1 - \eta) / 4, & N_2 &= (1 + \xi)(1 - \eta) / 4, \\ N_3 &= (1 + \xi)(1 + \eta) / 4, & N_4 &= (1 - \xi)(1 + \eta) / 4. \end{aligned} \quad (\text{A.3})$$

The shape functions for the 8-node 2D/3D elements are given

$$\begin{aligned} N_5 &= (1 - \xi^2)(1 - \eta) / 2, & N_6 &= (1 + \xi)(1 - \eta^2) / 2, \\ N_7 &= (1 - \xi^2)(1 + \eta) / 2, & N_8 &= (1 - \xi)(1 - \eta^2) / 2, \\ N_1 &= (1 - \xi)(1 - \eta) / 4 - (N_5 + N_8) / 2, \\ N_2 &= (1 + \xi)(1 - \eta) / 4 - (N_5 + N_6) / 2, \\ N_3 &= (1 + \xi)(1 + \eta) / 4 - (N_6 + N_7) / 2, \\ N_4 &= (1 - \xi)(1 + \eta) / 4 - (N_7 + N_8) / 2. \end{aligned} \quad (\text{A.4})$$

The shape functions for the 8-node and 20-node 3D elements are given, respectively

$$\begin{aligned} N_1 &= (1 - \xi)(1 - \eta)(1 - \zeta) / 8, & N_2 &= (1 + \xi)(1 - \eta)(1 - \zeta) / 8, \\ N_3 &= (1 + \xi)(1 + \eta)(1 - \zeta) / 8, & N_4 &= (1 - \xi)(1 + \eta)(1 - \zeta) / 8, \\ N_5 &= (1 - \xi)(1 - \eta)(1 + \zeta) / 8, & N_6 &= (1 + \xi)(1 - \eta)(1 + \zeta) / 8, \\ N_7 &= (1 + \xi)(1 + \eta)(1 + \zeta) / 8, & N_8 &= (1 - \xi)(1 + \eta)(1 + \zeta) / 8. \end{aligned} \quad (\text{A.5})$$

$$\begin{aligned} N_9 &= (1 - \xi^2)(1 - \eta)(1 - \zeta) / 4, & N_{10} &= (1 + \xi)(1 - \eta^2)(1 - \zeta) / 4, \\ N_{11} &= (1 - \xi^2)(1 + \eta)(1 - \zeta) / 4, & N_{12} &= (1 - \xi)(1 - \eta^2)(1 - \zeta) / 4, \\ N_{13} &= (1 - \xi^2)(1 - \eta)(1 + \zeta) / 4, & N_{14} &= (1 + \xi)(1 - \eta^2)(1 + \zeta) / 4, \\ N_{15} &= (1 - \xi^2)(1 + \eta)(1 + \zeta) / 4, & N_{16} &= (1 - \xi)(1 - \eta^2)(1 + \zeta) / 4, \\ N_{17} &= (1 - \xi)(1 - \eta)(1 - \zeta^2) / 4, & N_{18} &= (1 + \xi)(1 - \eta)(1 - \zeta^2) / 4, \\ N_{19} &= (1 + \xi)(1 + \eta)(1 - \zeta^2) / 4, & N_{20} &= (1 - \xi)(1 + \eta)(1 - \zeta^2) / 4, \\ N_1 &= (1 - \xi)(1 - \eta)(1 - \zeta) / 8 - (N_{17} + N_{12} + N_9) / 2, \\ N_2 &= (1 + \xi)(1 - \eta)(1 - \zeta) / 8 - (N_{18} + N_{10} + N_9) / 2, \\ N_3 &= (1 + \xi)(1 + \eta)(1 - \zeta) / 8 - (N_{19} + N_{11} + N_{10}) / 2, \\ N_4 &= (1 - \xi)(1 + \eta)(1 - \zeta) / 8 - (N_{20} + N_{12} + N_{11}) / 2, \\ N_5 &= (1 - \xi)(1 - \eta)(1 + \zeta) / 8 - (N_{17} + N_{16} + N_{13}) / 2, \\ N_6 &= (1 + \xi)(1 - \eta)(1 + \zeta) / 8 - (N_{18} + N_{14} + N_{13}) / 2, \\ N_7 &= (1 + \xi)(1 + \eta)(1 + \zeta) / 8 - (N_{19} + N_{15} + N_{14}) / 2, \\ N_8 &= (1 - \xi)(1 + \eta)(1 + \zeta) / 8 - (N_{20} + N_{16} + N_{15}) / 2. \end{aligned} \quad (\text{A.6})$$



## A.4 Gauss Quadrature

The numerical integration of 2D quadrilaterals is given by

$$\int_{-1}^1 \int_{-1}^1 f(x, y) dx dy = \sum_{j=1}^m \sum_{i=1}^l w_j w_i f(x_i, y_j). \quad (\text{A.7})$$

The 3D integration of bricks is given by

$$\int_{-1}^1 \int_{-1}^1 \int_{-1}^1 f(x, y, z) dx dy dz = \sum_{k=1}^n \sum_{j=1}^m \sum_{i=1}^l w_k w_j w_i f(x_i, y_j, z_k). \quad (\text{A.8})$$

The integration point locations and weighting factors are given in Table A.2.

Table A.2 Gauss numerical integration parameters

Integration points	Integration point locations $x_i$	Weighting factors $w_i$
quadrilateral 2×2 points	$\pm \frac{1}{\sqrt{3}}$	1.000
hexahedral 2×2×2 points	$\pm \frac{1}{\sqrt{3}}$	1.000

## A.5 Element Initial Stress Stiffness Matrix

In the derivation of element initial stress stiffness matrices it is convenient to reorder nodal degrees of freedom by introducing the element displacement vector  $\mathbf{u}$ , where translational DOFs are reordered so that first all  $x$ -direction DOF are given, then  $y$  and  $z$  as follows:

$$\mathbf{u} = \{u_1^x \dots u_n^x \ u_1^y \dots u_n^y \ u_1^z \dots u_n^z\}^T. \quad (\text{A.9})$$

The element initial stress stiffness matrix for the 3D isoparametric finite elements is given by

$$\mathbf{k}_S = \int_V \mathbf{G}^T \mathbf{S} \mathbf{G} dV, \quad (\text{A.10})$$

where  $\mathbf{G}$  is the matrix obtained by appropriate differentiation of shape functions  $\mathbf{N}$ ,  $\mathbf{S}$  is the matrix of initial stresses. The matrix  $\mathbf{G}$  is given by

$$\mathbf{G} = \begin{bmatrix} \mathbf{g} & 0 & 0 \\ 0 & \mathbf{g} & 0 \\ 0 & 0 & \mathbf{g} \end{bmatrix}. \quad (\text{A.11})$$

Each submatrix  $\mathbf{g}$  is given by

$$\mathbf{g} = \begin{bmatrix} \frac{\partial}{\partial x} N_i \\ \frac{\partial}{\partial y} N_i \\ \frac{\partial}{\partial z} N_i \end{bmatrix}, \quad i = 1, \dots, n. \quad (\text{A.12})$$

The stress matrix  $\mathbf{S}$  is given by

$$\mathbf{S} = \begin{bmatrix} \mathbf{s} & 0 & 0 \\ 0 & \mathbf{s} & 0 \\ 0 & 0 & \mathbf{s} \end{bmatrix}, \quad (\text{A.13})$$

and each submatrix  $\mathbf{s}$  is defined as

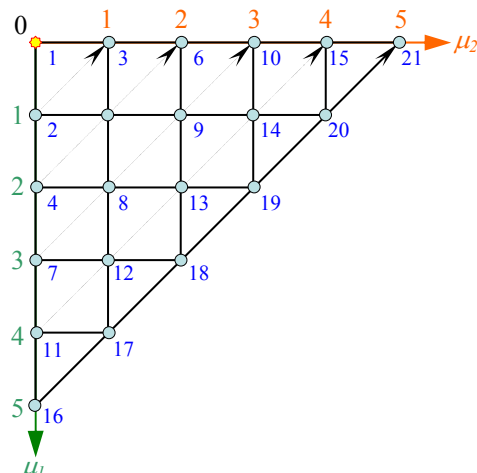
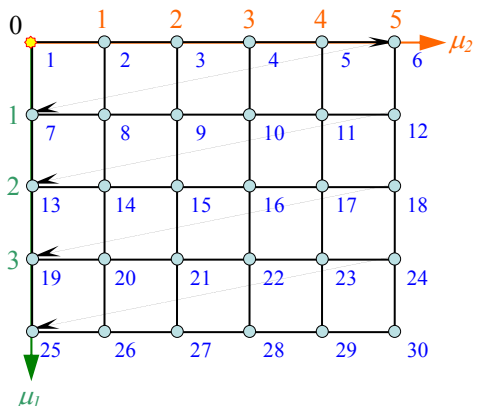
$$\mathbf{s} = \begin{bmatrix} \sigma_{xx} & \sigma_{xy} & \sigma_{xz} \\ \sigma_{xz} & \sigma_{yy} & \sigma_{yz} \\ \sigma_{xz} & \sigma_{yz} & \sigma_{zz} \end{bmatrix}. \quad (\text{A.14})$$

The stresses are obtained by an initial static stress analysis.

# Appendix B

## Polynomial Index Notation in 2D Case

Table B.1 Polynomial index notation

Pascal type: $\mu_1+\mu_2 \leq \max(\mu)$	Lagrange type: $\mu_1, \mu_2 \leq \max(\mu)$																																																																						
$size = C_{n_p}^{order+n_p}$ , $n_p = 2$ , $order = \max(\mu)$	$size = (\mu_1^{\max} + 1) \cdot (\mu_2^{\max} + 1)$																																																																						
$R(\mu) = \sum_{j=1}^{n_p} C_j^{K_j+j}$ , $K_j = -1 + \sum_{i=0}^{j-1} \mu_{n_p-i}$	$R(\mu) = 1 + \mu_2 + (\mu_2^{\max} + 1) \cdot \mu_1$																																																																						
<div><p><math>\mu = \{5,5\}</math></p></div> <div><table><tr><th rowspan="2"><math>R</math></th><th colspan="2"><math>\mu</math></th></tr><tr><th><math>\mu_1</math></th><th><math>\mu_2</math></th></tr><tr><td>1</td><td>0</td><td>0</td></tr><tr><td>2</td><td>1</td><td>0</td></tr><tr><td>3</td><td>0</td><td>1</td></tr><tr><td>4</td><td>2</td><td>0</td></tr><tr><td>5</td><td>1</td><td>1</td></tr><tr><td>6</td><td>0</td><td>2</td></tr><tr><td>7</td><td>3</td><td>0</td></tr><tr><td>8</td><td>2</td><td>1</td></tr><tr><td>9</td><td>1</td><td>2</td></tr><tr><td>...</td><td>...</td><td>...</td></tr></table></div>	$R$	$\mu$		$\mu_1$	$\mu_2$	1	0	0	2	1	0	3	0	1	4	2	0	5	1	1	6	0	2	7	3	0	8	2	1	9	1	2	...	...	...	<div><p><math>\mu = \{4,5\}</math></p></div> <div><table><tr><th rowspan="2"><math>R</math></th><th colspan="2"><math>\mu</math></th></tr><tr><th><math>\mu_1</math></th><th><math>\mu_2</math></th></tr><tr><td>1</td><td>0</td><td>0</td></tr><tr><td>2</td><td>0</td><td>1</td></tr><tr><td>3</td><td>0</td><td>2</td></tr><tr><td>4</td><td>0</td><td>3</td></tr><tr><td>5</td><td>0</td><td>4</td></tr><tr><td>6</td><td>0</td><td>5</td></tr><tr><td>7</td><td>1</td><td>0</td></tr><tr><td>8</td><td>1</td><td>1</td></tr><tr><td>9</td><td>1</td><td>2</td></tr><tr><td>...</td><td>...</td><td>...</td></tr></table></div>	$R$	$\mu$		$\mu_1$	$\mu_2$	1	0	0	2	0	1	3	0	2	4	0	3	5	0	4	6	0	5	7	1	0	8	1	1	9	1	2	...	...	...
$R$		$\mu$																																																																					
	$\mu_1$	$\mu_2$																																																																					
1	0	0																																																																					
2	1	0																																																																					
3	0	1																																																																					
4	2	0																																																																					
5	1	1																																																																					
6	0	2																																																																					
7	3	0																																																																					
8	2	1																																																																					
9	1	2																																																																					
...	...	...																																																																					
$R$	$\mu$																																																																						
	$\mu_1$	$\mu_2$																																																																					
1	0	0																																																																					
2	0	1																																																																					
3	0	2																																																																					
4	0	3																																																																					
5	0	4																																																																					
6	0	5																																																																					
7	1	0																																																																					
8	1	1																																																																					
9	1	2																																																																					
...	...	...																																																																					



# Appendix C

## Analytical Models in an Electrostatically Actuated Fixed-Fixed Beam

Analytical models [11, 116, 117, 119, 120] and scaling dependencies on length  $L$  for related properties in an electrostatically actuated fixed-fixed beam are summarized here.

Table C.1 Analytical models of a fixed-fixed beam

Property	Analytical model	$L$ dependence
Mass	$m = LBH\rho$	$L$
Stiffness (point force excitation at the center)	$K = 10.425 \frac{EBH^3}{L^3}$	$L^{-3}$
Third order stiffness coefficient	$\alpha = \frac{0.767}{B^2} K$	$L^{-3}$
Center deflection under uniform pressure $P$	$\delta = \frac{L^4}{32EH^3} P$	$L^4$
Maximum stress under uniform pressure $P$	$\sigma = \frac{L^2}{2H^2} P$	$L^2$
Bending energy	$W = \frac{\pi^4 EI \delta^2}{96L^3}, I = \frac{BH^3}{12}$	$L^5$
Resonant frequency	$f_i = \frac{n_i^2}{\sqrt{3}\pi} \frac{H}{L^2} \sqrt{\frac{E}{\rho}}$ $n_1 = 2.365$ $n_2 = 3.927$ $n_3 = 5.498$	$L^{-2}$
Modal mass	$m_i = \frac{k_i}{\omega_i^2}$	$L$

Table C.2 Analytical models in an electrostatically actuated fixed-fixed beam

Property	Analytical model	$L$ dependence
Pull-in voltage	$V_{PI} = \sqrt{\frac{8K_{eff}gap^3}{27\epsilon A}}$	$L^{-2}$
Optimal bias voltage	$V_{bias} \approx \sqrt{\frac{\alpha gap^5}{4\epsilon A}}$	$L^{-2}$
Power handling	$Power \geq 1.337 \frac{B\omega_0^3 m}{Q^2}$	$L^{-5}$

According to Blech [108] an analytical solution for the damping  $C$  and squeeze stiffness  $K$  coefficients for a rigid rectangular plate moving with a transverse motion is given by

$$C(\omega) = \frac{64\sigma(\omega)P_{amb}A}{\pi^6 d \omega} \sum_{m=odd} \sum_{n=odd} \frac{m^2 + n^2 c^2}{(mn)^2 \left[ (m^2 + n^2 c^2)^2 + \frac{\sigma(\omega)^2}{\pi^4} \right]}, \quad (C.1)$$

$$K(\omega) = \frac{64\sigma(\omega)^2 P_{amb}A}{\pi^8 d} \sum_{m=odd} \sum_{n=odd} \frac{1}{(mn)^2 \left[ (m^2 + n^2 c^2)^2 + \frac{\sigma(\omega)^2}{\pi^4} \right]}, \quad (C.2)$$

where  $c$  is the ratio of plate length  $a$  divided by plate width  $b$ ,  $d$  is the film thickness. The squeeze number is given by

$$\sigma(\omega) = \frac{12\eta_{eff}a^2}{P_{amb}d^2} \omega. \quad (C.3)$$

# References

- [1] E. LUND, “Finite Element Based Design Sensitivity Analysis and Optimization” PhD Thesis, Aalborg University, 1994.
- [2] PH. GUILLAUME AND M. MASMOUDI, “Computation of high order derivatives in optimal shape design”, *Numerische Mathematik*, **67**(2), pp. 231-250, 1994.
- [3] M. VARGHESE, “Reduced-order modeling of MEMS using modal basis function“, PhD Thesis, Massachusetts Institute of Technology, 2002.
- [4] F. BENNINI, “Ordnungsreduktion von elektrostatisch-mechanischen Finite Elemente Modellen für die Mikrosystemtechnik“, Dissertation, Technische Universität Chemnitz, 2005.
- [5] T. BECHTOLD, “Model Order Reduction of Electro-Thermal MEMS“, PhD Thesis, University of Freiburg, 2005.
- [6] J. LIENEMANN, “Complexity Reduction Techniques for Advanced MEMS Actuators Simulation”, PhD Thesis, University of Freiburg, 2006.
- [7] D. GUGEL, “Ordnungsreduktion in der Mikrosystemtechnik“, Dissertation, Technische Universität Chemnitz, 2009.
- [8] L. FENG, E.B. RUDNYI AND J.G. KORVINK, “Preserving the Film Coefficient as a Parameter in the Compact Thermal Model for fast Electro-thermal Simulation”, *IEEE Trans. Comput.-Aided Des. Integr. Circuits Syst.*, **24**(12), pp.1838-1847, 2005.
- [9] C. MOOSMANN, “ParaMOR - Modellordnungsreduktion parametrisierter MEMS Anwendungen“, Dissertation, Universität Freiburg, 2007.
- [10] “The Bosch Group: Automotive MEMS sales drop with auto market, but new EU requirements will help boost demand”, *MEMSentry*, **39**, pp. 15-17, 2009.
- [11] S.D. SENTURIA, “Microsystem Design”, *Kluwer Academic Publishers*, 2001.
- [12] G. GERLACH AND W. DÖTZEL, “Introduction to Microsystem Technology, A Guide for Students”, *Wiley*, Microsystem and Nanotechnology Series, 2008.
- [13] D. TENHOLTE, S. KURTH, K. HILLER, C. KAUFMANN, T. GESSNER, W. DÖTZEL AND J. MEHNER, “A MEMS Friction Vacuum Gauge”, *Proc. of Eurosensors XXII*, pp. 206-209, 2008.

- [14] Y.I. OZHIGOV, "Limitation of computational resource as physical principle", arXiv:quant-ph/0303127v1.
- [15] S.D. SENTURIA, N. ALURU AND J. WHITE, "Simulating the behavior of MEMS devices: Computational methods and needs", *IEEE Computational Science and Engineering*, **4**, pp. 30-43, 1997.
- [16] P. VOIGT, G. SCHRAG, E.-R. KÖNIG AND G. WACHUTKA, "Modeling Strategies for Microsystems", *Tech. Dig. of MSM'98*, pp. 517-521, 1998.
- [17] G. WACHUTKA, "The art of modelling coupled-field effects in microdevices and microsystems", *Int. Conf. on Modeling and Simulation of Microsystems*, pp. 697-703, 1999.
- [18] V. SHAPIRO AND I. TSUKANOV, "Mesh-free Method and system for modeling and analysis", Patent US6718291 B1.
- [19] M. PORFIRI, "Analysis by Meshless Local Petrov-Galerkin Method of Material Discontinuities, Pull-in Instability in MEMS, Vibrations of Cracked Beams, and Finite Deformations of Rubberlike Materials", PhD Thesis, Virginia Polytechnic Institute and State University, 2006.
- [20] S.D. SENTURIA, R.M. HARRIS, B.P. JOHNSON, S. KIM, K. NABORS, M.A. SHULMAN AND J.K. WHITE, "A computer-aided design system for microelectromechanical systems (MEMCAD)", *J. of Microelectromechanical Systems*, **1**(1), pp. 3-14, 1992.
- [21] S. SENTURIA, "CAD Challenges for Microsensors, Microactuators, and Microsystems", *Proc. IEEE*, **86**(8), pp. 1611-1626, 1998.
- [22] J. MEHNER, F. BENNINI AND W. DÖTZEL, "CAD for Microelectromechanical Systems", *System Design Automation - Fundamentals, Principles, Methods, Examples*, Kluwer Academic Publishers, pp. 111-132, 2000.
- [23] <http://intellisensesoftware.com>
- [24] <http://www.coventor.com>
- [25] <http://www.softmems.com>
- [26] <http://ansys.com>
- [27] <http://www.open-engineering.com>
- [28] <http://www.comsol.com>



- [29] J. CARTER, A. COWEN, B. HARDY, R. MAHADEVAN, M. STONEFIELD AND S. WILCENSKI, “PolyMUMPs Design Handbook”, Rev. 11.0, MEMSCAP Inc.
- [30] K. HILLER, M. KÜCHLER, D. BILLEP, B. SCHRÖTER, M. DIENEL, D. SCHEIBNER AND T. GESSNER, “Bonding and Deep RIE - a powerful combination for high aspect ratio sensors and actuators”, *Proc. of SPIE Micromachining and Microfabrication Process Technology X*, **5715**, pp. 80-91, 2005.
- [31] L.D. GABBAY, J.E. MEHNER AND S.D. SENTURIA, “Computer-Aided Generation of Nonlinear Reduced-Order Dynamic Macromodels – I: Non-Stress-Stiffened Case”, *J. of Microelectromechanical Systems*, **9**(2), pp. 262–269, 2000.
- [32] J.E. MEHNER, L.D. GABBAY AND S.D. SENTURIA, “Computer-Aided Generation of Nonlinear Reduced-Order Dynamic Macromodels – II: Stress- Stiffened Case”, *J. of Microelectromechanical Systems*, **9**(2), pp. 270–278, 2000.
- [33] W. BEDYK, M. NIESSNER, G. SCHRAG, G. WACHUTKA, B. MARGESIN AND A. FAES, “Automated Extraction of Multi-Energy Domain Reduced-Order Models Demonstrated on Capacitive MEMS Microphones”, *Proc. of the 14th Int. Conference on Solid-State Sensors and Transducers, TRANSDUCERS 2007*, pp. 1263-1266, 2007.
- [34] A.H. NAYFEH, M.I. YOUNIS AND E.M. ABDEL-RAHMAN, “Reduced-Order Models for MEMS Applications”, *Nonlinear Dynamics*, **41**(1-3), pp. 211–236, 2005.
- [35] S. REITZ, J. BASTIAN, J. HAASE, P. SCHNEIDER AND P. SCHWARZ, “System Level Modeling of Microsystems Using Order Reduction Methods”, *J. of Analog Integrated Circuits and Signal Processing*, **37**(1), pp.7-16, 2003.
- [36] J. MEHNER, V. KOLCHUZHIN, I. SCHMADLAK, T. HAUCK, G. LI, D. LIN AND T. MILLER, “The influence of packaging technologies on the performance of inertial MEMS sensors”, *Proc. of the 15th International Conference on Solid-State Sensors, Actuators and Microsystems, TRANSDUCERS 2009*, pp. 1885-1888, 2009.
- [37] J.J. SHAH AND M. MÄNTYLÄ, “Parametric and Feature-Based CAD/CAM: concepts, techniques, and applications”, *Wiley-Interscience*, 1995.
- [38] S. PERRIN, J-D. BELEY AND V. BAO, “Parametric and Topologic Optimization Applied To Powertrain Behaviour”, *FISITA 2002 World Automotive Congress*, 2002.
- [39] N. OLHOFF AND J.E. TAYLOR, “On structural optimization”, *J. of Applied Mechanics* **50**, pp. 1139–1151, 1983.
- [40] M. ENGESSER, A.R. FRANKE, M. MAUTE, D.C. MEISEL AND J.G. KORVINK, “An Optimization Technique for Area Shrinking Problems Applied to MEMS Accelerometers”, *Proc.of Smart Systems Integration*, pp. 111-118, 2009.

- [41] O. DAHLBLOM, A. PETERSON AND H. PETERSON, "CALFEM – a program for computer-aided learning of the finite element method", *Eng. Comput.*, **3**(2), 1986.
- [42] <http://www.colorado.edu/engineering/cas/courses.d/IFEM.d/>, "Introduction to Finite Element Methods", Department of Aerospace Engineering Sciences, University of Colorado.
- [43] ANSYS<sup>®</sup> Academic Research, Release 11.0, Documentation, ANSYS, Inc.
- [44] A.H. JAWED AND A.J. MORRIS, "Approximate Higher-Order Sensitivities in Structural Design", *Engineering Optimization*, **7**(2), pp. 121-142, 1984.
- [45] C. BISCHOF, G. CORLISS, L. GREEN, A. GRIEWANK, K. HAIGLER AND P. NEWMAN, "Automatic differentiation of advanced CFD codes for multidisciplinary design", *J. on Computing Systems in Engineering*, pp. 625-638, 1992.
- [46] I. OZAKI, F. KIMURA AND M. BERZ, "Higher-order sensitivity analysis of finite element method by automatic differentiation", *Computational Mechanics*, **16**(4), pp. 223-234, 1995.
- [47] F. VAN KEULEN, R.T. HAFTKA, AND N.H. KIM, "Review of options for structural design sensitivity analysis. Part 1: Linear systems", *Comput. Methods Appl. Mech. Eng.*, **194**, pp. 3213-3243, 2005.
- [48] HU HONG, "Application of an automatic differentiation method to a 2D Navier-Stokes CFD code", *Comput. Methods Appl. Mech. Eng.*, **156**, pp. 179-183, 1998.
- [49] P. PETIN, J.L. COULOMB AND PH. CONRAUX, "High Derivatives for Fast Sensitivity Analysis in Linear Magnetodynamics", *IEEE Trans. on magnetics*, **33**(2), 1997.
- [50] L. LEBENSZTAJN, "Sensitivity Analysis and High Order Derivatives Applied to the Modeling of Permanent Magnets," *IEEE Trans. on magnetics*, **34**(5), 1998.
- [51] T.N. NGUYEN AND J.-L.COULOMB, "High Order FE Derivatives versus Geometric Parameters. Implantation on an Existing Code", *IEEE Trans. on magnetics*, **35**(3), 1999.
- [52] IN-GU KWAK, YOUNG-WOO AHN, SONG-YOP HAHN, AND II-HAN PARK, "Shape Optimization of Electromagnetic Devices using High Order Derivatives", *IEEE Trans. on magnetics*, **35**(3), 1999.
- [53] B. THON, D. BARIANT, S. BILA, D. BAILLARGEAT, M. AUBOURG, S. VERDEYME, P. GUILLON, F. THEVENON, M. ROCHETTE, J. PUECH, L. LAPIERRE AND J. SOMBRIN, "Coupled Padé approximation-finite element method applied to microwave device design", *Microwave Symposium Dig. IEEE MTT-S International*, **3**, pp. 1889-1892, 2002.

- [54] J. MEHNER, A. SCHAPORIN, V. KOLCHUZHIN, W. DÖTZEL AND T. GESSNER, “Parametric Model Extraction for MEMS Based on Variational Finite Element Techniques”, *Proc. of Transducers '05 - 13th International Conference on Solid-State Sensors, Actuators and Microsystems*, **1**, pp. 776-779, 2005.
- [55] V. KOLCHUZHIN, J. MEHNER AND W. DÖTZEL, “Geometrically Parameterized Finite Element Model of the Silicon Strain Gauge”, *Proc. of 7. Chemnitzer Fachtagung Mikrosystemtechnik- Mikromechanik & Mikroelektronik*, pp. 190-195, 2005.
- [56] S. GARREAU, S. PERRIN AND M. ROCHETTE, “Application of high order derivatives to structural probabilistic analysis”, *Final Report*, CADOE / European Space Agency Project, 2005.
- [57] J. WIBBELER, J. MEHNER, F. VOGEL AND F. BENNINI, “Development of ANSYS /Multi-physics Modules for MEMS by CAD-FEM GmbH”, *19th CAD-FEM Users' Meeting*, 2001.
- [58] F. BENNINI, J. MEHNER AND W. DÖTZEL, “Computational methods for reduced order modeling of coupled domain simulations”, *Proc. of Transducers 2001*, pp. 260–263, 2001.
- [59] F. BENNINI, J. MEHNER AND W. DÖTZEL, “System Level Simulations of MEMS Based on Reduced Order Finite Element Models”, *Int. Journal of Computational Engineering Science*, **2**(2), pp. 385-388, 2003.
- [60] J.E. MEHNER, W. DÖTZEL, B. SCHAUWECKER AND D. OSTERGAARD, “Reduced order modeling of fluid structural interactions in MEMS based on modal projection techniques”, *Proc. of the Int. Conference on Solid-State Sensors, Actuators and Microsystems, TRANSDUCERS 2003*, **2**, pp. 1840–1843, 2003.
- [61] B. SCHAUWECKER, K.A. STROHM, W. SIMON, J. MEHNER AND J.-F. LUY, “Toggle-Switch - A new type of RF MEMS switch for power applications”, *Microwave Symposium Digest IEEE MTT-S International*, **1**, pp. 219-222, 2002.
- [62] C. DÖRING, S. REITZ, J. BASTIAN, M. MAUTE, P. SCHNEIDER AND P. SCHWARZ, ”Verhaltensmodellierung eines Drehratensensors mittels Verfahren der Ordnungsreduktion”, *Proc. of 10. GMM-Workshop*, 2004.
- [63] M. SCHLEGEL, F. BENNINI, J. MEHNER, G. HERRMANN, D. MUELLER AND W. DÖTZEL, “Analyzing and Simulation of MEMS in VHDL-AMS Based on Reduced Order FE Models”, *IEEE Sensors J.*, **5**(5), pp. 1019–1026, 2005.
- [64] T. HAUCK, M. THANNER AND G. O'BRIEN, “Dynamic Macromodels for Sensor Devices”, *Proc. of EuroSimE 2005*, pp. 50-54, 2005.

- [65] T. MÄHNE, K. KEHR, A. FRANKE, J. HAUER AND B. SCHMIDT, "Creating Virtual Prototypes of Complex MEMS Transducers Using Reduced-Order Modelling Methods and VHDL-AMS", *Applications of Specification and Design Languages for SoCs: Selected papers from FDL'05*, pp. 135-153, 2006.
- [66] D. GUGEL, W. DÖTZEL, T. OHMS AND J. HAUER, "Reduced Order Modeling in Industrial MEMS Design Processes", *Proc. of Eurosensors XX*, pp. 48-55, 2006.
- [67] T. HAUCK, I. SCHMADLAK AND J. MEHNER, "Stress Analysis of a Micromachined Inertial Sensor at Dynamic Load", *Proc. of ITherm 2008*, pp. 945-948, 2008.
- [68] G. LI, A. MCNEIL, D. KOURY, M. CHAPMAN, AND D. MONK, "Design of transducers and package at the same time", *Proc. of IPACK'05*, Ref. 73396, 2005.
- [69] V. KOLCHUZHIN, W. DÖTZEL AND J. MEHNER, "Challenges in MEMS parametric macro-modeling based on mode superposition technique", *Proc. of EuroSimE*, pp. 442-445, 2009.
- [70] P. SPELLUCCI, "Numerische Verfahren der nichtlinearen Optimierung", *Verlag Birkhäuser*, 1993.
- [71] V. KOLCHUZHIN, J. MEHNER, T. GESSNER AND W. DÖTZEL, "Parametric Finite Element Analysis for Reduced Order Modeling of MEMS", *Proc. of EuroSimE 2006*, pp. 507-510, 2006.
- [72] D. GUGEL AND W. DÖTZEL, "Parametric Reduced Order Modeling for Industrial MEMS Design Processes", *Proc. of Smart Systems Integration*, pp. 65-72, 2007.
- [73] J.L. LÓPEZ AND N.M. TEMME, "Multi-Point Taylor Expansions of Analytic Functions", *Tran. of the American Mathematical Society*, **356**(11), pp. 4323-4342, 2004.
- [74] C. BREZINSKI, "Padé type approximation and general orthogonal polynomials", *ISMN*, **50**, *Birkhauser Verlag*, 1980.
- [75] G.A. BAKER JR., "Essentials of Padé Approximations", *Academic Press, New York*, 1975.
- [76] P.R. GRAVES-MORRIS, D.E. ROBERTS AND A. SALAM, "The epsilon algorithm and related topics", *J. of Computational and Applied Mathematics*, **122**(1-2), pp. 51-80, 2000.
- [77] C. CHAFFY, "How to compute multivariate Pade approximants," *Proc. of the 5th ACM symposium on Symbolic and algebraic computation*, pp. 56-58, 1986.
- [78] P. GUILLAUME AND A. HUARD, "Multivariate Pade approximation", *J. of Computational and Applied Mathematics*, **121**, pp. 197-219, 2000.

- [79] D. ROY AND R. BHATTACHARYA, “Multivariate approximants with Levin-like transforms”, *Computer Physics Communications*, **172**(1), pp. 1-18, 2005.
- [80] S. BARGICCHI AND M. MASMOUDI, “Application of the Gevrey Theory to the Parameterization of Nonlinear Problems”. *The 3rd Int. Conference/Workshop on Automatic Differentiation: From Simulation to Optimization*, 2000.
- [81] Y. ANDRÉ, “Arithmetic Gevrey series and transcendence. A survey”, *J. de théorie des nombres de Bodeaux*, **15**(1), pp. 1-10, 2003.
- [82] S. BARGIACCHI, “Résolution de grands systèmes: du linéaire au non linéaire“, PhD Thesis, Université Paul Sabatier, 2004.
- [83] R. HAFTKA, “Second-order sensitivity derivatives in structural analysis”, *AIAA J.*, **20**, pp. 1765–1766, 1982.
- [84] P. LANCASTER, “On eigenvalues of matrices dependent on a parameter”, *Numer. Math.* **6**, pp. 377-387, 1964.
- [85] S. GARG, “Derivatives of eigensolutions for a general matrix”, *AIAA J.*, **11**, pp. 1191-1194, 1973.
- [86] A.L. ANDREW, “Eigenvalue problems with nonlinear dependence on the eigenvalue parameter. A bibliography”, *Technical Report*, La Trobe University, 1974.
- [87] A.L. ANDREW, “Convergence of an iterative method for derivatives of eigensystems”, *J. comput. Phys.*, **26**, pp. 107-112, 1978.
- [88] A.L. ANDREW, “Iterative Computation of Derivatives of Eigenvalues and Eigenvectors”, *J. Inst. Maths Applies*, **24**, pp. 209-218, 1979.
- [89] Z.-S. LIU, S.-H. CHEN, Y.-Q. ZHAO AND C.-S. SHAO, “Computing eigenvector derivatives in structural dynamics”, *Acta Mechanical Solida Sinica*, **6**(3), pp. 291-299, 1993.
- [90] R.B. NELSON, “Simplified calculations of eigenvector derivatives,” *AIAA J.*, **14**(9), pp. 1201-1205, 1976.
- [91] L.T. PILLAGE AND R.A. ROHRER, “Asymptotic waveform evaluation for timing analysis”, *IEEE Trans. Computer-Aided Design*, **9**, pp. 352-366, 1990.
- [92] MATLAB, The Mathworks, Inc., <http://www.mathworks.com/>
- [93] V.I. ZHULIN, S.J. OWEN AND D.F. OSTERGAARD, “Finite Element Based Electrostatic-Structural Coupled Analysis with Automated Mesh Morphing”, *Technical Proc. of the 2000 Int. Conf. on Modeling and Simulation of Microsystems*, pp. 501-504, 2000.

- [94] I. TSUKANOV AND M. HALL, "Data Structure and Algorithms for Fast Automatic Differentiation," *Int. J. for Numerical Methods in Engineering*, **56**(13), pp. 1949-1972, 2003.
- [95] K.H. CHANG, K.K. CHOI, C.S. TSAI, B.S. CHOI AND X.M. YU, "Design sensitivity analysis and optimization tool (DSO) for shape design applications", *Comput. System Eng.*, **6**(2), pp. 151-175, 1995.
- [96] K.J. BATHE, "Finite Element Procedures", *Prentice-Hall*, 1996.
- [97] C.H. BISCHOF AND A. CARLE, "Obtaining Fast and Reliable. Derivatives - Fast", *SIAM J. on Scientific Computing*, **15**(2), pp. 285-294, 1994.
- [98] G. CORLISS, C. FAURE, A. GRIEWANK, L. HASCOET AND U. NAUMANN, "Automatic differentiation of algorithms: from simulation to optimization", *Springer*, 2002.
- [99] C.H. BISCHOF, H.M. BÜCKER, B. LANG, A. RASCH AND E. SLUSANSCHI, "Automatic Differentiation of Large-Scale Simulation Codes is no Illusion", *Preprint of the Institute for Scientific Computing RWTH-CS-SC-02-12*, Aachen University, 2002.
- [100] <http://www.autodiff.org/tools>
- [101] M. SINGH, "n<sup>th</sup>-order derivatives of certain inverses and the Bell Polynomials", *J. Phys. A: Math. Gen.*, **23**, pp. 2307-2313, 1990.
- [102] K.K. CHOI AND K.H. CHANG, "A study of design velocity field computation for shape optimal design", *Finite Elements Anal Des*, **15**, pp. 317-341, 1994.
- [103] D.A. FIELD, "Laplacian smoothing and Delaunay triangulations", *Communications in Applied Numerical Methods*, **4**, pp. 709-712, 1988.
- [104] R. GUYAN, "Reduction of Stiffness and Mass Matrices", *AIAA Journal*, **3**(2), pp. 380, 1965.
- [105] R.R. CRAIG, "A Review of Time Domain and Frequency Domain Component Mode Synthesis Methods", *Int. J. of Analytical and Experimental Modal Analysis*, **2**(2), pp. 59-72, 1987.
- [106] R.R. CRAIG AND M.D.D. BAMPTON, "Coupling of Substructures for Dynamic Analysis", *AIAA Journal*, **12**, pp. 1313-1319, 1968.
- [107] D. OSTERGAARD AND J. MEHNER, "Using a Heat Transfer Analogy to Solve for Squeeze Film Damping and Stiffness Coefficients in MEMS Structures", 2003. <http://www.ansys.com/industries/mems/mems-downloads/thermal-analogy-damping.pdf>

- [108] J.J. BLECH, “On Isothermal Squeeze Films”, *J. of Lubrication Technology*, **105**, pp. 615-620, 1983.
- [109] M.-H. BAO, W.-J. QI AND Y. WANG, “Geometric Design Rules of Four-Terminal Gauge for Pressure Sensors”, *Sensors and Actuators*, **18**, pp. 149-156, 1989.
- [110] A.V. GRIDCHIN, V.A. KOLCHUZHIN, V.A. GRIDCHIN AND G. GERLACH, “FE Modeling of the four-terminal silicon piezoresistive structures”, *Proc. of 8. Chemnitzer Fachtagung Mikromechanik & Mikroelektronik*, pp. 117-122, 2007.
- [111] Y. NISHIDATE AND G.P. NIKISHKOV, “Generalized plane strain deformation of multi-layer structures with initial strains”, *J. of Appl. Phys.*, **100**(11), pp. 1-4, 2006.
- [112] A. MILEKHIN, S. MUTILIN, J. YUKECHEVA, M. PUTYATO, A. VOROB'EV, V. PRINZ, V. KOLCHUZHIN, J. MEHNER AND D.R.T. ZAHN, “Raman scattering on semiconductor microtubes”, *Physica status solidi (c)*, **6**(9), pp. 2060–2063, 2009.
- [113] <http://www.ioffe.ru/SVA/NSM/Semicond/>
- [114] V. KOLCHUZHIN, W. DÖTZEL AND J. MEHNER, “Efficient Generation of MEMS Reduced-Order Macromodels Using Differentiation of Finite Elements”, *Sensor Lett.*, **6**(1), pp. 97-105, 2008.
- [115] V. KOLCHUZHIN, W. DÖTZEL AND J. MEHNER, “A Derivatives-Based Method for Parameterization of MEMS Reduced Order Models”, *Proc. of EuroSimE 2008*, pp. 519-523, 2008.
- [116] M. AGARWALA, H. MEHTA, R.N. CANDLER, S.A. CHANDORKAR, B. KIM, M.A. HOPCROFT, R. MELAMUD, G. BAHL, G. YAMA, T.W. KENNY AND B. MURMANN, “Scaling of amplitude-frequency-dependence nonlinearities in electrostatically transduced microresonators”, *J. of Appl. Phys.*, **102**(7), 2007.
- [117] V. KAAJAKARI, T. MATTILA, A. OJA AND H. SEPPÄ, “Nonlinear Limits for Single-Crystal Silicon Microresonators”, *J. of MEMS*, **13**(5), 2004, pp. 715-724.
- [118] M. NIESSNER, G. SCHRAG, J. IANNACCI AND G. WACHUTKA, “Experimentally Validated and Automatically Generated Multi-Energy Domain Coupled Model of a RF MEMS Switch”, *Proc. of EuroSimE*, pp. 595-600, 2009.
- [119] D. BLEVINS, “Formulas for Natural Frequency and Mode Shape”, *Krieger Publishing Company*, 1995.
- [120] W.C. YOUNG, “Roark's formulas for stress and strain”, *McGraw-Hill*, 1989.





# List of Figures

2.1	Multilevel MEMS design flow process .....	19
2.2	Parametric transient multiphysics simulation.....	25
2.3	The levels of difficulty of the physical simulations.....	26
2.4	Derivatives based parametric FE simulation .....	26
2.5	A schematic view on the VHDL-AMS exported ROM model in ANSOFT/ Simplorer.....	27
2.6	Response surface method to the behavioral model extraction.....	33
3.1	Parametric harmonic response .....	43
3.2	Static behavior of a Duffing oscillator.....	47
3.3	Parametric modal analysis of a 2-DOF spring mass system.....	49
3.4	Frequency sweep response of a 2-DOF spring mass system.....	51
4.1	Block scheme of parametric FE technique .....	53
4.2	Parametric 3D eight node solid element.....	59
4.3	Surface load on the element.....	61
4.4	Body load on the element .....	61
4.5	Morphing process .....	65
4.6	Solid transformations.....	67
4.7	Comparison between FE mesh-morphing algorithms .....	68
4.8	3D array ( $n = 3$ , $order = 4$ ) and its compressed 2D representation .....	69
4.9	Substructure of a resonator .....	71
4.10	Error estimation in parametric analysis .....	73
5.1	FE-model of a fixed-fixed beam.....	75
5.2	Design curves of a fixed-fixed beam under pressure load.....	77
5.3	Comparison of the time cost between FE-reanalysis and HODM.....	78
5.4	Static response: Variation in orientation angle.....	78
5.5	Parametric modal study of a fixed-fixed beam.....	79
5.6	Undamped harmonic response of a fixed-fixed beam .....	80
5.7	Parametric model of a comb cell for computing capacitance stroke functions .....	80
5.8	Capacitance stroke function of a movable finger with regard to six degrees of freedom .....	81
5.9	Comparison between capacitance functions obtained by different approaches .....	82
5.10	Comparison between mesh-morphing and remesh approaches.....	83
5.11	Squeeze film analysis of a rectangular plate.....	85
5.12	FE-model of a perforated beam for discrete analysis .....	86
5.13	Result of a discrete static analysis of a perforated beam .....	86
5.14	Histogram: Discrete analyses of a perforated beam .....	86
5.15	Folded-flexure resonator.....	88

5.16	Parameterized four-terminal piezoresistive element .....	89
5.17	Parametric sequential coupled algorithm.....	90
5.18	Parametric analysis of a four-terminal piezoresistive element.....	91
5.19	Semiconductor Microtube .....	91
6.1	Overview of the data generation for MEMS reduced order macromodel by HOD technique .....	96
6.2	Accuracy of HOD method compared to ordinary FE sampling for ROM .....	98
6.3	Model of an electrostatically actuated fixed-fixed beam.....	101
6.4	Eigenfrequencies of a fixed-fixed beam vs. length .....	103
6.5	Mesh-morphing for parametric macromodeling of a fixed-fixed beam .....	104
6.6	Parametric ROM data extracted by HOD technique .....	105
6.7	Accuracy of HOD technique compared to ordinary FE sampling for parametric ROM .....	106
6.8	Parametric ROM model of a fixed-fixed beam in MATLAB/Simulink.....	107
6.9	Simulated transient response of the beams to an electric excitation .....	107

# List of Tables

2.1	Data for different disciplines nomenclature .....	24
4.1	Overview of AD software .....	63
5.1	Parameters summary for a fixed-fixed beam.....	76
5.2	Parameters summary for a comb cell .....	83
5.3	Results summary of the discrete analyses of a perforated beam .....	87
6.1	Summary of computation times: small signal case; number of modes = 3 (1,3,7) ....	99
6.2	Mode specifications for ROM .....	102
A.1	Finite element geometry .....	111
A.2	Gauss numerical integration parameters .....	113
B.1	Polynomial index notation.....	115
C.1	Analytical models of a fixed-fixed beam .....	117
C.2	Analytical models in an electrostatically actuated fixed-fixed beam .....	118



# Versicherung

Hiermit versichere ich, dass ich die vorliegende Arbeit ohne unzulässige Hilfe Dritter und ohne Benutzung anderer als der angegebenen Hilfsmittel angefertigt habe; die aus fremden Quellen direkt oder indirekt übernommenen Gedanken sind als solche kenntlich gemacht.

Bei der Auswahl und Auswertung des Materials sowie bei der Herstellung des Manuskripts habe ich Unterstützung von folgenden Personen erhalten:

KEINE

Weitere Personen waren an der Abfassung der vorliegenden Arbeit nicht beteiligt. Die Hilfe eines Promotionsberaters habe ich nicht in Anspruch genommen. Weitere Personen haben von mir keine geldwerten Leistungen für Arbeiten erhalten, die im Zusammenhang mit dem Inhalt der vorgelegten Dissertation stehen.

Die Arbeit wurde bisher weder im Inland noch im Ausland in gleicher oder ähnlicher Form einer anderen Prüfungsbehörde vorgelegt.

Chemnitz, 12. Februar 2010

.....  
Ort, Datum

.....  
Unterschrift



# Theses

1. Finite element techniques have become state-of-the-art for component design of MEMS. Physical effects related with mechanical, electromagnetic, thermal and fluid fields in complex devices are accurately described for static, harmonic and transient load situations. Drawback of existing finite element techniques is that those algorithms can only analyze a single model configuration with specified dimensions and physical parameters.
2. The key idea of the novel approach which accounts for parameter variations in a single finite element run is to compute not only the governing system matrices of the finite element problem but also high order partial derivatives with regard to design parameters. As result, Taylor vectors of the system's response can be expanded in the vicinity of the initial position capturing structural dimensions and physical parameter.
3. Behavioral models with singularities on the real axis, with singularities in the complex plane or with branching points cannot be presented efficiently by a Taylor series. Taylor expansions of functions with poles converge slowly or fail even with a high order of derivatives. In order to overcome the problem, rational polynomials (e.g. Padé approximation) can be utilized to extend the operating range over the poles, which are the zeros of the denominator term.
4. A Jacobian matrix is used for the isoparametric transformation of a finite element to a unit cell. Generally, the mathematical expression of a Jacobian matrix depends on the element type (through the shape functions) and the nodal coordinates of the element. The Jacobian matrix is expressed in terms of the derivatives of shape functions with respect to the local element coordinates evaluated at Gauss points of the element. The shape functions of the finite element depend only on the local coordinates within the element and thus are independent of the actual geometry of the element. Like Jacobian, the strain-displacement matrix depends on coordinates of the nodal points, whereas the constitutive matrix depends only on the material parameters. So, the derivatives of an elementary stiffness matrix can be done with respect to material properties, to geometrical parameters or to load and boundary conditions.
5. The derivatives of the inverse Jacobian matrix as well as the determinant of the Jacobian matrix can be obtained by using automatic differentiation (AD). AD technique utilizes generalized differentiation rules, which give an exact representation of the partial derivatives up to the specified order by combining derivatives of the arguments with binomial coefficients. AD allows to compute exact high order derivatives up to the machine precision.

6. A convenient way to transform global parameters to internal nodal coordinates is a Laplacian smoothing used for mesh-morphing. In contrast to iterative Laplacian smoothing, the electrical analogy can be effectively used to compute design velocities for nodal transformations with regard to geometrical parameters.
7. The mechanical components based on flexible beams and electrostatic components based on comb fingers are two important classes of MEMS applications. The beam performances scale with a power law dependence on its dimensions with exponent between -3 and 5. A proper chosen order of a Taylor series is vital to build an accurate approximation. Generally, HOD technique is limited to moderate parameters variations  $\pm 15\%$  due to the mesh-morphing procedures.
8. In contrast to traditional data sampling and function fit procedures, a novel HOD technique can be utilized to extract parametric reduced order models (macromodels) based on the mode superposition method. The implemented automatic differentiation technique provides high accuracy and efficiency in the frequency and time domains.



# Lebenslauf

**Vladimir A. Kolchuzhin**

## **Persönliche Daten:**

Geburtsdatum: 11. Januar 1974  
Geburtsort: Novosibirsk, UdSSR  
Staatsangehörigkeit: russisch  
Familienstand: verheiratet, 2 Kinder

## **Schulbildung:**

09/1984 – 06/1988 Oberschule in Novosibirsk  
09/1988 – 06/1992 Fachmittelschule für Radiotechnik in Novosibirsk  
Abschluss: Diplom mit Auszeichnung

## **Studium:**

10/1992 – 06/1997 Studium an der Staatliche Technische Universität Novosibirsk  
Fachrichtung: Elektronik und Mikroelektronik  
Abschluss: Bachelor der Technik und Technology  
Diplom mit Auszeichnung  
09/1997 – 06/1999 Masterstudium an der Staatliche TU Novosibirsk  
Fachrichtung: Elektronik und Mikroelektronik  
Abschluss: Magister der Technik und Technology

## **Berufliche Tätigkeit:**

09/1999 – 10/2004 wissenschaftlicher Mitarbeiter an der Professur  
für Halbleiter-baelemente und Mikroelektronik  
der Staatliche Technische Universität Novosibirsk  
seit 11/2003 wissenschaftlicher Mitarbeiter an der Professur  
für Mikrosystem- und Gerätetechnik der TU Chemnitz

Chemnitz, den 12.02.2010